FACULTY OF SCIENCE
UNIVERSITY OF COPENHAGEN

Master Thesis

Søren Nissen
Niels Bohr Institute

A Study of Solitons in Biological Membranes and Neurons

Academic Advisor: Thomas Heimburg
Submitted: 31st March 2014

The front page picture illustrate the concept of nerve signals trough neurons (istockphoto.com)

Copenhagen, 31st March 2014

A Study of Solitons in Biological Membranes and Neurons

An analytic study of bright and dark solitons stability, collisions and initiations in biological membranes

Søren Nissen
Membranes Biophysics Group
Niels Bohr Institute
University of Copenhagen

Academic Advisor: Thomas Heimburg

Søren Nissen

Note on programs

Algorithms has been written in *C++*. *Microsoft Visual Studio 2012* have been used for compilation. Data treatment have been carried out along with plotting and fitting in *Wolfram Mathematica 9.0.1.0*. Image handling has been done i *Adobe Photoshop CS6* and *Adobe Illustrator CS6*. Figures are unless otherwise specified made by myself. This document is designed in *Adobe InDesign CS6*.

Resume

Soliton-modellen introducere at anskue nerve signalet på en thermodynamisk måde, i modsætning til den anerkendte *Hodgkin-Huxley model*. I stedet for et elektrisk signal der løber ned langs nerve, menes der i *Soliton-modellen* at dette er en lydbølge. Lydbølger tage formen af og opfører sig som solitoner, en lokaliseret bølgepakke. Solitoner i en biologiske membran er en lokal ændring i membranens densitet der bevæger sig med konstant hastighed.

Målet med dette speciale er at bygge videre på forståelsen af solitoner i biologiske membraner. Der vil blive undersøgt, hvad der kræves af en membran for at kunne indeholde negative solitoner (negativ densitets ændring) og positive solitoner (positiv densitets ændring). Det vil blive vist, at sådan et miljø skal kunne vise to lokale maksima i kompressibiliteten over en bestemt temperatur vidde, hvor ligevægtstilstanden af membranen skal være i det lokale minimum mellem de to maksimum. Ydermere findes der, at solitoner af alle arter, negative og positive, kan kollidere uden noget nævneværdigt sker. Ved et sammenstød vil de to solitoner gå gennem i hinanden med det resultat, at de deres fremtidigt færd vil være forsinket, have tabt lidt af deres amplitude, have accelereret, samt at der er udskilt små bølge der forplanter sig foran dem. Forsinkelsen afhænger af deres hastighed, men der kan findes ved lave hastighed, at i stedet for at være forsinket i deres udbredelse, har sprunget længere frem på membranen.
Der findes også at små variationer i stabile solitoner, således at de er ustabile, vil resultere i at de henfalder til stabile solitoner inden for kort tid. Hvis variationen øges, vil det resultater i at solitonen deler sig i to soliton. Disse solitoner har ikke samme størrelse og vil løbe i hver sin retning.
Hvis der er en lokal forstyrrelse i membranen, vil dette efter kort tid resulterer i lige store solitoner. Der findes, at i en membran, som kan indeholde både negative og positive solitoner, at der vil optræde par, bestående af en negativ og positive soliton. Disse par optræder første efter et bestemt mønster, når forstyrrelsen har en hvis mængde energi fordelt ud over membranen. Det vil blive vist, at det er mest sandsynligt at have par af solitoner eller ingen solitoner, end kun at have en slags soliton i en menbrane, hvor begge type solitoner kan propagere.

Abstract

With the emergence of *the soliton model*, a different way to see nerve signal has been introduced. Instead of an electric signal that runs along the nerve, as described by *the Hodgkin-Huxley model*, *the soliton model* describes the nerve signal as a sound wave. These sound waves have the characteristics of and behave like solitons. Solitons in a biological membrane are a local density change of the membrane moving at constant speed.

The aim of this thesis is to get a better understanding of solitons in biological membranes. It will be investigated what is required of a membrane to sustain both negative and positive solitons. It will be shown, that such an medium must have two local maximum in the compressibility. In addition, the membrane should be in the state where the compressibility has a minimum between the two maximum. In such a membrane, collision of two solitons, of any kind, is shown to happen without annihilation. The two solitons will pass right through each other with a small amplitude loss, accelerated speed, and a delay in their future process. This delay is shown to depend on the velocity, and that the delay will be negative for solitons with a velocity near the lower limit velocity.
A small distortion of a soliton will result in a rapid decay from the unstable to a stable one. If the distortion exceeds a certain threshold, the soliton will split into two solitons, which will propagate in opposite direction. The solitons will not be of the same size and not have the same velocity.
It is shown that a local distortion in the membrane will result in solitons of same type propagating in opposite direction. The appearance of pairs of solitons (a negative and a positive soliton) depend on the energy given to the membrane, and over which range it is distributed. It is shown that it is more likely to have pairs of solitons or no solitons, than only have one type n a membrane where both types of solitons can propagate.

Contents

1 Introduction 1
1.1 Motivation 3
1.2 Objective 3

2 Background Theory 5
2.1 Biological Membranes 5
2.1.1 Lipids 7
2.1.2 Biological Membranes in Nature 8
2.1.3 Biomembrane Phases 10
2.1.4 Biomembrane Phase Transition 11
2.1.4.1 Cooperativity 14
2.1.4.2 Susceptibilities and fluctuations 14
2.1.4.3 Proportionality relations and compressibilities close to the transition. 17
2.1.5 Lipid Mixture 19
2.2 Theories of Nerve signal 22
2.2.1 Hodgkin & Huxley Model 23
2.2.2 Thermodynamics of the Nerve Pulse 24
2.2.2.1 Heat Changes during the Action Potential 24
2.2.2.2 Mechanical Changes during the Action Potential 25
2.3 The Soliton Model 26
2.3.1 Conservation laws 31
2.3.2 Energy of the soliton 32
2.3.3 Viscous dissipation 34
2.3.4 Collision of pulses and disturbances 35

3 Methods 37
3.1 Euler method 37
3.1.1 Error in Numerical Solution 38
3.1.1.1 Local Truncation Error 38
3.1.1.2 Global Truncation error 39
3.2 Two-Step Lax Wendroff 41
3.2.1 Algorithm 42
3.2.2 Error 44
3.2.2.1 Spatial noise 44
3.2.2.2 Temporal noise 44
3.2.2.3 Method stability and Small-amplitude perturbations 45
3.2.2.4 Small-amplitude waves 50

4 Sound Profiles 53
4.1 Sound profile for DPPC membrane 53
4.2 Sound profile for a 50:50 DMPC:DSPC membrane 55

5 Results 63
5.1 Solitons in DPPC LUV Membranes 63
5.1.1 Analytic Solution 63

5.1.2 Collision of negative solitons 65
5.1.2.1 Delay of the solitons 66
5.1.3 Disturbance in the soliton 67
5.2 Solitons in a mixed lipid membrane 70
5.2.1 Stable Soliton 70
5.2.2 Collision of Solitons 71
5.2.3 Disturbance in solitons 73
5.2.4 Initiation 75
5.2.4.1 Initiation in a system with viscosity 81
5.2.5 Thickness change and heat release 81

6 Discussion 83

7 Conclusion 87

8 Perspectives 88

Acknowledgments 90

References 91

Appendix 97
A. Small-amplitude waves 97
B. The initiations domains 98
C. Time series 100
C.1 Collision of two solitons 100
C.2 Initiation of solitons 104
D. Initiation (other similarities) 107
E. Best fit to 50:50 DMPC:DSPC sound profile 109
F. Soliton propagation in a shifted sound profile 110

Chapter 1

Introduction

Looking at the world's biological diversity, it is easy to believe that the difference in the domains, kingdoms and species are enormous. Even knowing that all life are just a combination of the same building blocks of life, it is easier to see the differences between a house cat and an *Escherichia coli*, than the similarities. All through that all living thing are cells, either living as a single-celled organism or a multicellular organism, they all follow the same set of fundamental rules and elements. All living things today can be traced back to the first self-replication ribonucleic acid (RNA) molecule, which have been an essential role to all life. Today, RNA is still in use in the protein synthesis, but the storage function and its role as the self-replication molecule are evolved to be DNA. They both follow the same specific rules across the whole biological diversity. In the same way, as in biology, the different fields of physics have many similarities than what first meets the eyes. Mathematics is the common language in physics, and as RNA and DNA can be used to describe every living cell, mathematics can be used to describe the principles of the nature. The mathematics develop to describe a principle of one thing in nature can be used to describe another thing, like the principle of genes in DNA can be used to describe the similarity between a house cat and bacteria, and their differences.
In this thesis the concept of solitons is used, this phenomena was first described by *John Scott Russell* in 1834 and he write the following about his first encounter with a soliton, which summarise the characteristic of a soliton well:

> *"I was observing the motion of a boat which was rapidly drawn along a narrow channel by a pair of horses, when the boat suddenly stopped – not so the mass of water in the channel which it had put in motion; it accumulated round the prow of the vessel in a state of violent agitation, then suddenly leaving it behind, rolled forward with great velocity, assuming the form of a large solitary elevation, a rounded, smooth and well-defined heap of water, which continued its course along the channel apparently without change of form or diminution of speed. I followed it on horseback, and overtook it still rolling on at a rate of some eight or nine miles an hour, preserving its original figure some thirty feet long and a foot to a foot and a half in height. Its height*

gradually diminished, and after a chase of one or two miles I lost it in the windings of the channel. Such, in the month of August 1834, was my first chance interview with that singular and beautiful phenomenon which I have called the Wave of Translation." [1]

In his work he established some key properties of solitons – the waves where stable and obtain same shape, and can travel over very large distances. The speed depend on the size of the wave and is constant, and they do not merge, like other waves. If a wave is too big, compared to the conditions, it will split into a big and a small wave. However, what he did see and investigated, was not truly solitons, but *near-solitons* or solitary waves. Near-solitons do not emerge from a collision unchanged, but have a small amplitude loss. The loss is mostly insignificant, and therefore they is often called solitons. In physics, solitons can be found in a wide range of fields, e.g. optic, hydrodynamic, quantum mechanics, and biological membranes.

Besides solitons, the phase transition has a present role in this thesis, since it is in this phase a biological membrane is giving rise to the needed non-linearity in the compressibility. The most recognizable phase transition has it component in common with the first described soliton, water. The transition from ice to water, and from water to steam, is one of the most fascinating phase transition and violent in nature, which has been a pivot to science in decades. That all matter can be transform from a solid to a fluid by just raising the temperature, reshaped and back to solid again, has resulted in the world. And that fluid turns into gas has lead to the civilisations we know today. In the phase transition, different odd properties take place when the matter is a mix of the two states. One of these properties is compressibility, which turn out not to be the average between the compressibility of the two state around the phase transition. The compressibility was used by scientist in the 18th and 19th century, in the discussion about the atomic theory. The compressibility is a measure of the relative volume change of a gas, fluid or solid as a response to pressure or change in stress.

In the phase transition, a biological membrane has a characteristic change in the compressibility. Together with the dispersive nature of the membrane, it give the condition for solitons to propagate. This led to the proposal of *the soliton model* in 2005 by *Heimburg* and *Jackson*, that the nerve signal is a soliton travelling through the nerve [2]. However, it was seen as a controversy to the accepted theory, *Hodgkin* and *Huxley* [3], which describe the primary signal as an action potential travelling through the nerve cells. Where it is in *the soliton model* is an effect of the soliton. *The soliton model* is of thermodynamic nature, and can therefore explain most of the thermodynamic nature of the nerve. *The Hodgkin-Huxley model* is a macroscopic model and use the ion-channel to explain the action potential, which is not directly incorporated in *the soliton model*.

1.1 Motivation

Neurophysiology is a field where a lot of common knowledge is based on few or inaccessible literary works. However, the common knowledge has been accepted, because it is in agreement with the accepted theory, *the Hodgkin-Huxley model*. But much of this knowledge, like annihilation of colliding pulses, has almost no recorded evidence in the literature. And as shown recently by our lab, in *Membrane Biophysics Group*, that this common knowledge is properly not accurate [4]. In Denmark we learn kids in primary school that the nerve signal is something electrical running around in the brain cell and with some "magic" you get a consciousness. The "magic" is still unexplained, but the electrical signal is understood in the way *Hodgkin* and *Huxley* described it in 1952 [3]. Over the years, different variations of *the Hodgkin-Huxley model* have been presented, but no theories has varied from the carrying signal is the electric signal. *The soliton model* challenged the view of the nerve signal, by introducing a new way to look at the nerve signal. It is still a new theory, is less developed and have yet to be widely applied. But to have the opportunity to be a part of the development of and contribute to this theory, which some day could be the accepted one, and could alter the knowledge of entire generations, rewrite the school books, has been a big motivation for me and I am respectfully for the opportunity I have been given.

1.2 Objective

The aim of this thesis is to get a better understanding of solitons in biological membranes. This will be done by investigate in which kind of environment it is possibility to have solitons with a negative and positive lateral density change. Further, what such an environment give of properties in the interaction between solitons of different kinds, instability of solitons and how solitons can be initiated in such an environment.

The thesis is structure as following: Starting introducing the reader to the *Background Theory* in chapter 2, containing introduction to lipids, biological membranes, phase transition for membranes and the two theories of the nerve signal, the accepted theory *the Hodgkin-Huxley model*, and *the soliton model*. Then the numerical methods used to calculate the result is presented and analysed with their errors in *Methods* (chapter 3). The thermodynamic theory of sound profile and calculation of the used sound profiles is given in *Sound Profile* (chapter 4). The result of the numerical methods using the sound profiles is given in *Results* (chapter 5) and the findings is discussed in chapter 6 and conclusions in drawn in chapter 7. The work in this thesis is set into perspective in chapter 8.

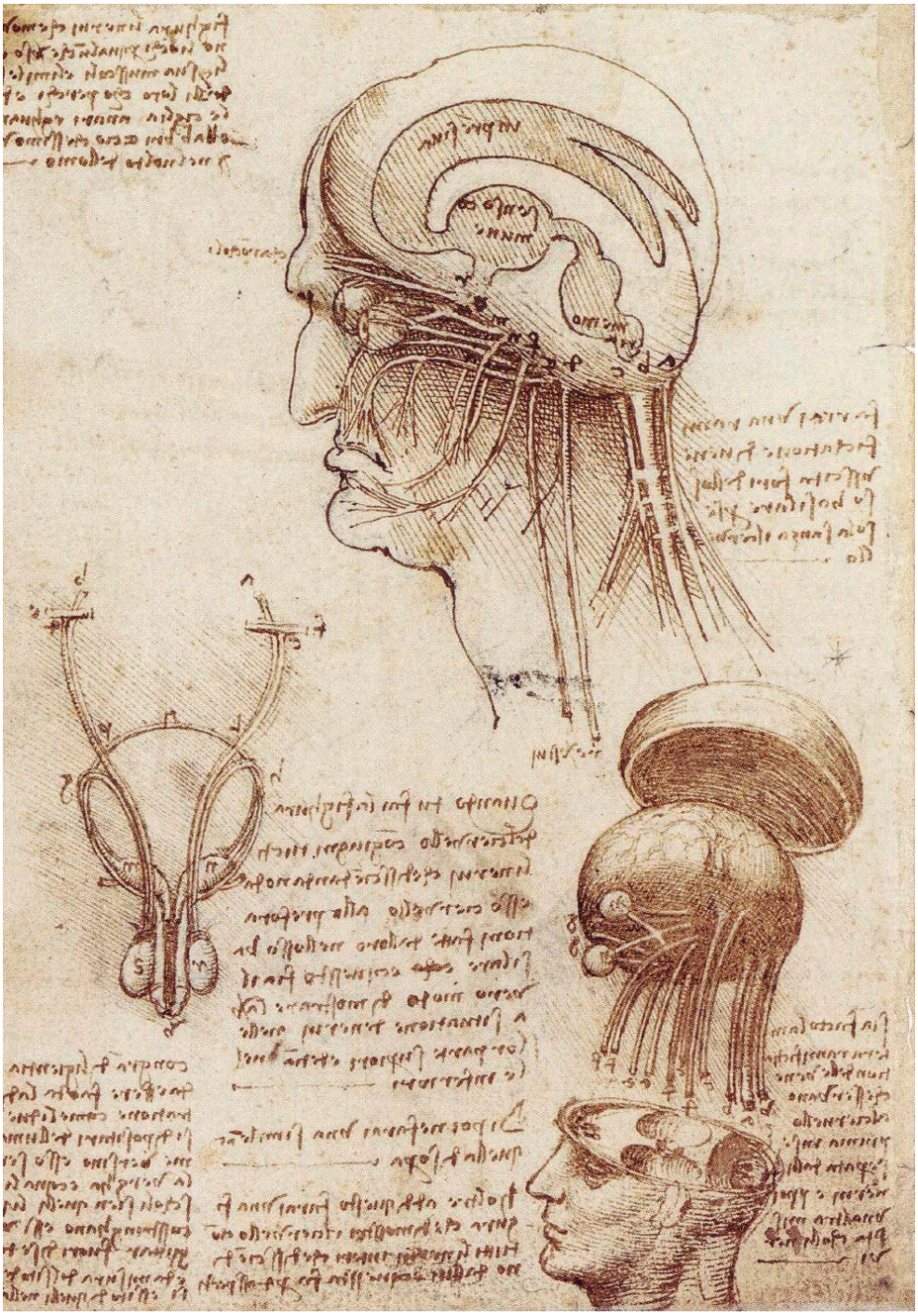

Study of Brain Physiology, By Leonardo da Vinci, 1508. He made the drawing based on what he was told that behind the eyes there were three cavities, where the spirit was housed. Later, after he had investigated brains on his own, Leonardo da Vinci draw new drawing without the cavities.

Chapter 2

Background Theory

This chapter will give the introduction needed to fully understand this thesis. First the biological membranes is introduced, what they consists of and their characteristics related to *the soliton model*. Thereafter, an introduction to the nerve signal, its properties and *the Hodgkin-Huxley model* for the nerve signal. And last a detailed introduction to *the soliton model*.

2.1 Biological Membranes

Many people do not think of the skin as the largest organ in the human body. Many just think the skin as a waterproof, flexible, and inert container. Moreover, it's not seen as an organ that support a variety of essential processes, such as temperature regulation. In the same way, the skin that surrounds each of the biological cells of the bacteria to the cells in the organs is not just a dynamic and flexible container, but is essential to the cell's inner to function. These dynamic, flexible and essential containers called biological membranes or biomembrane, are not just a container for the cell organelles, but also provide the surface of these organelles. Biomembranes have the function of carry different tasks out, like transport of ions and molecules across the membrane, communication with other cells and shield the inner from the surroundings by obtaining a chemical favourable environment. Other biomembranes have a role of separating other biomembranes and cells from the external environment, like the myelin cells is separating the axon in the neurons from the external environment.

The best way to get an understanding of the biological membrane structure is to look on how the understanding of biological membranes has develop throughout history. The first encounter of the biomembrane was made by the Swiss botanist *Carl Wilhelm von Nägeli*, in his work *Botanische Beiträge* from 1955. *Carl Nägeli* noted the different in rates of penetration of pigments into damaged and undamaged plants cells and concluded that there must be an outer layer with its own special properties. He named it the *plasma membrane*. In 1899, *Ernst Charles Overton* showed that the view created by *Wilhelm Pfeffer*, two years before in 1897, needed to be modified. *Wilhelm Pfeffer* [5] demonstrated that the membrane was a barrier to the passage of water and solute. *Overton* [6] demonstrated that non-polar molecules such as alkyl chains and cholesterol have a relatively easy passage though the

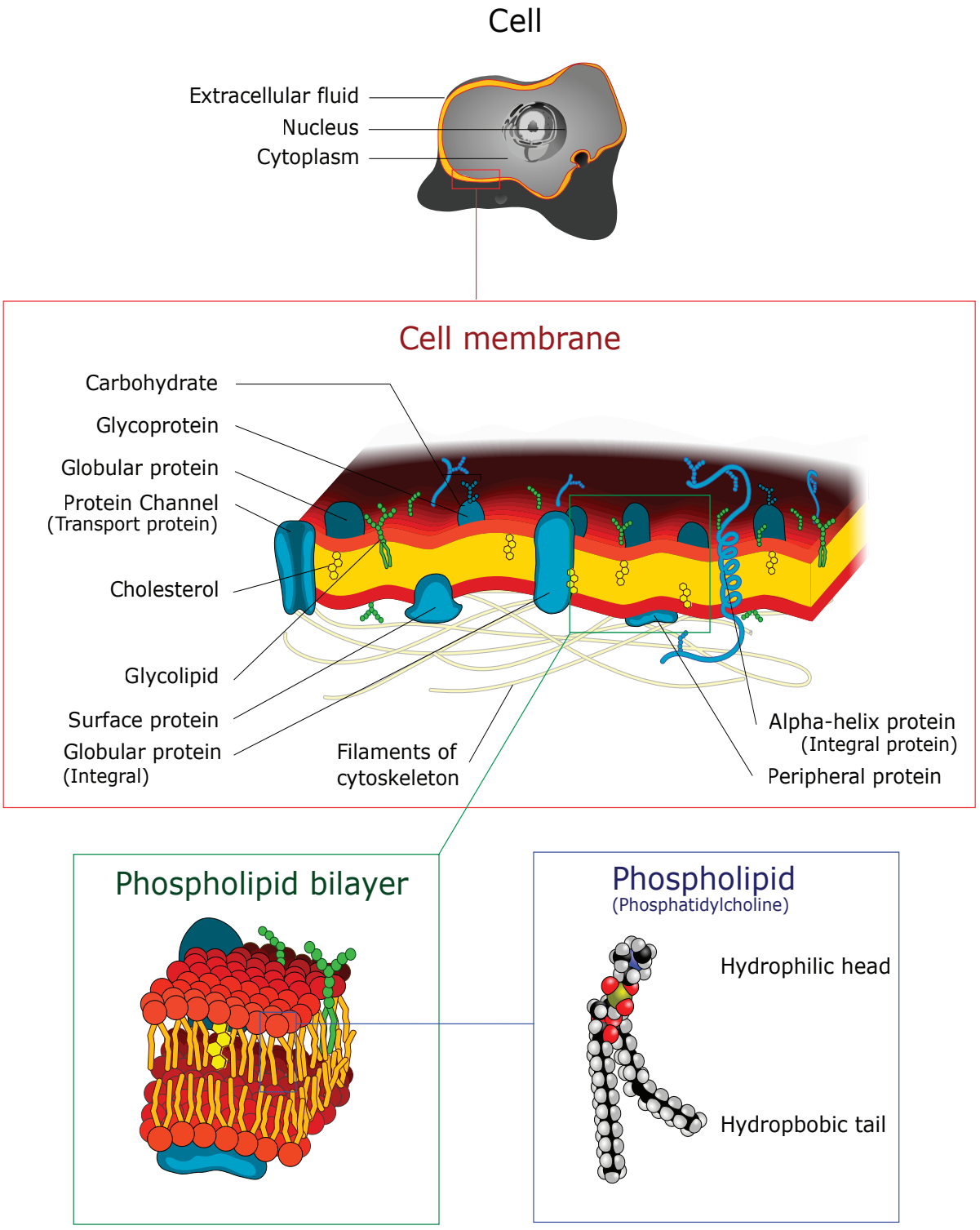

Figure 2.1.1 – Illustration of a Eukaryotic cell membrane. ("Cell membrane detailed diagram 4" by Dhatfield licensed under CC BY-SA 3.0)

membrane compared to polar molecules, such as water. On that, he concluded that the membrane exercises selective control through its differential permeability and that it is composed of certain types of liquid crystals known as lipids.
In 1925, *Evert Gorter* and *F. Grendel* [7] measured the surface area of a red blood cell and the area of a reconstructed film formed by the lipids extracted from the red blood cell membrane. The ratio was approximately one-to-two. They conclude that the membrane may consist of a double layer of lipids molecules. Later, in the mid-1930s, *James Danielli*, *Hugh Davson* [8] and *E. Newton Harvey* [9], [10] made accurate measurements of the surface tension of the plasma membrane and found this to be considerably lower than for most lipids. They proposed a membrane model (*Davson-Danielli model*), where the lipids made a bilayer, while the proteins, knowing to lower the surface tension in an addition to lipids, formed a thin film at the lipid-water interface. The membrane itself could be either liquid or solid and considered homogeneous. In 1954, *Danielli* [11] revised the model. The hydrophobic parts of the lipid were conjectured to lie in the bilayer interior, while the hydrophilic regions of the lipids facing the water at either side, in the gaps between the proteins. *J. D. Robertson* [12], in 1957, confirmed that the bilayer hypothesis, while observing the membrane in an electron microscope. He was able to resolve two dark parallel lines and between a lighter area. The dark lines was linked to the two protein layers, and the lighter area to the lipid bilayer. The interpretation was that all cell membranes must have a universal structure, so-called unit-membrane.

Singer and Nicolson [13] eventually refined this model, in 1972, with the proposal of the *Fluid Mosaic model* for the gross organisation and structure of the proteins and lipids of biomembranes. The model proposed that the lipids are arranged in the form of a bilayer, like in *the Davson-Danielli model*, in which the proteins are embedded and are free to diffuse laterally. An illustration is shown of an *Eukaryotic* membrane in Figure 2.1.1.
In 1984, *Mouritsen and Bloom* [14] extended *Fluid Mosaic model* with *the Mattress model*. *The Mattress model* introduce that the lipids and the proteins may distribute inhomogeneously, because of the mismatch between the hydrophobic regions of the lipids and the proteins. With these models the biomembrane was describe as a dynamics system.

2.1.1 Lipids

Lipids are a group of naturally occurring molecules that include fats, waxes, and sterols. Chemically the lipids can be divided into eight groups: fatty acids, glycerolipids, glycerophospholipids, sphingolipids, saccharolipids, polyketides, sterol lipids and prenol lipids. Lipids are either hydrophobic or amphiphilic.
Glycerophospholipids or phospholipids are the main component of the biomembrane, and like the majority of the other lipids in membranes, these have a polar and non-polar region, making them amphiphilic molecules.

This thesis will mainly focus on phospholipids, and therefore an introduction to its structure and property is necessary. In Figure 2.1.2 the chemical structure of a phospholipids is illustrated. A phospholipid can be divided into two regions, a

polar and a non-polar region (Figure 2.1.2: Green: non-polar, Red and blue: polar). The non-polar region is composed of two hydrocarbon chains, normally containing 16 or 18 carbons molecules [15]. The hydrocarbon groups can vary between 12 to 22 molecules, where the chains can be either saturated (with hydrogen atoms) or unsaturated. The most common is that one chain is saturated and the other unsaturated. The hydrocarbon chains are linked through to a carbon in a glycerol backbone. In the other end of the glycerol backbone, one find, in this case a phospholipid, a negative charged phosphate group. The phosphate group is attach to the backbone thought an ester bond. To this phosphate is the head group attached, and making up the polar region of the lipid. The head group can make the region either a negative charged, with serine glycerol as head group, or a Zwitterionic[1] with choline and ethanolamine as head group.
The lipids are named after the carbons chain and the head group. An example is dipalmitoylphosphatidylcholine (DPPC) a lipid with two palmitic acids linked to a choline group.

Due to the amphiphilic nature of most lipids, they will self-organize to a structure that minimize their unfavourable polar-nonpolar interaction, when they are with a polar solvent, e.g. water. The self-organization will mostly result in macroscopic structures, such as micelles, planar bilayers or vesicles. Vesicles are especially in of general interest in the context of biological membranes. Because the bilayer structure are energetically favourable and comparable to the cells membrane.

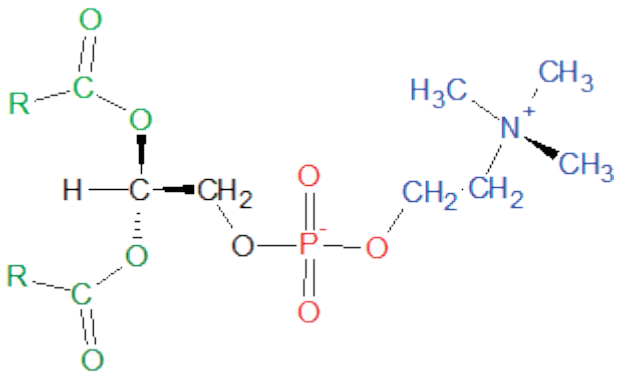

Figure 2.1.2 – A chemical drawing of a phospholipid with a head group of phosphatidylcholine, and the carbon chain starting the two "R".

2.1.2 Biological Membranes in Nature

Biomembranes varies in lipid composition across the nature and organisms. Even for the same organisms, the lipid composition can vary when raised in different environments. Bacteria grown under different environments, where the change could be in temperature, pressure or pH, showed different lipid composition in the membrane [16]. The bacteria have different processes to vary the lipid compo-

1 From German *zwitter* "hybrid", meaning a neutral molecule with a positive and a negative electrical charge within the molecule

sition, such as changing the length of the carbon chains or make carbon-carbon double bonds. These processes is often introduced by enzymes, which expression genes is temperature controlled, and become inactive with a protein binding to the enzyme at higher temperature. The ability to regulate the composition to the environment is known as homeoviscous adaptation [17], [18].
Similar response to the environment is found in cells of eukaryotic organisms. Where the cells regulate the carbon-carbon double bonds in the carbon chains, and the concentration of cholesterol in the membrane to adapt to the environment. When poikilothermic animals[2] are living in a low temperature environment, compared to them living in a higher temperature, the amount of double bonds and the concentration of cholesterol is higher [19].
This form of adaption to the environment is observed in varies types of biomembranes. *Escherichia coli* (E. coli) grown at different temperatures changes their lipid composition such that the membrane obtain a similar physical properties at their growth conditions (see Figure 2.1.3) [15]. There have also been observed different lipid composition in deep-sea bacteria grown under different pressure [20]. Even in homoeothermic animals, this adaption can be observed. Arctic animals, such as reindeers has a relative higher concentration of unsaturated lipids, than near the thigh. Even in humans such adaption to the environment is found, where chronic alcoholics have a relative higher amounts of saturated lipids and cholesterol in their red blood cells. The higher concentration compensate for the changes induced by the alcohol.

All these findings strongly indicate that the organisms is trying to obtain a biomembrane with the same physical properties relative to its environment. The state of the membrane is often just after the phase transition, where the membrane is in a fluid and soft state.

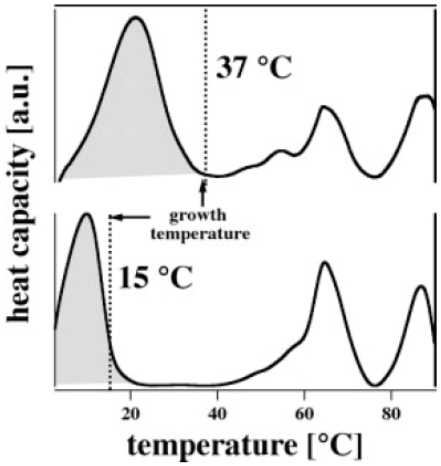

Figure 2.1.3 – Heat capacities for E.coli grown at 37 °C and 15 °C , show different lipid melting properties. The lipid melting transition is always found slightly below growth temperature. The peaks at higher temperature is protein unfolding peaks. (Taken from T. Heimburg (2007) [15]*)*

2 Cold-blooded animals, which do not obtain a constant internal temperature, e.g. frogs and fish.

2.1.3 Biomembrane Phases

Biological membranes have thermodynamic properties, and these properties can be studied in detail by using model systems prepared from pure lipids bilayers.
Lipid bilayers will in a system with a temperature decreasing over time, go from a gel phase to a fluid phase through different transition and phases. One can find similar phases in the transition from ice to water. The phases are a result of the lipid carbon chains different conformations and the crystal organisation of the head-group. The lipid chains have a trans-gauche isomerization, and can therefore be in an all-trans configuration, which results in a lower energy state than a configuration of trans-isomers and gauche-isomers mixed. Trans-gauche isomerization is a rotation around a C-C bond, where a rotation of 120° result in a different structure in the molecule.
Lipids in water will group together and form structures depending on the concentration. First micells will form. These are groups of lipids arranged in a spherical or cylindrical configuration, where the polar heads shield the hydrocarbon tails from the water. When the concentration is increased, the lipids can undergo a transition to other configuration. E.g. where the micelles are ordered in a cubic or hexagonal array, or a sponge phase. Other transition can be a unilamellar vesicle, where the lipids group together and form a bilayer. These unilamellar vesicles can be compared to bubbles, where air is both inside and outside.

A lipid bilayer containing the same spies of lipid can be found in four phases (illustrated in Figure 2.1.4):

- L_c: Crystalline, in which the lipids are ordered in three dimensions.
- L'_β: Solid-ordered, also called "gel phase", is crystalline molecular order phase, where the chains are "all-trans" and tilted.
- P'_β: Ripple-phase, where the lipids in partially solid and partially fluid in a periodic structure in the plane of the lamellae.
- L_α: Liquid-disordered phase, also called "Fluid phase", is where all lipids chains are disordered and the lateral order of lipids is random.

The transition between these phases occur at well-defined temperatures, which is depending on the chain length, chain saturation, and the head group size and charge.

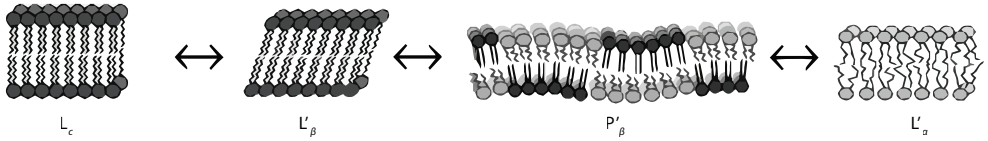

Figure 2.1.4 – The lipid membrane phases that occur in lipid membranes with increasing temperature display a decreasing order of the chains. (Originated from Heimburg [15]*)*

The focus in this thesis will be on the main lipid melting transition between L'_{β} and L_{α}, and the ripple-phase (P'_{β}-phase) will be ignored. It has been shown that the presence of various biomolecules in the membrane can result in the ripple-phase can be abolished, and the phase is rarely seen in biological membranes [21].

2.1.4 Biomembrane Phase Transition

Biomembrane undergo a transition when it transform from one phase to another, and is often referred to lipid melting. When the membrane undergo a transition, it can display a number of extraordinary properties, such as change in volume, area and compressibility.

The phase transition from a solid-ordered phase to a liquid-disordered phase hold both in protein-free and natural membranes. While the transition range over a very wide range of temperature (from -20° and up to 60°C). The phase transition of biological membranes in organisms is slightly below (on the order of 15°C) the growth temperature, see Figure 2.1.5. As previously mentioned, organisms have been found to adapt their lipid composition such that their membranes conserve their physical properties, here the phase transition. The relation between the lipid melting transition and growth conditions indicates, that for the organisms, it is an importance to have this transition for the function of biological membranes and therefore biology in general. This area, of the transition between the gel- and the fluid-phase, have been intensive researched by [22]–[24].

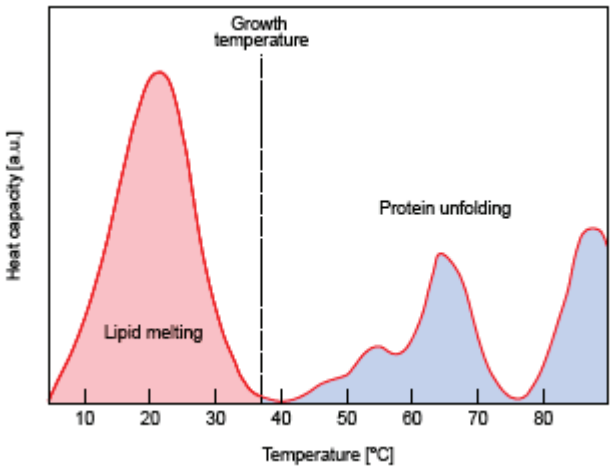

Figure 2.1.5 – Heat capacity for a intact Escherichia coli, show two regimes, the first where the lipid is melting and the second where the protein is unfolding. Notice that the growth temperature is just above the lipid transition. (Taken from T. Heimburg (2007) [15]*)*

The lipid melting transition is an exothermic transition, which happens over a narrow temperature range. The transition is driven by the entropy gain of collective melting of lipid chains. The melting transition can be measured with many methods, such as differential scanning calorimetry and various spectroscopic methods. Calorimetry has the advantage that it directly yields important thermodynamic information, such as enthalpy and entropy changes. At the lipid melting transition the calorimetry show a spike in the heat capacity. During the transition, a number of other susceptibilities likewise display spikes, such as compressibility, which have a major importance for this thesis.
In the thermodynamic description, the lipids can be found in two phases, gel- and fluid-state. This is of course an oversimplification, since it mean that both the head groups and the chains undergo a structural change at the same temperature. However, this does not imply that the membrane is well described by only two distinct states. During the transition the membrane can be found in a number of intermediate states where the two lipid states are mixed.

To describe the phase transition one have to look at the lipid melting. If one assume that a lipid, and the lipid carbon chain, can only be in one of two states, an all-trans state (gel-state) or a disordered state (fluid-state). Then will the melting point, T_m, be defined as the temperature at which the gel state and the fluid states are equally likely:

$$\frac{P_{fluid}\left(T_m\right)}{P_{gel}\left(T_m\right)} = K\left(T_m\right) = e^{-\Delta G^{\ominus}/RT_m} = 1 \tag{2.1.1}$$

Where *K(T)* is the equilibrium constant and *Van't Hoff equation* have been used, *R* the molar gas constant and *ΔG* is the difference in the Gibbs free energy. When the ground state and the excited state are equivalently, the difference in Gibbs free energy is zero:

$$\Delta G^{\ominus} = G_{fluid} - G_{gel} = \Delta H^{\ominus} - T_m \Delta S^{\ominus} = 0 \tag{2.1.2}$$

,

Where the definition of Gibbs free energy is used. *ΔH* and *ΔS* is the change in enthalpy and entropy for the transition between fluid and gel.
The melting temperature can then be said as the temperature, where the Gibbs free energy of the two states is the same. The melting temperature can be defined through the enthalpy and entropy, following from eq. (2.1.2):

$$T_m \equiv \frac{\Delta H^{\ominus}}{\Delta S^{\ominus}} \tag{2.1.3}$$

As mentioned the melting temperature for lipids depends on the structure of it. From (2.1.3) one can see that a change in enthalpy or entropy give a different melting temperature. Entropy has been found to increase linearly with the chain length in lipids. In biological membrane other things have influence on the melt-

ing temperature, such as hydrostatic pressure, pH and any other things that make a change in the difference in enthalpy and entropy between the phases.
The equilibrium constant *K(T)* define the probability that a lipid has enough thermal energy to be in a excited state. When the assumption is that the system is characterised by only two states, one can express the probability of a lipid in a membrane is in a particular state with the use of the equilibrium constant:

$$P_{fluid} = \frac{K(T)}{1+K(T)} \qquad P_{gel} = \frac{1}{1+K(T)} \tag{2.1.4}$$

P_{fluid} and P_{gel} can also be seeing as the fraction of the membrane there is in the fluid-state and in the gel-state at a given temperature. Lipids melting in a vesicle is shown in Figure 2.1.6. The mean enthalpy change per mole of lipid is therefore given by

$$\langle \Delta H(T) \rangle = \Delta H^{\ominus} \frac{K(T)}{1+K(T)}. \tag{2.1.5}$$

For $\Delta H = 35\ kJ/mol$ one obtains that the transition between gel and fluid happens over a temperature range of *100 °C*. This is not in agreement with experimental data, where the transition can happen in a range of less than *1 °C*. The explanation for this disagreement is that lipid melting is a cooperative phenomenon.

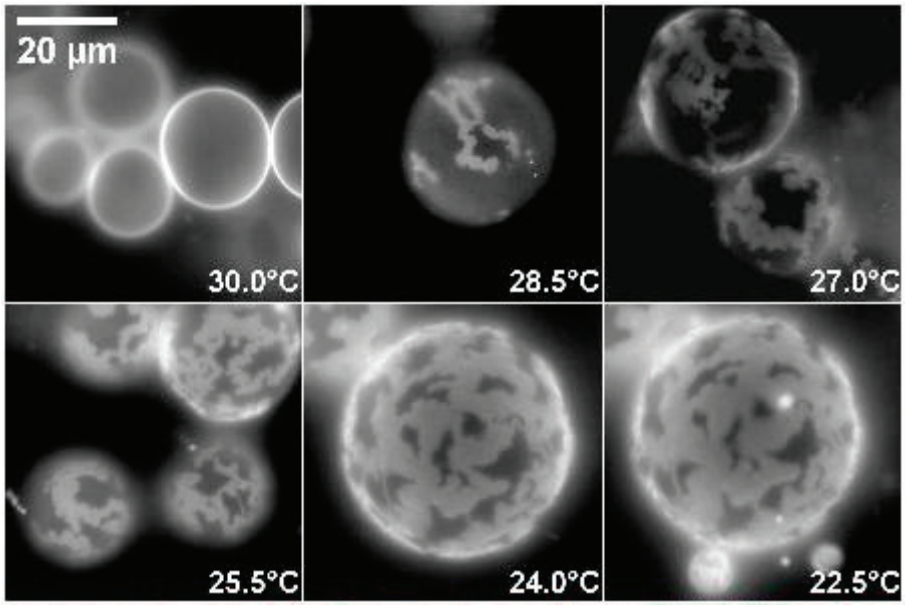

Figure 2.1.6 – Lipid vesicle at different temperature show that the lipids melt in cluster. Dark area is lipids in fluid state and light is gel solid state. (Taken from C. Leirer (2008) [69])

2.1.4.1 Cooperativity

In the phase transition, the membrane can be found in a number of intermediate states; where the two lipid states are mixed. These states with mixed lipid states are a result of a cooperation between the lipids. This means that lipid do not melt independently from each other but rather form macroscopic domains that melts in a cooperative way [15]. The extent of the cooperativity is reflected in the width of the transition, which varies from more than 30 K for biological membranes to 0.1 K for multilamella vesicles.
The cooperativity between the lipids under the melting transition results in a topography, where the membrane is dominated by the formation of domains of various sizes and compositions. These domains are more compact, the larger the coopeartivity is at the melting point, as the system will seek to minimize the length of the domain boundaries, which is energetically unfavourable.

Under the assumption that lipids do not melt independently of each other, but rather in clusters of n lipids. One have to consider these lipids as a part of a cooperative unit, with size n, and the enthalpy and entropy will for such a system be $n\Delta H$ and nΔS. The Gibbs free energy is then expressed as $n\Delta G$, and the equilibrium constant can be expressed as:

$$K(T) = \exp\left(-\frac{n\Delta G^{\ominus}}{RT}\right) = \exp\left(-\frac{n\Delta H^{\ominus} - T\Delta S^{\ominus}}{RT}\right) = \exp\left(-\frac{n\Delta H^{\ominus}}{R}\left(\frac{1}{T} - \frac{1}{T_m}\right)\right), \quad (2.1.6)$$

where the equilibrium constant is a function given by enthalpy and the entropy or melting temperature, which can be determinate experimental, e.g. from a heat capacity profile. Figure 2.1.7 shows the results of the calculation for the fraction of lipid in the excited state.

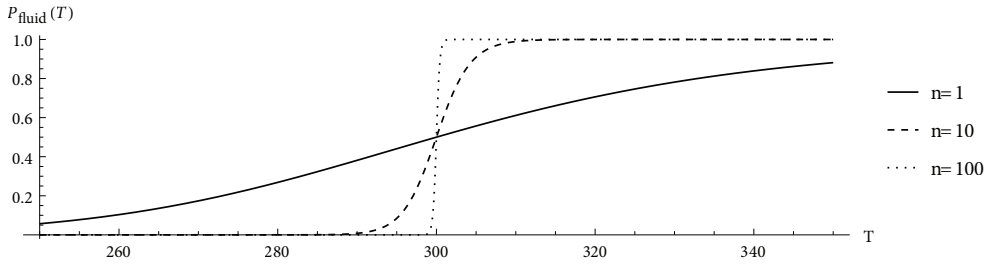

Figure 2.1.7 – The fraction of melted lipids as a function of temperature for different n, cluster size.

2.1.4.2 Susceptibilities and fluctuations

There is different experimental methods to make measurement on a membrane with phase transition, and the most suitable method to derive the thermodynamically properties of the membrane is calorimetry. Calorimetric measurement is defined as a method to measure the heat capacity of a sample as a function of temperature. Heat capacity is defined as the amount of heat added to a substance of a certain amount to change the temperature. Phase transitions are characterised by a peak in the heat capacity, since the heat required to change the state of the

substance is maximum during the transition. At constant pressure, thermodynamically it is defined as:

$$c_P = \left(\frac{dQ}{dT} \right)_P \tag{2.1.7}$$

Enthalpy is defines as $H \equiv U + PV$, where U is the internal energy, P the pressure and V the volume. The differential become:

$$dH = dU + PdV + VdP = dQ + VdP \,, \tag{2.1.8}$$

where $dQ = dU - PdV$ have been used. At constant pressure (2.1.8) will take the form:

$$c_P = \left(\frac{dH}{dT} \right)_P \tag{2.1.9}$$

Since $dQ = TdS$, the heat capacity at constant pressure is also given by:

$$c_P = T\left(\frac{dS}{dT} \right)_P \tag{2.1.10}$$

From this follows that the change in enthalpy and entropy from the gel-phase to fluid-phase can be calculated from the heat capacity:

$$\Delta H^{\ominus} = \int_{T_{gel}}^{T_{fluid}} c_P dT \qquad \Delta S^{\ominus} = \int_{T_{gel}}^{T_{fluid}} \frac{c_P}{T} dT \tag{2.1.11}$$

The boundary temperatures, T_{gel} and T_{fluid}, is the temperature before and after the phase transition. The change in enthalpy and entropy in the range before and after the transition can be neglected.

Normally one cannot directly measure the enthalpies of the individual states, but rather the thermodynamics averages over all states. When a system is in thermal equilibrium, it is in a state around the most likely state. This is because of the fluctuations there is in a thermodynamic system. Each states is weighted by its Boltzmann probability

$$P_i = \frac{\exp\left(-H_i / kT\right)}{\sum_i \exp\left(-H_i / kT\right)} \,, \tag{2.1.12}$$

where the numerator is the Boltzmann distribution and the denominator is the sum over all states. One can then obtain for the mean enthalpy:

$$\langle H \rangle = \sum H_i P_i = \frac{\sum H_i \exp\left(H_i / kT \right)}{\sum \exp\left(H / kT \right)}, \tag{2.1.13}$$

where $\langle \cdot \rangle$ denotes the statistical mean. Similar, calculation can be made for every observable, *X*, e.g. specific volume or the area:

$$\langle \mathrm{X} \rangle = \sum_i \mathrm{X}_i P_i \tag{2.1.14}$$

In an experiment with a high concentration of lipid, e.g. 10 mM, one will have a large amount of unilamellar lipid vesicles, 10^{13} vesicles/cm^3. Which will be in a macroscopic scale. Each vesicles will display a fixed enthalpy at a given moment. The average enthalpy is given by (2.1.13), and therefore one can show that the heat capacity is given by

$$c_P = \frac{d\langle H \rangle}{dT} = \frac{\langle H^2 \rangle - \langle H \rangle^2}{RT^2}, \tag{2.1.15}$$

where the *fluctuation theorem* have been used, and one can show that the heat capacity is proportional with the fluctuation.
Similar relations hold between all the other susceptibilities of the system and magnitude of the fluctuation of the related extensive variable. Susceptibilities are defined as the derivative of an extensive variable with respect to an intensive variable. The susceptibilities of a system are closely related to the fluctuations of the extensive variable, which can be seen considering the isothermal volume compressibility, κ_T^V, and the isothermal area compressibility, κ_T^A:

$$\kappa_T^V = -\frac{1}{\langle V \rangle} \cdot \left. \frac{d\langle V \rangle}{dP} \right|_T = \frac{1}{\langle V \rangle} \cdot \frac{\langle V^2 \rangle - \langle V \rangle^2}{RT} \tag{2.1.16}$$

$$\kappa_T^A = -\frac{1}{\langle A \rangle} \cdot \left. \frac{d\langle A \rangle}{d\Pi} \right|_T = \frac{1}{\langle A \rangle} \cdot \frac{\langle A^2 \rangle - \langle A \rangle^2}{RT} \tag{2.1.17}$$

This means that the isothermal area and volume compressibilities are proportional to the fluctuation in area and volume, respectively.
The heat capacity can be dissected into two part; an intrinsic, $c_{P,0}$, and an excess heat capacity, Δc_P, derived from the enthalpy. Let $H_0(T)$ be the intrinsic heat of the membrane lipids and $\Delta H_0(T)$ be the excess heat linked to the chain isomerizations. The heat capacity can then be expressed as:

$$c_P(T) = \left.\frac{dH(T)}{dT}\right|_P + \left.\frac{d\Delta H(T)}{dT}\right|_P = c_{P,0}(T) + \Delta c_P(T) \tag{2.1.18}$$

Similarly can the volume compressibility be expressed, when letting $V_0(T)$ be the intrinsic volume of the membrane lipids and $\Delta V(T)$ is the excess volume change

$$\kappa_T^V(T) = -\frac{1}{V}\left.\frac{dV_0(T)}{dP}\right|_T - \frac{1}{V}\left.\frac{d(\Delta V(T))}{dP}\right|_T = \kappa_{T,0}^V(T) + \Delta\kappa_T^V(T), \tag{2.1.19}$$

where $\kappa_{T,0}^V$ is the intrinsic volume compressibility of the lipids and $\Delta\kappa_T^V$ is the excess volume compressibility linked to the fluctuation in the membrane state. The intrinsic change is related to the volume fluctuations at the molecular level, which are unrelated to the physical state. The isothermal compressibilities are different in the gel- and fluid-phase, and therefore $\kappa_{T,0}^V$ may adopt different values below and above the transition. Normally the isothermal compressibilities are lower in the gel-phase than in the fluid-phase [25].
Similarly, for the area compressibility one obtains

$$\kappa_T^A(T) = -\frac{1}{A}\left.\frac{dA_0(T)}{d\Pi}\right|_T - \frac{1}{A}\left.\frac{d(\Delta A(T))}{d\Pi}\right|_T = \kappa_{T,0}^A(T) + \Delta\kappa_T^A(T), \tag{2.1.20}$$

where $\kappa_{T,0}^A$ as the intrinsic compressibility of a lipid membrane in a given state at temperature T, and $\Delta\kappa_T^A$ as the excess lateral compressibility, linked to the fluctuation in the membrane state.
In the absence of lateral stress or at constant bulk pressure, one obtains, with use of *Maxwell relations*, respectively for the adiabatic volume compressibility, κ_S^V, and the two-dimensional adiabatic compressibility, κ_S^A:

$$\kappa_S^V = \kappa_T^V - \frac{T}{V \cdot c_P}\left(\frac{dV}{dT}\right)_P^2, \tag{2.1.21}$$

$$\kappa_S^A = \kappa_T^A - \frac{T}{A \cdot c_\Pi}\left(\frac{dA}{dT}\right)_\Pi^2, \tag{2.1.22}$$

where c_Π is the heat capacity at constant lateral tension, equal to the bulk heat capacity, c_P.

2.1.4.3 Proportionality relations and compressibilities close to the transition

The membrane undergo in the transition significant changes in both the area and volume. This change is mainly related to the change in the lipids chains, and is showed through experimental work, that this change is proportional to the change in enthalpy. *Anthony et al.* [26] showed that the enthalpy change, ΔH, and the relative volume change, ΔV, are proportional in the lipid chains melting transition

range:

$$\left\langle \Delta V\left(T\right)\right\rangle = \gamma_V \left\langle \Delta H\left(T\right)\right\rangle \tag{2.1.23}$$

This relation was also found to be true in lipid mixture over a wide temperature range, and in lipid membranes and biological membranes [27]. Further has it been shown by molecular dynamics simulation that this proportionality relation is valid in general [28].
Based on this proportionality relation between enthalpy and volume, *Heimburg* [29] proposed that a similar proportionality relation should hold between change in the enthalpy and change of area. It is known that the area of a lipid membrane in the transition change considerably. The postulation has been justified indirectly by lipid monolayer experiments [30], and yield:

$$\left\langle \Delta A\right\rangle = \gamma_A \left\langle \Delta H\right\rangle \tag{2.1.24}$$

This means that the change in area and volume can be linked directly to the measurable excess heat capacity, Δc_P. From eq. (2.1.23) and (2.1.24) one obtain:

$$\frac{d\left\langle \Delta V\right\rangle}{dT} = \gamma_V \frac{d\left\langle \Delta H\right\rangle}{dT} = \gamma_V c_P \tag{2.1.25}$$

$$\frac{d\left\langle \Delta A\right\rangle}{dT} = \gamma_A \frac{d\left\langle \Delta H\right\rangle}{dT} = \gamma_A c_P \tag{2.1.26}$$

It can be shown that $\Delta V_i = \gamma_V \Delta H_i$ holds for every available substrate, and this implies that:

$$\left\langle \Delta V^2\right\rangle = \gamma_V^2 \left\langle \Delta H^2\right\rangle \tag{2.1.27}$$

This can then give an expression for the excess volume compressibility

$$\Delta\kappa_T^V = -\frac{1}{\left\langle V\right\rangle}\frac{d\left\langle \Delta V\right\rangle}{dp} = \frac{\left\langle \Delta V^2\right\rangle - \left\langle \Delta V\right\rangle^2}{\left\langle V\right\rangle RT} = \frac{\gamma_V^2 T}{\left\langle V\right\rangle}\frac{\left\langle \Delta H^2\right\rangle - \left\langle \Delta H\right\rangle^2}{RT^2} = \frac{\gamma_V^2 T}{\left\langle V\right\rangle}\Delta c_P, \tag{2.1.28}$$

where eq. (2.1.15), (2.1.16) and (2.1.19) have been used.
Similarly, the isothermal lateral compressibility can be expressed:

$$\Delta\kappa_T^A = \frac{\gamma_A^2 T}{\left\langle A\right\rangle}\Delta c_P, \tag{2.1.29}$$

where eq. (2.1.17) and (2.1.20) have been used instead. This is of great interest for this thesis since it give an expression for the change in lateral compressibility as a function of measurable variables.

2.1.5 Lipid Mixture

Biological membranes consist of many different lipids. The melting transition of a biological membrane is complex, since the biological membrane show melting reactions slightly below body temperature with a broad transition half-width. And the various lipids in the membrane have all different melting temperatures and different melting enthalpies. The lipid species in mixtures are not likely to melt independently, because of the cooperativity.

To get an understanding of a system with two lipid species, one can consider the case where the free energy of the interaction between all lipids in a state are the same. This means that the free energy is not changing, when one exchange the lipids within the gel phase or the fluid phase. The lipids will then randomly distribute in each of the lipid states. This is called "ideal mixing".
In this system it only make sense to see what happens between the two lipid species, A and B, melting temperatures, since the system either will be fully in the gel- or fluid-phase outside the melting temperatures. For such a system, where species A have the melting temperature $T_{m,A}$ and melting enthalpy ΔH_A, and species B have the melting temperature $T_{m,B}$ and melting enthalpy ΔH_B, it obey:

$$x^f = \frac{x_B^g - x_B}{x_B^g - x_B^f} \qquad \text{and} \qquad x^g = 1 - x^f \tag{2.1.30}$$

Where the equation to the left is the fraction of the lipid in the fluid-state. The equation to the right is the *lever rule*. $x^f{}_B$ and $x^g{}_B$ is the mole fraction of species B in the fluid- and gel-state respectively. x_B is the fraction of species B in the system. Similar, exist $x^f{}_A$ and $x^g{}_A$ as the mole fraction of species A in the two phases. For all fractions $0 \leq x_A^g, x_A^f, x_B^g, x_B^f \leq 1$ has to be fulfilled. The fractions are found by the equilibrium constant for each of the species, and that it must follow that the sum of the mole fraction of A and B must be one in the gel- and fluid-state. For the derivation see *Lee* (1977) [31].
From (2.1.30) one can also write:

$$\frac{x^f}{x^g} = \frac{x_B^g - x_B}{x_B - x_B^f} \tag{2.1.31}$$

The *lever rule* allows one to calculate the fractions of lipids in the gel- and fluid-state as a function of the fraction of component B and the temperature. One can then make a phase diagram, which tells at what temperature the system of varying x_B will be in the gel- or fluid-phase, or in a mixture of gel and fluid. A phase diagram for a system with two species with $\Delta H_A = \Delta H_B = 24$ *kJ/mol*, $T_{m,A} = 270$ *K*, $T_{m,B} = 314$ *K* is presented in Figure 2.1.8. In the figure one can see that the lipids melt after the melting temperature for species A, and all the lipids are melted before the system reach species B melting temperature.
One can also calculate the enthalpy and the heat capacity as a function of temperature:

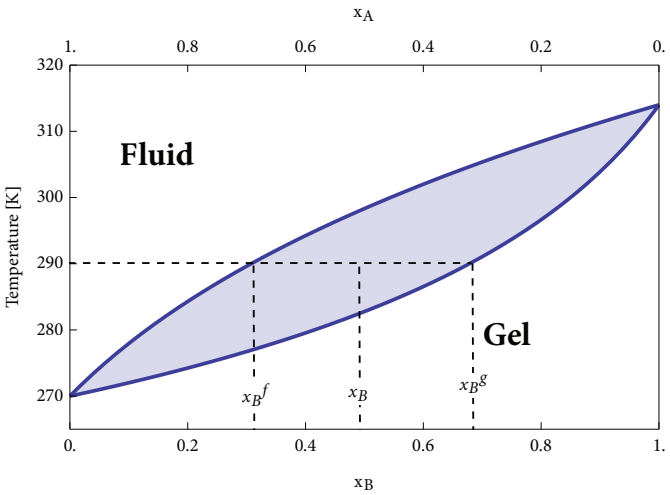

Figure 2.1.8 – The relative amounts and the compositions of gel phase and fluid phase for given x_B and temperature can be obtained from using the lever rule. The diagram was calculated for $\Delta H_A = \Delta H_B =$ 24kJ/mol, $T_{m,A}$=270 K, $T_{m,B}$=314 K.

$$\Delta H(T) = \frac{x_B^g - x_B}{x_B^g - x_B^f} \cdot \left(x_B^f \cdot \Delta H_B + \left(1 - x_B^f\right) \cdot \Delta H_A \right) . \qquad (2.1.32)$$

The heat capacity is given by $c_P = d\Delta H / dT$. For $x_B = 0.5$ and with the same system as mention above, one get the enthalpy and heat capacity as shown in Figure 2.1.9. The sharp peaks at the upper and lower temperature limits of the heat capacity are due to the assumption that the pure components display an infinitely sharp transition.

In general a mixture between two components is not ideal, and the interaction between two molecules of species A and B cannot be ignored. The lipids may also diffuse, resulting in a change in the free energy. In Figure 2.1.9 the heat capacity has sharp peaks, this sharpness is not found in experiments because the mixture is not infinitely cooperative, where the peaks are smoother. Experimental heat capacity profiles and phase diagrams is shown in Figure 2.1.10 with smoother peaks at the transitions.

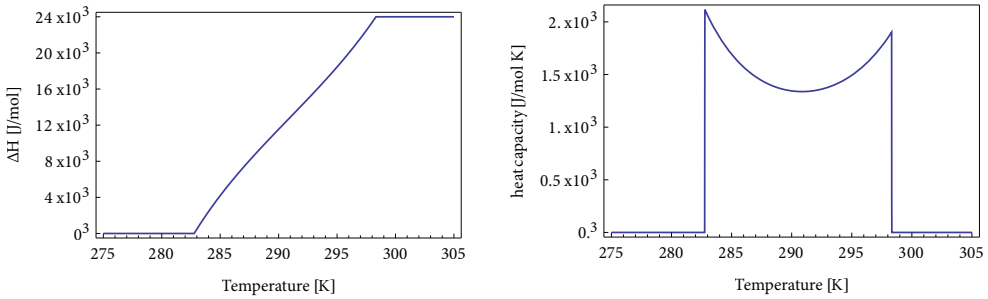

Figure 2.1.9 Enthalpy and heat capacity as a function of temperature calculated for $X_B = 0.5$ with $\Delta H_A = \Delta H_B =$ 24kJ/mol, $T_{m,A}$=270 K and $T_{m,B}$=314 K.

To model a real mixture one can use Monte Carlo simulation, where in a two-component membrane one have two melting enthalpies, ΔH_A and ΔH_B, and entropies, ΔS_A and ΔS_B. Furthermore, there are six nearest neighbour interaction parameters: between gel and fluid lipids of species A, between gel and fluid lipids of species B, between fluid lipids of species A and B, and between gel lipids of species A and B. Totally six parameters. The Gibbs free energy of each configuration of such a system is given by:

$$\begin{aligned}\Delta G = {} & N_{f_A}\left(\Delta H_A - T\Delta S_A\right) + N_{f_B}\left(\Delta H_B - T\Delta S_B\right) \\ & + N_{g_A,f_A}\omega_{g_A,f_A} + N_{g_B,f_B}\omega_{g_B,f_B} + N_{g_A,g_B}\omega_{g_A,g_B} \\ & + N_{f_A,f_B}\omega_{f_A,f_B} + N_{g_A,f_B}\omega_{g_A,f_B} + N_{f_A,g_B}\omega_{f_A,g_B}\end{aligned} \tag{2.1.33}$$

Where N_{fA} and N_{fB} are the numbers of lipid of species A and B in a fluid state. The $N_{gA,fB}$ is the number of interactions between lipid species A in the gel state and the lipid species B in the fluid state. The simulation may also take into account that the lipids will diffuse in the mixture [32]–[35].

Throughout this thesis the *phase transition* will be referred to the main transition, and be the point at the maxima at a heat capacity profile. In lipid mixture there will be referred to two *phase transition*, even though there only is one. Each *phase transition* correspondent to the maxima at the two peaks in a heat capacity profile, if two peaks present.

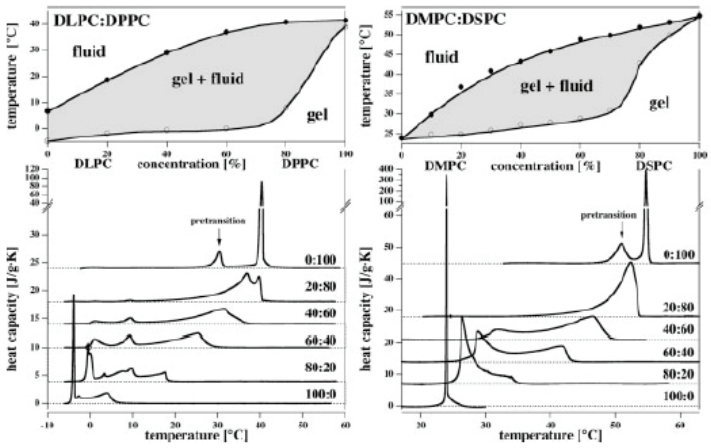

Figure 2.1.10 - Phase diagram of DLPC-DPPC mixtures (left) and DMPC-DSPC (right). The solidus line (transition from gel to gel-fluid-line) has a smaller slope than the liquids line indicating that the interaction between gel- and the coexistent-phase is smaller than the interaction between the fluid- and the coexistent-phase. The bottom panels show the heat capacity profiles. (Taken from T. Heimburg (2007) [35]).

2.2 Theories of Nerve signal

Through the years of the western civilisation, humankind has philosophized over humans, and thereby animals, ability to control its limbs and sensation. Ancient medical practitioners did understand that nerves served two functions, but how it operated and under the direction of which principal organ, was the mystery. The word *"nerve"* originate from Greek and mean tendon or sinew. Through time, it has been difficult to categorize the nerve system, where it had been a common confusion to distinguish between connective tissues and other more subtle types of physical connections within the body. Tendon and sinew can be categorize as fibrous which bind the muscle to the bones.

The Greek philosopher *Aristotle* (384 BC – 322 BC) believed that the nerves were controlled by and originated in the heart. Six centuries later *Galen* (129 AD – circa 217), a Roman physician, concluded that the brain was there nerves emanating. He imagined that the nerves to be hollow tubes, which allow the animal spiritus to roam, and control the limbs.

In many centuries after, the concept and understanding of nerves did not change, and the mystery of how the head communicated with the body, was still a mystery. Even though new findings, it did not change this ancient view of the nervous system. *Leonardo da Vinci* (1452 -1519) made drawings of nervous system. The first drawings of the brain was with three cavities behind the eyes, believed to be the house of the spirit. Later, after *Leonardo da Vinci* had dissected brains on his own, he made new drawings without the cavities and much more specific drawings.

Santiago Ramón y Cajal, designated by many as the father of modern neuroscience, discovered that the nervous system consist of millions of cells, called neurons. He also discovered that the nerve signal only travels one way. *Santiago* was awarded the *Nobel Prize in Physiology or Medicine* in 1906. In the late 19th century *Emil du Bois-Reymond*, *Johannes Peter Müller*, and *Herman von Helmholtz* showed neurons were electrically excitable and that their activity predictably affected the electrical state of adjacent neurons.

In 1952 *Alan Lloyd Hodgkin* and *Andrew Huxley* [3] presented a mathematical model for the initiation and propagation of nerve pulses. The model was originally only intended as an empirical description of the experiments by *Kenneth S. Cole and Howard J. Curtis* [36]. *Cole* and *Curtis* found transient voltage change of a nerve signal in giant squid axons. The nerve signal was called *action potential*. However, this was in the description not meant to be a universal description of the nerve signal, but gained quickly widespread acceptance as the nerve signal theory. They were awarded with *the Nobel Prize in Physiology or Medicine* in 1963.

The neuron, the nerve cell, differ not much from other cells, they have nucleus, mitochondria, cell membrane et cetera. However, they differ from ordinary cell in its geometry. The nerve cell is a cell who directly communicates with others. Meaning that the signal from other neurons is received by the dendrites, travel along the axon and communicated out of the neuron to other via the axon terminal.

The axon can span from nanometres to meters. Geometrically the axon can be forked, but a single cylindric geometry is commonly assumed for simplification. The longest neuron in the human body is the *sciatic nerve*. It begins in the lower back and runs down to the toes. Axon can be supported by number of tissues surrounding it. Special interest is the myelin sheaths, which are formed by *Schwann*

cells. Between the myelin sheaths, exist myelin sheath gap or *node of Ranvier*. Myelinated neurons have been found to transmit signals with a velocity of order *100 m/s* and non-myelinated neuron in the order of *1-5 m/s* [15]. Recently, it just has been showed, what has been accepted for years, that the distance between the myelin sheath gaps have an influence on the propagation velocity. The longer between the gaps the faster the signal can travel, meaning that the more the axon is myelinated the faster the nerve signal will be [37]. With the velocity and the duration of the nerve signal, one can calculated the range and size to be in the scale of millimetres and centimetres, marking nerve signal a macroscopic phenomenon.

2.2.1 Hodgkin & Huxley Model

In a typical nerve, the ion concentration of sodium and potassium is very different inside and outside. One finds a higher concentration of potassium inside than outside. Moreover, for sodium it is just reversed. These concentration differences give rise to a voltage difference over the nerve membrane. *Hodgkin* and *Huxley* assumed that the cell membrane, in a giant squid axon, acts like a barrier with ion channels [3]. Ion channels are trans-membrane proteins that open and close in a complex time- and voltage-dependent manner and allow for selective conduction of different ions. In *the Hodgkin-Huxley model* (*HH-model*), the membrane is considered impermeable to ions and is assumed equivalent to function as a capacitor with constant capacitance. The protein channels can be assumed resistors of variable conductance, with the ionic currents (I_K, potassium, I_{Na}, sodium and I_l, leak current), where the current flowing through the membrane is the sum of the ionic and capacitive contributions.

The idea of nerve pulse propagation is that a local depolarization will lower the potential difference over the membrane causing a local flux of ions through the channels. This will result in further depolarization of the membrane, which in turn will cause additional channels to conduct ions. This depolarization create a cascade effect through the nerve, where the nerve signal is propagating. However, the equivalent circuit seem quite simple and straightforward. The detailed dynamics of the ion channels is rather complicated. The ion channels have a complex time and voltage dependence, which have to be empirically fitted for any system.

Hodgkin and *Huxley* proposed the following differential equation for describing the propagation of the voltage pulse in a giant squid axon:

$$\frac{a}{R}\frac{\partial U}{\partial} = C_m \frac{\partial U}{\partial t} + g_K\left(U - E_K\right) + g_{Na}\left(U - E_{Na}\right) + g_l\left(U - E_l\right) \qquad (2.2.1)$$

The voltage, U, is a function of space and time. R_i is the specific intracellular resistivity and a is the radius of the axon, which is assumed to be a perfect cylinder. C_m is the capacitance of the membrane. E_K and E_{Na} are the respective resting potentials associated to potassium and sodium. E_l being the leak potential. g_K and g_{Na} are conductance of potassium and sodium, and g_l is the leak conductance. All being functions of voltage and time.

With this model *Hodgkin* and *Huxley* could be able to describe action potentials in a giant squid axon. However, they were quite careful in their original paper from

1952 to make this model as a generalization. The empirical aspect of their model makes its application to any other systems hard to calculate, because many of the parameters cannot be measured in experiments directly.
The Hodgkin-Huxley model assume that the membrane is a constant structure with no drastic changes in geometry or any other physical property. This assumption is in conflict with the dynamic nature of biological membrane. Experimental findings indicates occurrence of a phase transition during the nerve pulse, which cause, as mention before, a drastic changes in the membrane [38], [39]. *Tasaki et al.* showed that the nerve pulse could still propagate without monovalent cations (e.g. Na, K) in the exterior solution. Therefore, the role of ion channels can be questioned, and this observation has been attributed to secondary selectivity of the ion channels.

2.2.2 Thermodynamics of the Nerve Pulse

The Hodgkin-Huxley model is based on equivalent circuits and on *Kirchhoff's laws*, and the model is based on electrophysiology, the discipline of measuring voltage, current, and capacitance changes across biological membranes. The model is not a thermodynamically model, since it does not explicitly contain temperature, entropy, pressure, etc. Not many thermodynamic properties of the nerve pulse have been researched, but some have, such as temperature change, thickness changes of the membrane, and forces in the membrane. None of them is described directly by *the Hodgkin-Huxley model*, and some of them are in conflict with the model.

2.2.2.1 Heat Changes during the Action Potential

It has been found that during the action potential, the temperature of the nerve increases during the first phase, and decreases back. The heat release is entirely reabsorbed in the second phase of the signal [40], shown in Figure 2.2.1. This found has been confirmed in great detail for nerves originating from a number of different myelinated nerves [41] and non-myelinated nerves [42], [43]. Abbott *et al.* also found that the heat release is most likely proportional to the area of the nerve membrane. This indicate that a physical process related to the membrane generates the heat [40]. For myelinated nerves, *Abbott et al.* also found that the heat release occurs along the whole nerve, rather than just in the *nodes of Ranvier*. From all this they concluded that the whole nerve is active through the nerve signal and not just in the nonisolated segments.
A reversible heat change means that the action potential is isentropic (or adiabatic, and that the entropy is conserved since $dQ = TdS$). Isentropic processes is reversible, therefore must the action potential be reversible. However, this is not described in *the Hodgkin-Huxley model*, which is not reversible. In the equivalent circuit terminology, the ion channels is viewed as resistors. When a current is running through a resistors it release heat, independent of the currents direction. In *the Hodgkin-Huxley model*, ions flow through the ion channels, making the current, and produce the action potential, and thereby generating the heat during the action potential. No processes in the model describe reabsorption of the heat released. Moreover, since the model is based on equilibration of ion gradients, the entropy of the system is increasing.

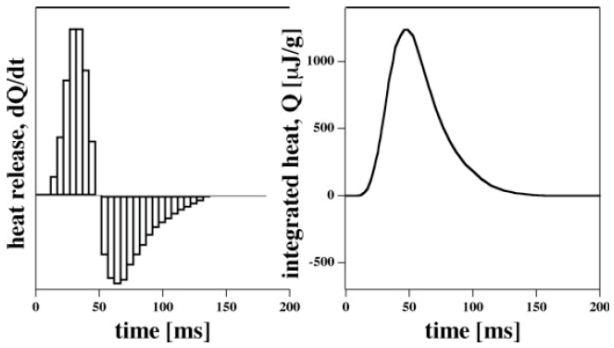

Figure 2.2.1 – Heat release in garfish olfactory nerve. Left: During the nerve signal one find that the heat release and absorbing is similar to the action potential. Right: The total heat release within error is zero, calculated by integrated the heat release. (Taken from T. Heimburg [15]*)*

2.2.2.2 Mechanical Changes during the Action Potential

During the action potential other recordings have been made. It was found that a dislocation of the membrane surface could be observed (Figure 2.2.2, right) which is strictly coupled to the potential changes of the surface. It was also found that one can measure force on a piston which is in contact with the nerve (Figure 2.2.2, left) [44]. In other words, will the internal pressure in the axon membrane change during the nerve signal.

These found and others (changes in fluorescence intensity and anisotropy in the membrane) were taken as evidence for the occurrence of a phase transition during the nerve signal [38], [39]. As mention in section 2.1.4, one will expect, when changing the lipid state from fluid to gel: heat release, increase in membrane thickness, and reduction of area. The revers, changing the lipid state from gel to fluid, one will expect the opposite.

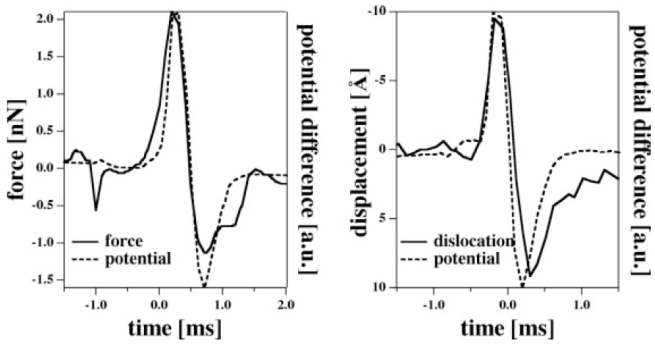

Figure 2.2.2 – Mechanical changes during the action potential. Left: Force on a piston during the action potential in a squid axon. The solid line represent the force, and the dotted the voltage potential. Right: Solid line represent the displacement (thickness of the membrane) and the dotted the voltage potential. (Taken from T. Heimburg [15]*)*

2.3 The Soliton Model

All these founds, mentioned in last section - the adiabatic nature of the nerve signal and the mechanical changes have many similarities with a sound wave. This lead in 2005 to the proposal of *the Soliton Model* by *Thomas Heimburg* and *Andrew D. Jackson* [2], which this thesis will investigate further.

Solitons are localized wave packet that propagate without attenuation and without changes in shape. One can say that a soliton is a particle-like solitary wave state, and are known from area of physics such as plasmas, fluid, mechanics, lasers, optics, solid-state physics, and elementary-particle physics. Solitary waves and solitons are not exactly the same, but throughout this thesis solitary waves will be mentioned as solitons.

For the existence of solitary waves, the medium has to display nonlinear elastic constants upon density changes, and dispersion. In other words, the medium must have a speed of sound, which has to be a nonlinear function of density, and the compressibility must be frequency dependent.

Biological membranes show these properties near its phase transition, and as mention, this phase transition is just below the body or grown temperature. When lowering the body temperature one moves the physical state of the membrane through the phase transition, and the lipids will be in the gel-state. During this transition, the lateral area of the membrane decreases by about 25 %. One could also increase the lateral pressure instead of lowering the temperature to move the membrane through its phase transition. As mention in section 2.1.4 during the phase transition the lateral compressibility increases. This means that the lateral compressibility can also be expressed as a function of lateral area or density, instead as a function of the temperature. One can see the membrane as a spring that becomes softer when compressed, until at a point where it becomes rigid. When membranes under physiological conditions are compressed and is moved towards the phase transition it becomes softer. After the phase transition, it become more rigid. These properties is characterize by nonlinear elastic constants. Furthermore, it has been found experimentally that the adiabatic compressibility is frequency depend [45]. When the biological membrane both display nonlinear elastic constants and dispersion, solitary waves can propagate.

The Soliton Model is based on the equation of sound. By assuming the nerve axon is an infinitely long homogeneous cylinder, the 3-dimensional geometry problem of the nerve axon is degenerate into a 1-dimensional problem. In the absence of dispersion, sound propagation is governed by the equation

$$\frac{\partial^2}{\partial \tau^2}\Delta\rho^A = \frac{\partial}{\partial z}\left(c^2 \frac{\partial}{\partial z}\Delta\rho^A \right), \tag{2.3.1}$$

where $\Delta\rho^A = \rho^A - \rho_0^A$ is a function of z and τ, and $c = 1/\sqrt{\rho^A \kappa_S^A}$ is the lateral sound velocity in the membrane also referred to as the phase velocity. This equation originates from the *Euler equation* in fluid hydrodynamics. As illustrated in Figure 2.3.1, the phase velocity is a non-linear function of density around the phase transition. One can thus expand the phase velocity as a function of the density change:

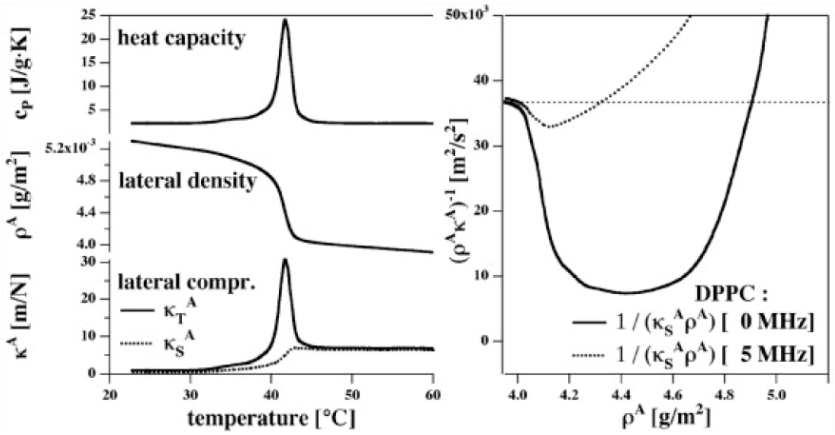

Figure 2.3.1 – Left: Heat capacity of DPPC LUV (top), the lateral area density, ρ^A (middle), and the corresponding isothermal area compressibility for low frequency case (bottom, solid curve) and adiabatic area compressibility for a 5 MHz ultrasonic case (bottom, dotted curve). Right: The lateral sound velocity for the low frequency and the 5MHz case, as a function of membrane area density at T = 45 °C. (Figure has been adopted from Heimburg and Jackson (2005) [2]*.)*

$$c^2 = \frac{1}{\rho^A \kappa_T^A} = c_0^2 + p \cdot \Delta\rho^A + q \cdot \left(\Delta\rho^A\right)^2 + \cdots \,, \tag{2.3.2}$$

where ρ_0^A is the equilibrium lateral density. *Heimburg* and *Jackson* neglected higher orders than quadratic terms, and obtained the values for p and q by fitting the experimental values of c^2. They obtain, for the DPPC LUV case $c_0 = 176.6$ *m/s*, $p = -16.6\ c_0^2/\rho_0^A$, $q = 79.5\ c_0^2/(\rho_0^A)^2$ and $\rho_0^A = 4.035\times10^{-3}$ *g/m²*, assuming a bulk temperature above the melting temperature of $T = 45$ °C.
Frequency dependence of the phase velocity below kHz region is experimentally difficult to probe. Therefore, *Heimburg* and *Jackson* assumed that the dispersion term took the simplest possible form, resulting in the final formulation of the model:

$$\frac{\partial^2}{\partial\tau^2}\Delta\rho^A = \frac{\partial}{\partial z}\left(\left(c_0^2 + p\cdot\Delta\rho^A + q\cdot\left(\Delta\rho^A\right)^2\right)\frac{\partial}{\partial z}\Delta\rho^A\right) - h\frac{\partial^4}{\partial z^4}\Delta\rho^A \tag{2.3.3}$$

where $h > 0$ is the dispersion constant. The dispersion constant is independent of the density, and have only the effect of setting the linear scale of the soliton. They define $h = 2\ m^4/s^2$ to produce pulses of few centimetres width as found in some nerves. Eq. (2.3.3) can be recognized as a generalization of the *Boussinesq equation*, and it is known to have exponentially localized soliton-like solutions that propagate without distortion for a finite range of sub-sonic velocities.
For periodic low-amplitude solutions of the form $\Delta\rho^A = \rho_0^A \sin\left(\omega\tau - kz\right)$, where $k = \omega/v$, and v the velocity of the waves and ω angular frequency. Inserting this in eq. (2.3.3), with the assumption that $c = c_0$ for the high frequency case, one obtain the dispersion relation:

$$v^2 = \frac{\omega^2}{k^2} = c_0^2 + hk^2 \approx c_0^2 + \frac{h\omega^2}{c_0^2} \tag{2.3.4}$$

Last term has use the approximation $v \approx c_0$. The dispersion relation show that the sound velocity thus increase with increasing frequency, as required by the experimental observation of decreasing compressibility with increasing frequency (see Figure 2.3.1, left, bottom, where the *5 MHz* case show less lateral compressibility than the *0 MHz* case).
One can choose to work with the dimensionless variables *u, x* and *t* defined as:

$$u = \frac{\Delta\rho^A}{\rho_0^A}, \quad x = \frac{c_0}{\sqrt{h}} z, \quad t = \frac{c_0^2}{\sqrt{h}} \tau, \quad B_1 = \frac{\rho_0}{c_0^2} p, \quad B_2 = \frac{\rho_0^2}{c_0^2} q, \quad \beta = \frac{v}{c_0}. \tag{2.3.5}$$

With this choice of variables, eq. (2.3.5) takes the form

$$\frac{\partial^2 u}{\partial t^2} = \frac{\partial}{\partial x}\left(B(u) \frac{\partial u}{\partial x} \right) - \frac{\partial^4 u}{\partial x^4}, \tag{2.3.6}$$

with

$$B(u) = 1 + B_1 u + B_2 u^2. \tag{2.3.7}$$

For the case with DPPC LUV (shown in Figure 2.3.1) and other cases one require that $B_1 < 0$ and $B_2 > 0$.
Assuming that the general solution propagates without distortion, one can set *u* as a function of $\xi = x - \beta t$ and rewrite eq. (2.3.6) as:

$$\beta^2 \frac{\partial^2 u}{\partial \xi^2} = \frac{\partial}{\partial \xi}\left(B(u) \frac{\partial u}{\partial \xi} \right) - \frac{\partial^4 u}{\partial \xi^4} \tag{2.3.8}$$

With the assumption that *u* is localized and vanishes for $|\xi| \to \infty$, one can integrate eq. (2.3.8) twice to yield:

$$\frac{\partial^2 u}{\partial \xi^2} = (1 - \beta^2) u^2 + \frac{1}{2} B_1 u^3 + \frac{1}{3} B_2 u^4 \tag{2.3.9}$$

For a localize solutions it is requires that $|\beta| < 1$, since it vanish far away:

$$u \sim \exp\left(-\sqrt{1 - \beta^2}\, |\xi| \right) \quad \text{for} \quad |\xi| \to \infty \tag{2.3.10}$$

Eq. (2.3.9) can be multiplied on both sides by $\partial u / \partial \xi$ and integrate once more to yield:

$$\left(\frac{\partial u}{\partial \xi}\right)^2 = \left(1-\beta^2\right)u^2 + \frac{1}{3}B_1 u^3 + \frac{1}{6}B_2 u^4 \tag{2.3.11}$$

From the equation, one can see that the soliton profile must have a maximum, and it must be symmetric about this maximum, when it have to be localize and vanish far from it. This relation is only possible when:

$$1 > |\beta| > \beta_0 = \sqrt{1-\frac{B_1^2}{6B_2}} \tag{2.3.12}$$

Where β_0 is the minimum velocity corresponds to the maximum amplitude solitons. From *Heimburg* and *Jackson* [2] this value is about *100 m/s* and should correspond to the velocity of the nerve signal above threshold excitation.
Eq. (2.3.11) can be solved numerical as done by *Heimburg* and *Jackson* [2], or analytic done by *Lautrup et al.* [46].
The analytic solution to eq. (2.3.11) can be found when one expect localized solutions for $\beta_0 < |\beta| < 1$. When this condition is met, the right side of the eq. (2.3.11) will have two real roots, $u = a_\pm$, with:

$$a_\pm = -\frac{B_1}{B_2}\left(1 \pm \sqrt{\frac{\beta^2-\beta_0^2}{1-\beta_0^2}}\right) \tag{2.3.13}$$

Where the relation in eq. (2.3.12) have been used. The solution will then have the analytic form:

$$u(\xi) = \frac{2a_+a_-}{\left(a_+ + a_-\right) + \left(a_+ - a_-\right)\cosh\left(\xi \cdot \sqrt{1-\beta^2}\right)} \tag{2.3.14}$$

Solutions for different velocities is shown in Figure 2.3.2.
Vargas et al. [47], in their work on periodic solution to eq. (2.3.6) introduce a mechanical analogy to understand the equation. The equation could be transform to a form similar to the equation of motion $\frac{1}{2}mv^2 + V(x) = const$. From the two integration of eq. (2.3.6) to eq. (2.3.8) they introduce two integration constant, the first one disappears for reasons of symmetry. From this they multiply with $\partial u/\partial \xi$ and integrate once more (same method as in eq. (2.3.11)) to yield:

$$\left(\frac{\partial u}{\partial \xi}\right)^2 = \left(1-\beta^2\right)u^2 + \frac{1}{3}B_1 u^3 + \frac{1}{6}B_2 u^4 + C \cdot u + V_0 \tag{2.3.15}$$

Where *C* will depend on experimental constraints and V_0 is an integration constant with no influence on the solutions. There is only one term there is proportional to the derivative of *u*, which can be seen as a "*kinetic term*" and the second

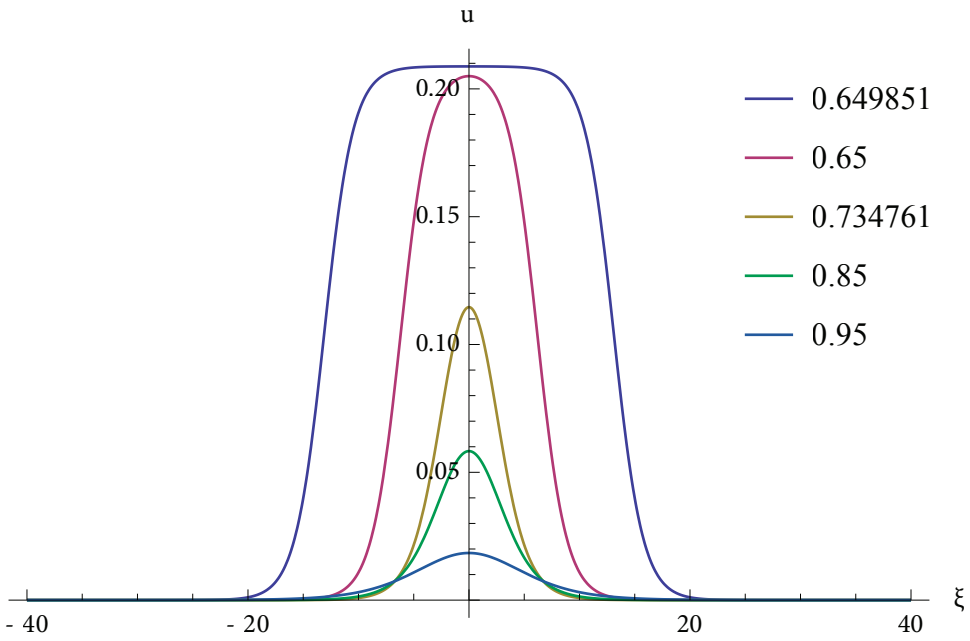

Figure 2.3.2 – Soltion profiles for the velocities, 0.649850817, 0.65, 0.734761, 0.85 and 0.95. The maximum height diminishes as a function of β.

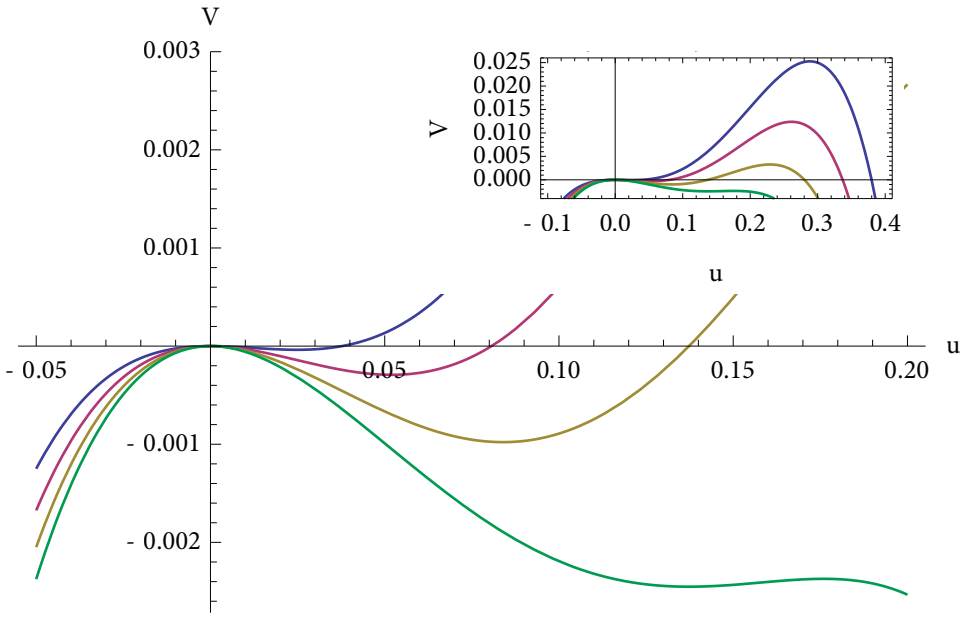

Figure 2.3.3 – The potential V(u) for four different velocities. The soliton correspond to a movement in the potential, with start in 0. If the potential do not reach 0 again, the movement will continue down the potential, and therefore there will be no solution with a velocity of 0.6. The insert show the potentials in a larger density range, showing that for all velocity with a solitary solution possess two maxima and one minimum.

term depends on u and can be seen as a "*potential term*":

$$\underbrace{\left(\frac{\partial u}{\partial \xi}\right)^2}_{\text{"Kinetic term"}} \underbrace{-\left[\left(1-\beta^2\right)u^2-\frac{1}{3}B_1u^3-\frac{1}{6}B_2u^4-C\cdot u\right]}_{\text{"Potential term"}\equiv V(u)}=\left(\frac{\partial}{\partial \xi}u\right)^2+V\left(u\right)=V_0 \quad (2.3.16)$$

The potential, $V(u)$, can be plotted as shown in Figure 2.3.3, where one can imagine a particle in the potential rolling back and forward. For velocities with no solitary solutions, the particle will only roll forward and down the potential.
When a nerve pulses is propagating the nerve length becomes shorter [43], and *Vargas et al.* linked this effect to the integration constant C from eq. (2.3.15). They conclude that when the overall nerve length is constant, one obtains periodic solutions, and $C > 0$. When the nerve length can be shortening it generates a localized pulse, $C = 0$. Meaning that because of mass conservation, the nerve can as an effect of the propagation of the nerve signal either, shorter itself and have a localize pulse, or be at constant length and allow periodic pulses.

2.3.1 Conservation laws

It is clear that if u is a smooth solution of (2.3.6) that vanishes, along with its derivatives, as $|x|\to\infty$, then the quantity

$$J\left(u\right)=\int_{-\infty}^{\infty}\frac{\partial u}{\partial t}dx \quad (2.3.17)$$

is an invariant of motion, and can been seen as the mass flux into the system. Whereas

$$I\left(u\right)=\int_{-\infty}^{\infty}u\,dx \quad (2.3.18)$$

varies in time as $I = Jt + const$, and can be seen as the total mass in the system at time t. Since the solutions is localize and remain bounded as t increases, the mass will not change, and therefore $J = 0$. One can then introduce a new function v defined by

$$v=\int_{-\infty}^{x}\frac{\partial u}{\partial t}dx \quad (2.3.19)$$

which also vanishes with its derivatives as $|x|\to\infty$. v can be seen as the velocity field. For the soliton described by eq. (2.3.14) v become:

$$v=\int_{-\infty}^{x}\frac{\partial u}{\partial t}dx=\int_{-\infty}^{x}\beta\frac{\partial u}{\partial x}dx=\beta u \quad (2.3.20)$$

Where the relation $\xi = x - \beta t$ have been used. Equation (2.3.8) can then be expressed with functions *v* and u:

$$\frac{\partial v}{\partial t} = B(u)\frac{\partial u}{\partial x} - \frac{\partial^3 u}{\partial x^3} \tag{2.3.21}$$

This is a system that conserves the functional *I*.

2.3.2 Energy of the soliton

The Energy of a soliton can be calculated by introducing the displacement *s(x,t)*, the compression is then given by:

$$u = \frac{\partial s}{\partial x} \tag{2.3.22}$$

Inserting this in eq. (2.3.6) and integrate to yield

$$\frac{\partial^2 s}{\partial t^2} = B(u)\frac{\partial^2 s}{\partial x^2} - \frac{\partial^4 s}{\partial x^4} \tag{2.3.23}$$

This equation can be seen as a *Euler-Lagrange equation* with the *Lagrangian density*

$$\mathcal{L} = \frac{1}{2}\left(\frac{\partial s}{\partial t}\right)^2 - \frac{1}{2}\left(\frac{\partial u}{\partial x}\right)^2 - \frac{1}{2}A(u), \tag{2.3.24}$$

where

$$A(u) = \int_0^u Q(u)du = \int_0^u B(u)du\,du = u^2\left(1 + \tfrac{1}{3}B_1 u + \tfrac{1}{6}B_2 u^2\right). \tag{2.3.25}$$

Since the *Lagrangian* may be written as kinetic minus potential energy, the *Lagrangian* density can be expressed similar as kinetic energy density minus potential density energy. The dimensionless energy density becomes:

$$\varepsilon = \frac{1}{2}\left(\frac{\partial s}{\partial t}\right)^2 + \frac{1}{2}\left(\frac{\partial u}{\partial x}\right)^2 + \frac{1}{2}A(u) \tag{2.3.26}$$

The three dimensionless terms represent respectively the kinetic energy, the energy of dispersion, and the energy of compression.
Energy for a soliton, where *s* is only a function of $\xi = x - \beta t$, e.g. the stable soliton shown in this chapter, becomes:

$$\varepsilon = \frac{1}{2}u^2\beta^2 + \frac{1}{2}\left(\frac{\partial u}{\partial \xi}\right)^2 + \frac{1}{2}A(u) \quad (2.3.27)$$

Using the soliton equation (2.3.9) which may be rewritten to:

$$\left(\frac{\partial u}{\partial \xi}\right)^2 = A(u) - \beta^2 u^2 \quad (2.3.28)$$

The sum of the kinetic energy density plus the dispersive energy density thus equals the compressive energy density, such that the total energy density can be expressed as:

$$\varepsilon = A(u) \quad (2.3.29)$$

The total dimensionless energy of the soliton is then the integral of the energy density over all space, and is conserved and independent of time. The main contribution to the energy of the soliton is mainly from the compressibility, as shown, and from the kinetic. In Figure 2.3.4, the energise are shown as a function of the velocity, β. For the limit case when the velocity goes againt the lower limet, $\beta \rightarrow \beta_0$ will the energy goes againt infinity $E \rightarrow \infty$. The energy density have a limit, because u is limited by eq. (2.3.13), meaning that the soliton become wider when $\beta \rightarrow \beta_0$ and therefore the energy goes to ∞.

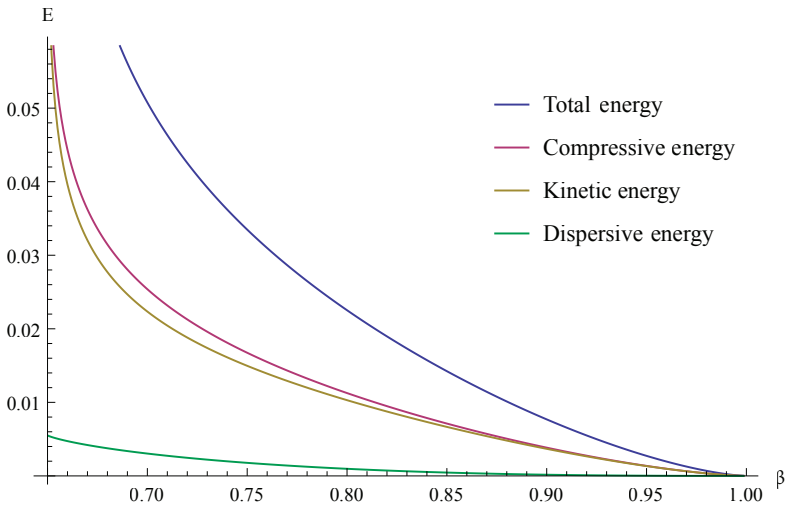

Figure 2.3.4 – The energy for a soliton as a function of the velocity. When $\beta \rightarrow \beta_0$ the energy $\rightarrow \infty$.

2.3.3 Viscous dissipation

One can introduce viscosity in the system the solitons are propagating in, and look at the consequences of dissipation. The solitons will lose energy and amplitude while they accelerate [46]. It can be seen as the soliton, while it lose energy and amplitude, try to remain stable, and therefore accelerate as a consequence of eq. (2.3.14).

The dissipation term can be introduce by first consider the one dimension *Navier-Stokes equations* for compressible fluids are:

$$\rho\cdot\left(\frac{\partial v}{\partial \tau}+\frac{\partial v}{\partial z}\right)=-\frac{\partial p}{\partial z}+\eta\frac{\partial^2 v}{\partial z^2},\qquad \frac{\partial \rho}{\partial \tau}=-\frac{\partial\left(\rho v\right)}{\partial x} \tag{2.3.30}$$

Where $v(z,\tau)$ is the velocity field, and $\rho(z,\tau)$ the density field. The pressure field p is assumed to obey a barotropic constitutive equation, $p = p(\rho)$, and depends indirectly on z and τ through ρ. The viscosity η is assumed constant. Using that

$$\frac{\partial\left(\rho v\right)}{\partial \tau}+\frac{\partial\left(\rho v^2\right)}{\partial z}=\rho\left(\frac{\partial v}{\partial \tau}+v\frac{\partial v}{\partial x}\right) \tag{2.3.31}$$

one can rewrite these equations as mass and momentum balance:

$$\frac{\partial \rho}{\partial \tau}=\frac{\partial\left(\rho v\right)}{\partial z},\qquad \frac{\partial\left(\rho v\right)}{\partial t}=-\frac{\partial M}{\partial z} \tag{2.3.32}$$

where

$$M=p+\rho v^2-\eta\frac{\partial v}{\partial z} \tag{2.3.33}$$

Combining the balance equations one get an equation, that has the basic form of a standard wave equation:

$$\frac{\partial^2 \rho}{\partial \tau^2}=\frac{\partial^2 M}{\partial z^2} \tag{2.3.34}$$

By assuming that the second term in M is negligible, and that the last term is small, one get

$$\frac{\partial^2 \rho}{\partial \tau^2}=\frac{\partial}{\partial z}\left(c^2\frac{\partial \rho}{\partial z}\right)+\nu\frac{\partial^2}{\partial z^2}\frac{\partial \rho}{\partial t} \tag{2.3.35}$$

where $\nu = \eta/\rho$ and $c^2 = \partial p/\partial\rho$, and used the equation of continuity to eliminate v. This equation is similar to equation (2.3.1) and introduce a dispersive term and dimensionless variables, one have eq. (2.3.6):

$$\frac{\partial^2 u}{\partial t^2} = \frac{\partial}{\partial x}\left(B(u)\frac{\partial u}{\partial x}\right) - \frac{\partial^4 u}{\partial x^4} + \kappa \frac{\partial^2}{\partial x^2}\frac{\partial \rho}{\partial t} \tag{2.3.36}$$

where $\kappa = \nu/\sqrt{h}$. *Lautrup et al.* [46] did a numerical study on the soliton with a κ = *0.05* (water; $\kappa = 10^{-7}$), and found out that the solitons have lost *70 %* of theirs height at $t = 990$ and has travelled more than 100 times theirs initial width.
The nerve pulse change only little over distances, and the small dissipation of heat in experiments of nerves [42] imply that the magnitude of dissipation is smaller than the one considered by *Lautrup et al.*. Further, was solitons not found to breakdown into small-amplitude waves noticed, which one could have expected by a high dissipation.

2.3.4 Collision of pulses and disturbances

It is a common belief in neuroscience that nerve pulse collision are blocked upon collision [48]. However, very little literature is written on this subject. *The FitzHugh-Nagumo model* [49], [50], which is a simplified mathematical representation of the Hodgkin-Huxley model, allows for both the cancellation and penetration of pulses depending on parameters [51].
Lautrup et al. studied head-on collision of solitons and showed that it seems like they passed through each other [46]. Figure 2.3.5 show results for collision of solitons. The only effect of the collision is small-amplitude noise travelling ahead of the post-collision solitons. When two solitons with a velocity close to the minimum velocity and therefore maximum possible amplitude collide, the density change exceed the density of the solid phase. Therefore, they introduce a "soft barrier" at the density of the solid phase:

$$B(u) = \left(1 + B_1 u + B_2 u^2\right)\left(1 + e^{\alpha(u-u_{\max})}\right) \tag{2.3.37}$$

With this condition a collision of two solitons close to the minimum velocity, result post-collision in several solitary peaks with different amplitude and velocity. This effect is also present in the situation without the soft barrier, but not as prominent, and not with the same amount of solitary peaks and small-amplitude waves. The energy loss from the solitons, and the energy in the small-amplitude waves, are for extreme cases under 4 %. For collision of soliton with velocity larger and not close to minimum velocity, have energy loss very under 1 %.
For solitons, one have to notice that they are not normal linear waves that obey the principle of superposition. The principle of superposition means that the amplitudes of two waves traveling through the same medium at the same time simply add together and interfere with each other. Solitary waves, instead of interacting through interference and simple addition, they collide in a nonlinear and complicate manner [52]. When soliton collide it appears that they jump through each other or just exchange the properties of velocity, energy, size and shape. After the collision they are not in their relative locations one would have expected them to be in, if they simply passed through each other, but are delayed. These soliton delays are found in many research field [53], [54].

Further, *Lautrup et at.*, investigate solitons with an initial velocity lower than the corresponding analytic value, given that

$$v(x,0) = p\beta u(x,0) \tag{2.3.38}$$

where $0 < p < 1$. Thus the initial field is not solitonic, this will be referred to unstable solitons, given that they over time will decay to a stable solitons. This is resulting in, that just after initiation the unstable soliton divided into two solitons of different sizes, which propagate in opposite directions. The soliton, which decay to a velocity in the same direction as the initial soliton, is larger than the one in the opposite directions, and can be seen as the initial soliton. Theirs amplitude and shape corresponds to theirs analytic amplitude and shape given by the velocity. A head of the two solitons travels small-amplitude noise. The small-amplitude waves travels with velocities over $\beta > 1$ and carry about 0.3 % of the system's total energy. The area between the two solitons has no change in the density.

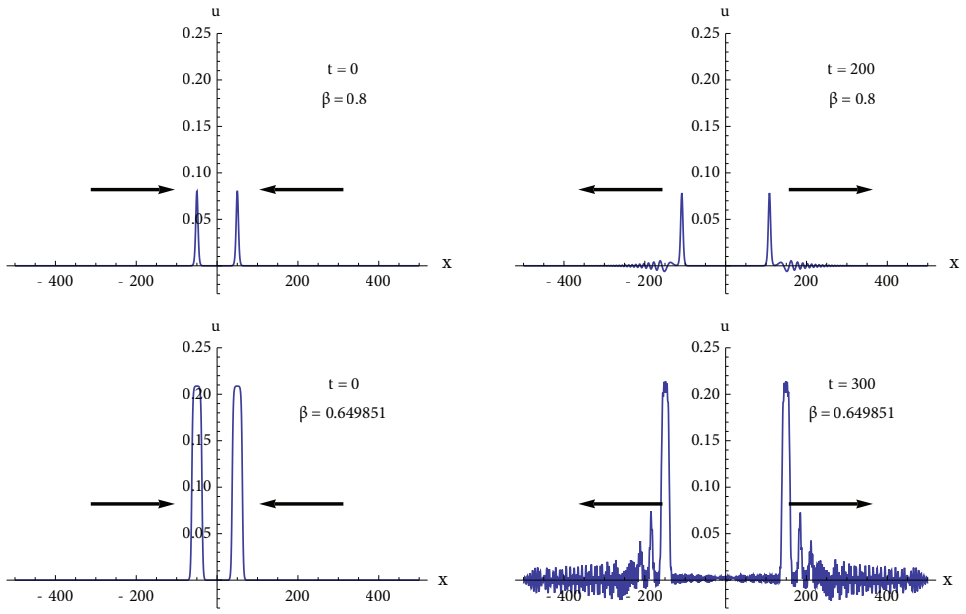

Figure 2.3.5 –Collision of two solitons before (left) and after (right) shown for $\beta = 0.8$ (top) and $\beta = 0.649851$ (bottom). One obtains small-amplitude noise traveling ahead of the post-collision pulse.

Chapter 3

Methods

The Soliton Model is based on the density change in a lipid membrane which is described by a partial differential equation – sound equation for lipid membranes. This equation can be transform into an ordinary differential equation to find stable solitons. To solve the ordinary differential equation, *the Eurler method* is used. To solve the partial differential equation *the two-step Lax Wendroff method* is used. In this chapter the two numerical methods will be presented and the solution to the the sound equation for lipid membranes will be analysed.

3.1 Euler method

The sound equation presented as eq. (2.3.6) and later as eq. (5.1.1) and (5.2.1) can be numerically solved by introducing the variable $\xi = x - \beta t$ (will in this section be referred to as time for simplicity, even though it also denotes place), which turns the partial differential equation into an ordinary differential equation. After integrations, one arrives at eq. (2.3.11):

$$\frac{\partial u}{\partial \xi} = \mp\sqrt{\left(1-\beta^2\right)u^2 + \frac{1}{3}B_1 u^3 + \frac{1}{6}B_2 u^4} \tag{3.1.1}$$

Which can be solved using a numerical method, such as *Euler Method*. Using numerical methods to solve a differential equation have the advantage that they are easier than finding the analytic solution and the result is a good approximation of the real solution to the equation.
The *Euler method* can be used when one wants to approximate the solution of the initial value problem:

$$\frac{dy(\xi)}{d\xi} = y'(\xi) = f\left(\xi, y(\xi)\right) \qquad y(\xi_0) = y_0 \tag{3.1.2}$$

Choosing a value h for the size of every step and setting $\xi_n = \xi_0 + nh$, then one step of the *Euler method* from ξ_n to $\xi_{n+1} = \xi_n + h$ is

$$y_{n+1} = y_n + hf\left(\xi_n, y_n\right) \tag{3.1.3}$$

With the assumption that one seek negative solitons, where

$$u \sim -\exp\left[-\sqrt{(1-\beta)}\,|\xi|\right] \qquad |\xi| \to \infty\,, \tag{3.1.4}$$

equation (3.1.1) is negative until the solution reaches its minimum, and the solution is symmetric around its minimum. One can then determinate a value for y_0 and step by step calculate the solution.

3.1.1 Error in Numerical Solution

When using a numerical approximation to solve a differential equation, one has to expect a difference between the solution and the real solution; the error in the numerical method. The local truncation error (LTE) is the difference made in a single step, where the global truncation error (GTE) is the cumulative effect of the local truncation errors committed in each step.

3.1.1.1 Local Truncation Error

The local truncation error of the Euler method is the difference between the numerical solution after one step, y_{n+1}, and the exact solution at time $\xi_{n+1} = \xi_n + h$. The numerical solution is given by eq. (3.1.3), and the exact solution can be given by a Taylor expansion around ξ_n:

$$y\left(\xi_n + h\right) = y\left(\xi_n\right) + hy'\left(\xi_n\right) + \frac{1}{2}h^2 y''\left(\xi_n\right) + O\left(h^3\right) \tag{3.1.5}$$

The local truncation error is given by the difference between these equations:

$$\tau_n = y\left(\xi_n + h\right) - y_{n+1} = \frac{1}{2}h^2 y''\left(\xi_n\right) \tag{3.1.6}$$

This shows that for small h, the local truncation error is approximately proportional to h^2. In Figure 3.1.1 the relative error taken in each step is shown for different step sizes. It is clear to see that the error is proportional to h^2 and the error is smallest near the peak of the soliton.

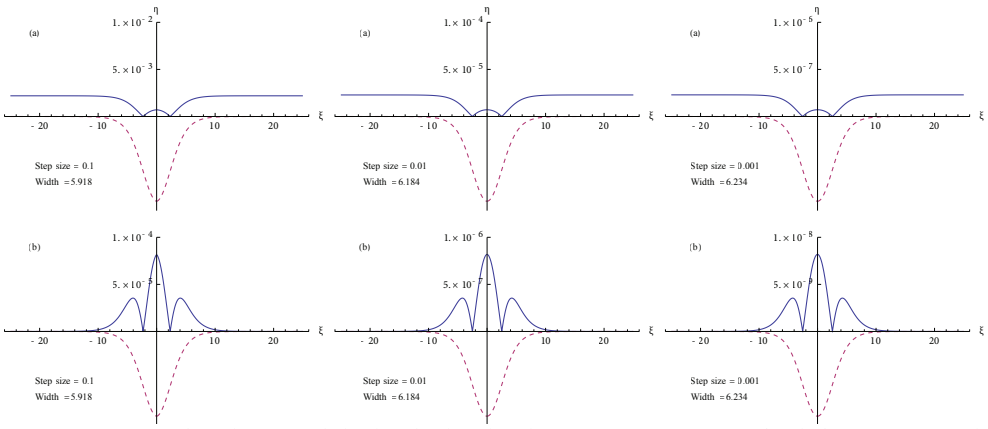

Figure 3.1.1 – (a) The relative and (b) the absolute local truncation error given for different step size (h = 0.1, 0.01, 0.001) for a soliton with velocity β = 0.735, the unit on the x-axis is the step, n, times step size, h, ξ = nh. The dashed line show the solution shape for each step size, its amplitude is approximately u = -0.114. It is shown that the smallest relative error is near the peak of the soliton. The size of the error in each step size clearly follow h^2.

3.1.1.2 Global Truncation error

The global truncation error is the error at time $\xi_n = nh$ and is the cumulative effect of the local truncation error committed in each step. The steps between time ξ_0 and ξ_n is proportional to *1/h*, and the error committed in each step is proportional to h^2. Therefore, it is expected that the global truncation error is proportional to *h*. The error is the different between the exact solution at ξ_n and the numerical solution after *nh* step:

$$e_n = y(\xi_n) - y_n = y(\xi_n) - y_0 + hy'(\xi_0) + hy'(\xi_1) + \cdots + hy'(\xi_{n-1}) \qquad (3.1.7)$$

The error is shown in Figure 3.1.2 for different step size, *h*, for all ξ. One can notice that the error is not exactly proportional to *h*, which can be lead to be an effect of the width (*i.e.* full width of half-maximum) of the solution (in Figure 3.1.2 the width is shown for each step size). The exact solution has a width of roughly 6.24. At its minimum, equation (3.1.1) is developing slower for each step, and therefore the larger step size is reaching the minimum in less time than the smaller step size, therefore the solution has a smaller width for larger step. One of the assumption was that the solution was symmetric around its minimum, and force the width to be equal to the exact width, by making the area around the minimum wider, the error will be almost perfectly proportional to *h*. In Figure 3.1.3 the relative error for different velocities, *β*, is shown, one can see that the numerical solution has the same amplitude as the analytic, and the relative error is in the same scale for all solutions. The largest error occurs when the derivative of the solution is largest, which has the effect that the solution from the numerical methods differ a little from the solution calculated by the analytic method. However, these errors are small for small step size and justifies the use of *Euler method* for solving equations where the result takes the form of a soliton.

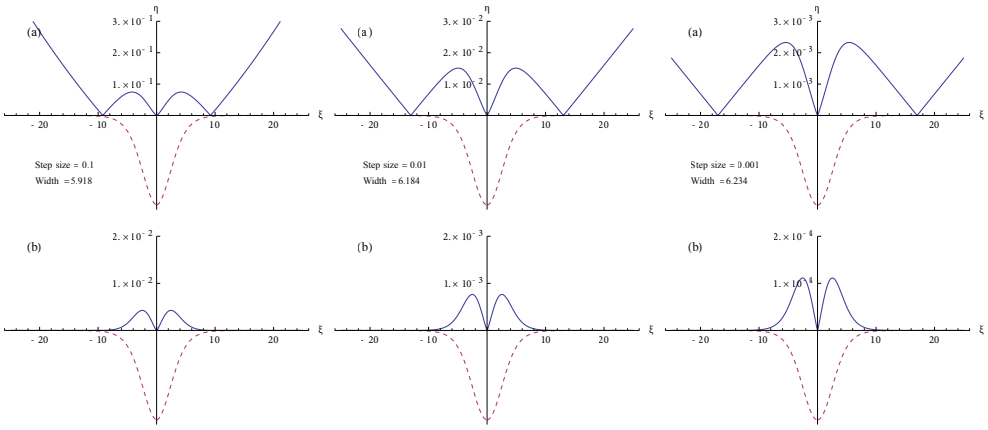

Figure 3.1.2 – (a) the relative and (b) the absolute global truncation error for all ξ at different step size, h, shown that the error is almost approximately to h. Dashed line illustrate the shape of the solution.

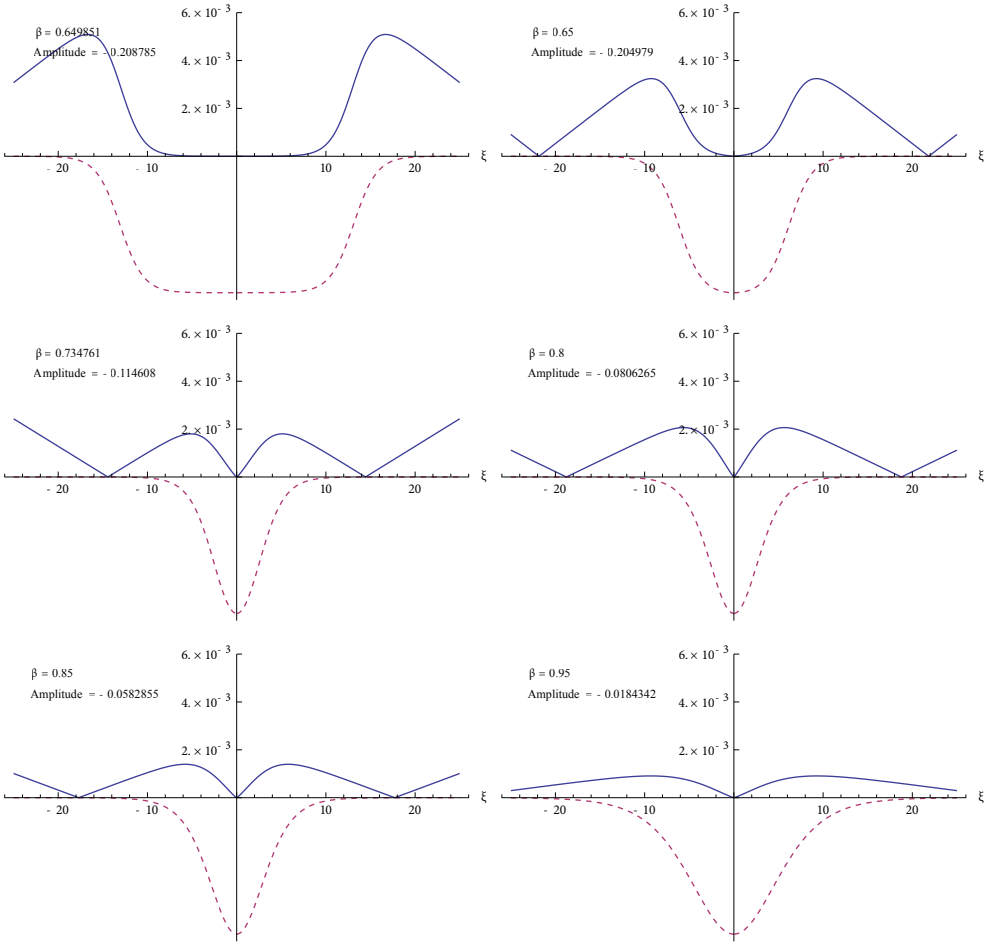

Figure 3.1.3 – The relative error for solutions with different velocities, β, with step size h = 0.001, show that the error is biggest for high amplitude, low velocities solitons. The error is low for all solitons

3.2 Two-Step Lax Wendroff

The thesis has the aim to investigate a number of questions associated with the stability of negative and positive solitons. However, solving the equation analytically in time and space has shown to be too difficult, if not impossible. Therefore, it has been chosen to consider this problem numerically. A well suited method to solve *the soliton model* for the expanded sound profile (eq. (5.2.1)) when the initial state *u(x,0)* is known, is the *Two-Step Lax Wendroff method* [55]. The method is second-order accurate in both space and time, and it avoids large numerical dissipation and mesh drifting.
By defining the operator for the half-interval average of a function:

$$\hat{\Sigma}_x F(x) \equiv \frac{F\left(x+\frac{1}{2}\Delta x\right)-F\left(x-\frac{1}{2}\Delta x\right)}{2} \tag{3.2.1}$$

The operator for the spatial derivatives are likewise of the central form, implying that corrections to an arbitrary function *f(x)* are of second order in Δx:

$$\hat{\nabla}_x F(x) \equiv \frac{F\left(x+\frac{1}{2}\Delta x\right)-F\left(x-\frac{1}{2}\Delta x\right)}{\Delta x} \tag{3.2.2}$$

In section 2.3.1 the flux conservation law was introduced. These can be rewritten as

$$\frac{\partial u}{\partial t}=\frac{\partial v}{\partial x}, \qquad \frac{\partial v}{\partial t}=\frac{\partial f}{\partial x}, \tag{3.2.3}$$

where

$$f=Q(u)-\frac{\partial w}{\partial x}, \qquad w=\frac{\partial u}{\partial x}-\kappa v, \tag{3.2.4}$$

with *Q(u)* from eq. (2.3.25) and κ is the dimensionless viscosity constant introduced in section 2.3.3. Using this rewrite, one can define the discrete functions:

$$f(x,t)=Q\left(u(x,t)\right)-\hat{\nabla}_x w(x,t) \tag{3.2.5}$$

$$w(x,t)=\hat{\nabla}_x u(x,t)-\kappa\hat{\Sigma}_x v(x,t) \tag{3.2.6}$$

Where *w(x,t)* can be seen as the mass flow through a point between two grids at the same time, *t*, and *f(x,t)* as the force. The discretized equation of motion then take the form:

$$u\left(x,t+\tfrac{1}{2}\Delta t\right)=\hat{\Sigma}_x u(x,t)+\tfrac{1}{2}\Delta t\hat{\nabla}_x v(x,t) \tag{3.2.7}$$

$$v\left(x,t+\tfrac{1}{2}\Delta t\right)=\hat{\Sigma}_x v\left(x,t\right)+\tfrac{1}{2}\Delta t\hat{\nabla}_x f\left(x,t\right) \tag{3.2.8}$$

Where u is the density change, and v the velocity field. Finally, the values after one time step, Δt, can be calculated:

$$u\left(x,t+\Delta t\right)=u\left(x,t\right)+\Delta t\hat{\nabla}_x v\left(x,t+\tfrac{1}{2}\Delta t\right) \tag{3.2.9}$$

$$v\left(x,t+\Delta t\right)=v\left(x,t\right)+\Delta t\hat{\nabla}_x f\left(x,t+\tfrac{1}{2}\Delta t\right) \tag{3.2.10}$$

The order of errors can be found just by expanding eq. (3.2.1) and eq. (3.2.2) in Δx to smooth function:

$$\hat{\Sigma}_x F\left(x\right)=F\left(x\right)+\frac{1}{8}\Delta x^2 F''\left(x\right)+\cdots \tag{3.2.11}$$

$$\hat{\nabla}_x F\left(x\right)=F'\left(x\right)+\frac{1}{24}\Delta x^2 F'''\left(x\right)+\cdots \tag{3.2.12}$$

Since the operators give F and it derivative F' at x, it can be seen that both smooth functions have the errors of second order.
Figure 3.2.1 show a scheme of the calculation, the method from $t+\Delta t/2$ to $t+\Delta t$ is called *staggered leapfrog method*. To calculate x at $t+\Delta t$, one has to calculated the temporary values u, v and f at $x-\Delta x/2$ and $x+\Delta x/2$ for time $t+\Delta t/2$ from the values for $x-1$, x and $x+1$ at time t. And w at x for time $t+\Delta t/2$ from w for $x-\Delta x/2$ and $x+\Delta x/2$ at time t. When these three temporary grid values in the $t+\Delta t/2$ layer are calculated, u and v for x at time $t+\Delta t$ can be calculated with the values for x at time t.

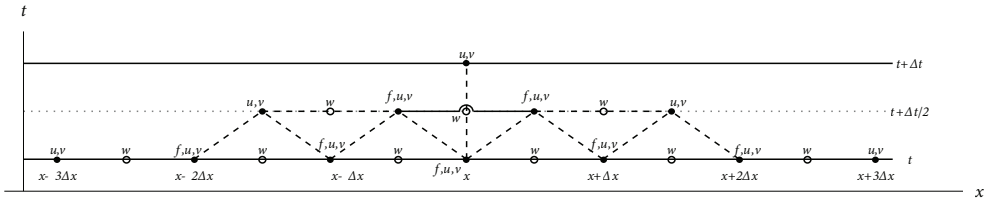

Figure 3.2.1 – Scheme of the Two-Step Lax Wendroff method, the solid dots on the grid have the values for u, v and f, where the open dots have the values for w. The values at the layer at time t+Δt, can be calculated from the layer with temporary values, t+Δt/2, and the values at the layer at time t.

3.2.1 Algorithm

Consider a lattice of the size N over the periodic interval $L = N\Delta x$, with u and v represented by the arrays $U[N + 1]$ and $V[N + 1]$ at integer coordinates $x_i = i\Delta x$ and integer times $t_n = n\Delta t$. The array elements $[0]$ and $[N]$ takes the same values. Further more the temporary values are identified with $N + 1$ arrays $W[N + 1]$, $F[N + 1]$, $U'[N + 1]$ and $V'[N + 1]$.

The fundamental time-cycle consists of the following steps. The periodicity condition is imposed in each algorithmic step (*[0] = [N]*). For each time step, Δt, the algorithm starts at step 1.

1. Calculate the flow between U_i and U_{i+1} for $i = 0,\ldots, N–1$, which represents the function w at the spatial half-way point $x_i+\Delta x/2$ at time t_n:

$$W_i = \frac{U_{i+1,n} - U_{i,n}}{\Delta x} - \kappa \frac{1}{2}\left(V_{i+1,n} + V_{i,n}\right) \tag{3.2.13}$$

2. Calculate the force for $i = 1,\ldots, N$, which represents the function f at x_i at time t_n:

$$F_i = Q\left(U_{i,n}\right) - \frac{W_i - W_{i-1}}{\Delta x} \tag{3.2.14}$$

3. Advance $\Delta t/2$ and calculated the temporary values U' and V', which represents u and v for $x_i+\Delta x/2$ at time $t_n+\Delta t/2$:

$$U_i' = \frac{1}{2}\left(U_{i+1,n} + U_{i,n}\right) + \frac{1}{2}\Delta t \frac{V_{i+1,n} - V_{i,n}}{\Delta x} \tag{3.2.15}$$

$$V_i' = \frac{1}{2}\left(V_{i+1,n} + V_{i,n}\right) + \frac{1}{2}\Delta t \frac{F_{i+1} - F_i}{\Delta x} \tag{3.2.16}$$

4. Calculate the flow with periodic boundary conditions, w for x_i at time $t_n+\Delta t/2$:

$$W_i = \frac{U_i' - U_{i-1}'}{\Delta x} - \kappa \frac{1}{2}\left(V_i' - V_{i-1}'\right) \tag{3.2.17}$$

5. Calculate the force with boundary conditions, f for $x_i+\Delta x/2$ at time $t_n+\Delta t/2$:

$$F_i = Q\left(U_i'\right) - \frac{W_{i+1} - W_i}{\Delta x} \tag{3.2.18}$$

6. Advance by Δt and calculate U and V, u and v for x_i at time $t_{n+1} = t_n+\Delta t$:

$$U_{i,n+1} = U_{i,n} + \Delta t \frac{V_{i-1}' - V_i'}{\Delta x} \tag{3.2.19}$$

$$V_{i,n+1} = V_{i,n} + \Delta t \frac{F_{i-1} - F_i}{\Delta x} \tag{3.2.20}$$

7. The algorithm now resumes from step 1.

3.2.2 Error

When using a numerical method leads to numerical errors, for any solutions of problems on an artificial grid will necessarily lead to grid noise, which take the form of grid-spacing dependent corrections to the continuum equation.

3.2.2.1 Spatial noise

Spatial noise is the error that the lattice produce to the exact solution. Expanding the discrete derivatives (eq. (3.2.11) and eq. (3.2.12)) to second order in Δx, and assume time to be continuous, one find the equations of motion:

$$\frac{\partial u}{\partial t} = \frac{\partial v}{\partial x} + \frac{1}{24}\Delta x^2 \frac{\partial^3 v}{\partial x^3} \tag{3.2.21}$$

$$\frac{\partial v}{\partial t} = \frac{\partial f}{\partial x} + \frac{1}{24}\Delta x^2 \frac{\partial^3 f}{\partial x^3} \quad \frac{\partial v}{\partial t} = \frac{\partial f}{\partial x} + \frac{1}{24}\Delta x^2 \frac{\partial^3 f}{\partial x^3} \tag{3.2.22}$$

$$f = Q(u) - \frac{\partial w}{\partial x} - \frac{1}{24}\Delta x^2 \frac{\partial^3 w}{\partial x^3} \tag{3.2.23}$$

$$w = \frac{\partial u}{\partial x} - \kappa v + \frac{1}{24}\Delta x^2 \frac{\partial^3 u}{\partial x^3} - \kappa \frac{1}{8}\Delta x^2 \frac{\partial^2 v}{\partial x^2} \tag{3.2.24}$$

These corrections will all contribute to a derivation between the analytic solution and the solution on the lattice. These corrections will also introduce grid-generated dispersion and dissipation. Differentiate eq. (3.2.21) with respect to time t, and substitute with eq. (3.2.22)-(3.2.24) to obtain a single differential equation for u:

$$\begin{aligned} \frac{\partial^2 u}{\partial t^2} = {} & \frac{\partial^2 Q(u)}{\partial x^2} - \frac{\partial^4 u}{\partial x^4} + \kappa \frac{\partial^3 u}{\partial x^2 \partial t} \\ & + \frac{1}{24}\Delta x^2 \left(\frac{\partial^4 Q(u)}{\partial x^4} + 4\kappa \frac{\partial^5 u}{\partial x^5} - 3\frac{\partial^6 u}{\partial x^6} \right) \end{aligned} \tag{3.2.25}$$

The first line is the basic area density change equation and the last line shows that the lattice produces extra terms proportional to Δx^2. This show that this method is second order accurate in space x.

3.2.2.2 Temporal noise

In the two-step method, with half-step integers, will the temporal discretization

will also generate grid noise. This noise can be consider by looking at a simple differential equation:

$$\frac{dy(t)}{dt} = F(t) \tag{3.2.26}$$

Where F is a known function of time. The half-time solution is then defined to be:

$$y(t + \Delta t/2) = y(t) + \frac{1}{2}\Delta t F(t) \tag{3.2.27}$$

This is a temporary result from which the full time-step can be calculated:

$$y(t + \Delta t) = y(t) + \Delta t F(t + \Delta t/2) \tag{3.2.28}$$

Using equation (3.2.27) the full time-step can be calculated to:

$$y(t + \Delta t) = y(t) + \Delta t \frac{dy(t + \Delta t/2)}{dt} = y(t) + \Delta t\left(F(t) + \frac{1}{2}\Delta t F'(t)\right) \tag{3.2.29}$$

Expanding the right hand side of (3.2.28) in Δt to second order to get:

$$y(t + \Delta t) = y(t) + \Delta t\left(F(t) + \frac{1}{2}\Delta t F'(t) + \frac{1}{8}\Delta t\ F''(t)\right) \tag{3.2.30}$$

This is similar to the *midpoint method*, and it shows that the two-step approximation is second order accurate in time t, and that the error is of third order in the time interval.

3.2.2.3 Method stability and Small-amplitude perturbations

The primary concern using numerical methods is the stability of the solutions when it is evolved in time. *Lautrup et al.* [46] made a study on small-amplitude perturbations and stability of solitons in *the two-step Lax-Wendroff method* for the basic density change equation of the form of equation (2.3.6). This study conclusions can be transfer to the time evolved solutions, where only negative solitons can exist, in section 5.1.2, because the basic equation is in the exact same form. However, the conclusions cannot be directly transferred to the study of coexistent negative and positive solitons, since the basic density change equation is being expanded to equation (5.2.1), and the initial values of u and v is not established from an analytic and exact solution, but a numerical solution.

As shown the use of the numerical methods introduced an inevitably small-amplitude perturbation (eq. (3.2.25)) proportional to Δx^2 to the exact solution into the numerical system. When the initial values only can be found by using a numerical method, e.g. the Euler method, a bigger perturbation is expected compared to

the initial values established from an analytic solution. If the perturbation grows exponentially over time, then the initial solitonic solution will be locally unstable. Also the finite size of Δx means that there is a smallest wavelength perturbation which can be studied on the lattice. Such potential instabilities involving such wavelengths, is not impossible but is unlikely.

The small-amplitude perturbations will be investigated with $\Delta x = 0.1$ and $\Delta t = 0.001$ on a spatial lattice, which was chosen to be periodic with length 100. From *Lautrup et al*. it is known that the energy is not strictly conserved by the algorithm, but rather decreases linearly with a rate of 1.9×10^{-7} of the initial energy with time over the time intervals considered. Further more they follow solitons for times as long as 1000 units, where the energy loss is negligible, and there is no indication of instability. Other things found in the transition from analytic to numerical was that the initial energy was a bit lower, the velocity was found stable but a bit lower, fluctuation in the location of the maximum was 25 times smaller than the spatial size, Δx, and the shape of the soliton was slightly higher and narrower. Another thing was that the soliton was not found unstable under large-amplitude noise. These things is also found to be valid for the basic equation for the negative soliton and the expanded density change equation.

One can illustrate soliton stability by first determining the location of the maximum[3] of the soliton as a function of time. If the velocity of this point is constant, and the density change too, it is an initial indication of the stability of the soliton. However, there are small fluctuations in the location of both the maximum density and the velocity due to the perturbations. When the position of the soliton is defined, it can be used to shift every time frame, so the soliton is kept at a fixed position. From this a time-averaged soliton can be constructed in order to minimize the effects of the perturbations. The difference between the time-averaged soliton and the initial soliton or analytic, if exist, can be seen as an indication of the error introduce by the numerical methods. The difference for the basic equation for a negative soliton with velocity $\beta = 0.735$ is shown in Figure 3.2.2(a), the difference is of the same order as in *Lautrup et al*., and the only different in the shape is that it is mirrored in the x-axis. The figure show that the analytic solitons are not identical to solitons on a finite mesh.

The noise is an effect of the perturbation, and can give an indication of the level of fluctuation in the numerical method. This can be considered as a function of time by subtracting the time-average soliton from $u(x,t)$ each time frame and construct the root mean square (r.m.s.) of the resulting difference as a function of time. This is shown in Figure 3.2.2(b) for a soliton with velocity $\beta = 0.735$ from the basic equation for a negative soliton. If the soliton is stable, the resulting r.m.s. is bounded as a function of time. Otherwise, if the soliton is unstable, the resulting r.m.s. is not bounded and one would expect to find a systematic difference. Because the soliton's maximum will grow exponentially over time, and the difference in the vicinity of this maximum will be the main contributor to this growth. As shown in Figure 3.2.2(b) no sign of instability is present, since the r.m.s. over time do not grow, and that the magnitude of the spatial distribution of the r.m.s. is the same all over time.

3 "Maximum" is referenced to the point in the soliton where the derivative of the density change is zero, for a positive soliton the maximum, for a negative soliton the minimum.

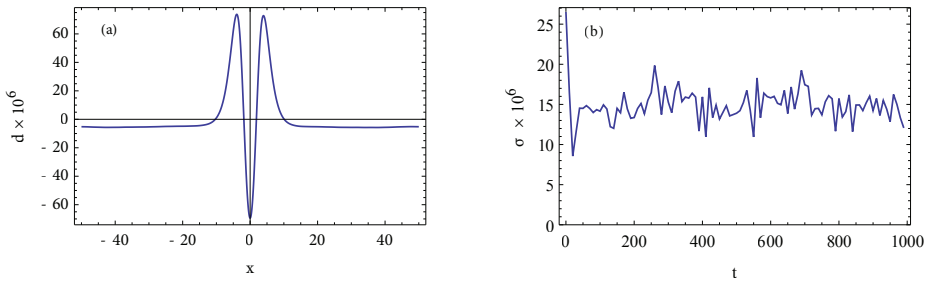

Figure 3.2.2 – (a) The difference between the time-averaged numerical soliton and the analytic soliton for a soliton with velocity β = 0.735. The average has been performed over 1000 units of time, during which the soliton travels more than 100 times its own width. (b) Time evolution of r.m.s. noise level σ for the soliton with velocity β = 0.735 over 1000 units of time.

When the analytic solution is not known, one has to use other methods to establish the initial state. Two methods have been developed in this thesis to make the initial state in *the two-step Lax-Wendroff method*. These two methods will be analyzed, where one has been exclusively used to set the initial state.
In section 5.2.1 stable soliton is calculated with the *Euler method*, these was calculated with a step size much smaller than the spatial size in *the two-step Lax-Wendroff method*. By choosing the values correspond to the same x value, the result from the *Euler method* can be transformed to the mesh:

$$u_{Lax-Wendroff}\left(x_i,0\right)=u_{Euler}\left(x_j,0\right) \tag{3.2.31}$$

Where step x_j in the Euler method corresponds to the x value for x_i from *the Two-step Lax-Wendroff method*, and j can be expressed as:

$$j=i\frac{\Delta x_{Lax-Wendroff}}{\Delta x_{Euler}} \tag{3.2.32}$$

Where Δx is the step size for one of the methods. One could also take the average value between the step j - ½ and j + ½. This average has no significant influence on the error in the method. In Figure 3.2.3 the difference between the time-average soliton and an initial negative soliton is shown. It is clear that the soliton has a larger amplitude and is narrower compared to the initial soliton. The difference is almost a factor 1000 bigger than the previous difference for an analytic soliton. The initial soliton had a velocity of $\beta = 0.88$, but the time evolved soliton had a velocity of $\beta = 0.87$ average over all time, which is below the calculated minimum velocity of $\beta_0 = 0.875681$. When this soliton starts to propagate in the simulation it emits small-amplitude waves and a larger small-amplitude wave, with a shape of a soliton with an amplitude of 13% of the initial soliton and a velocity approximately below $\beta > 1$ in front of it. This is also seen in the case for the basic equation for negative solitons, where the amplitude was greater than the analytic soliton with the same velocity. The solitons was consider unstable until it emit small-amplitude waves and become stable. As seen in Figure 3.2.3(b) the r.m.s. noise seems to be

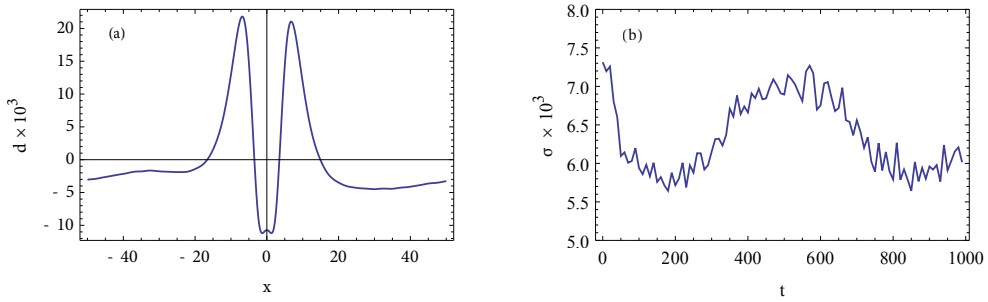

Figure 3.2.3 – (a) The difference between the time-averaged numerical soliton and the numerical initial soliton calculated with Euler method for a velocity β = 0.88. The average has been performed over 1000 units of time, during which the soliton travels more than 100 times its own width and decay to the velocity β = 0.87. (b) Time evolution of r.m.s. noise level σ for the soliton over 1000 units of time, show a periodic pattern, because of the small-amplitude emits a wave which overleap the soliton.

periodic over time. This is a result of the two waves, the soliton and the large wave, overlapping the time between $t = 0$ and ~ 350 and between ~ 700 and ~ 1000. The noise is calculated by subtracting the initial soliton from every time frame, and therefore when the two waves are overlapping the noise becomes smaller, hence they both originate from the initial soliton and mass is conserved, and when they are not overlapping it become larger. When they are not overlapping the soliton's velocity is above the minimum velocity. As mentioned before, a similar energy loss is found with this method, however, where the situation before had an almost perfect linear loss over time, this fluctuates in the loss, due the small-amplitude waves, however, the energy decay is averagely linear over time. The maximum fluctuates about $x = 1$ (10 times larger than Δx), which is a result of the larger small-amplitude wave. If the length of the lattice was infinity, the fluctuation would be less. This method introduces a lot of noise into the simulation, and another method with reduced noise will be preferable.

In section 5.1.3 it is shown that a small increase in the amplitude of the soliton leads to a velocity change, such that the velocity corresponds to the amplitude. In this situation small-amplitude waves was created, however the energy and amount was determinated by the size of the perturbation. In section 3.1 it was shown that the error in the maximum of the solution calculated numerically from *the Euler method* was approximately zero. Meaning that the *Euler method* gets the right amplitude of the solution, and that the error in *the Euler method* was in the shape of the soliton.

Using these properties one can construct a soliton on the form of an analytic soliton, and by having the right amplitude and shape. The main contributor to the error should be the velocity. This was made by first finding suitable values for the sound velocity on the form of the basic density change equation to both sides of the sound profile. The values were found by fitting the sound profile to one of the sides, and then tweak the value to obtain values where the difference between the solution of the expanded and the basic equation was within a small range for a large range of soliton velocities, and at all-time below the right velocity. Meaning that, if one wants a soliton in *the two-step Lax-Wendroff method* with velocity β = 0.88, the analytic soliton used to establish the initial state, must be below this velocity, but have the same amplitude. The analytic solution to the basic density

change equation is known, and from the Euler method the right amplitude can be calculated. The velocity of the analytic solution can then be found. The initial state can now be established, with a soliton of the right amplitude and shape, but with a lower velocity than the exact soliton.
In Figure 3.2.5(a) the difference between the time-average soliton with a velocity of $\beta = 0.88$ and the initial soliton with a velocity of $\beta = 0.85$. Compared to the other method, where the initial state was established with *the Euler Method*, the difference is 10 times lower. The noise is 30 times bigger than the case where the exact solution was known. The soliton is over all-space smaller than the initial soliton, where the other methods have been narrower, but with a larger amplitude. In (b) one can see that also the r.m.s. noise is 10 times smaller than the other method and 40 times bigger than when the exact solution is known, and have no sign of systematic errors in it. When the soliton starts to propagate in the simulation, it emits small-amplitude waves. These waves are small and carry less than 0.02 % of the initial energy. By establishing the initial state this way, one have reduces the noise and one still obtain stable solitons over time.

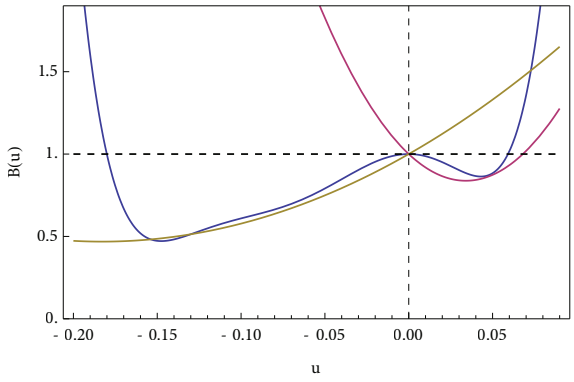

Figure 3.2.4 – The sound profiles, where the sound velocity from the basic density change equation is fitted to both side. Blue – the expanded sound velocity. Purple – the sound velocity for negative density change. Yellow – the sound velocity for positive density change.

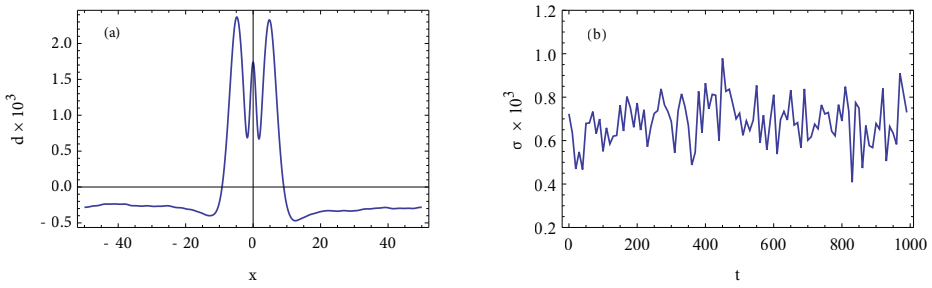

Figure 3.2.5 – (a) The difference between the time-averaged numerical soliton and the analytic soliton from the fitted sound profile for a velocity $\beta = 0.85$. The soliton decay to the velocity $\beta = 0.88$. (b) Time evolution of r.m.s. noise level σ for the soliton over 1000 units of time, show no sign of a periodic pattern, and is 10 times smaller than method where Euler method was used.

3.2.2.4 Small-amplitude waves

Small-amplitude waves is a common phenomena in this study, and it is therefore interesting to know how these small-amplitude waves are handled by *the two-step Lax Wendroff method*. As mentioned, the method has problems with waves where the wave length is shorter than Δx, because these waves cannot be expressed in the lattice. Waves with wave length larger than Δx tend to disappear in the method too. The small-amplitude waves carry energy, and when the waves disappear the energy disappears too. This is demonstrated in Figure 3.2.6 for the relative energy loss as a function of the wavenumber for different times t, on a periodic lattice $N = 100$, with $\Delta x = 0.1$ and $\Delta t = 0.001$. The initial state was set by a sinusoidal wave with the amplitude as a function of the wavenumber, k:

$$u(0,x) = A(k)\sin(kx) \tag{3.2.33}$$

It is found that the amplitude depend on the wavenumber (see appendix B). The velocity is also found to be a function of wavenumber, k, and the velocity field is then:

$$v(0,x) = \beta(k)u(0,x) \tag{3.2.34}$$

The periodic lattice gives rise to discontinuities in the initial state (where *U[0] = U[1000]*), but this is found to be insignificant, and the one discontinuities wave will only contribute with a small error, since the wave length is much smaller than the lattice size. As seen in Figure 3.2.6, at high wave lengths the relative energy loss is high, even after few iterations.

For example for waves with wavenumber $k = 5$ (wave length $\lambda = 1.26$) after $t = 30$ more than 30 % of the initial energy is gone, and at time $t = 100$ almost all of the initial energy has disappeared from the system, where waves with small wavenumber is unaffected by the method and have almost none energy loss over time.

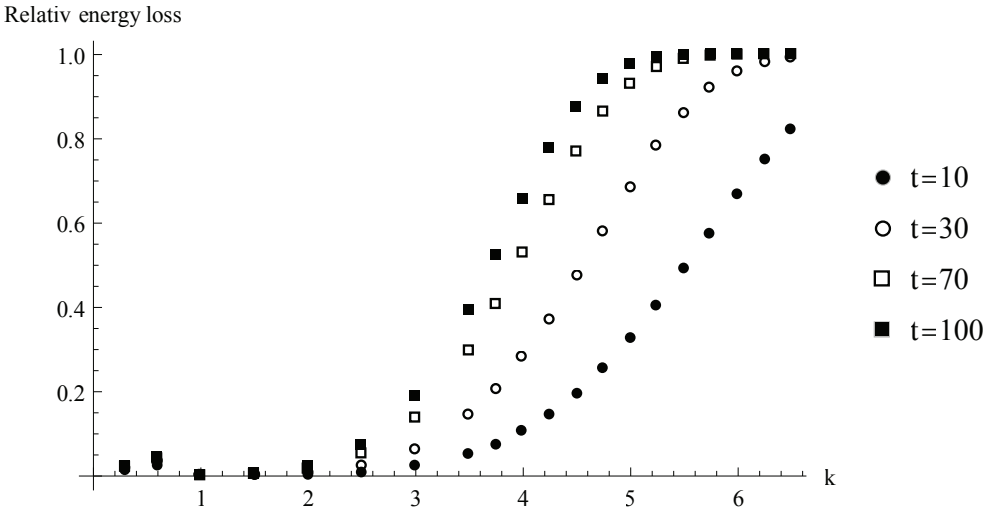

Figure 3.2.6 – Energy loss as a function of wavenumber, for different time t. For larger wavenumber the energy loss is high.

It is therefore expected that situations with small-amplitude waves with large wavenumber, energy will disappear from the system over time, due to the method's handling of small-amplitude waves.
When introduction a viscosity in the systems, it is seen that the energy in the small-amplitude waves decay quickly. Even for small-amplitude waves where the wavenumber is low and could propagate in a viscosity-less system without any energy loss, they disappear in a small amount of time, as seen in Figure 3.2.7.

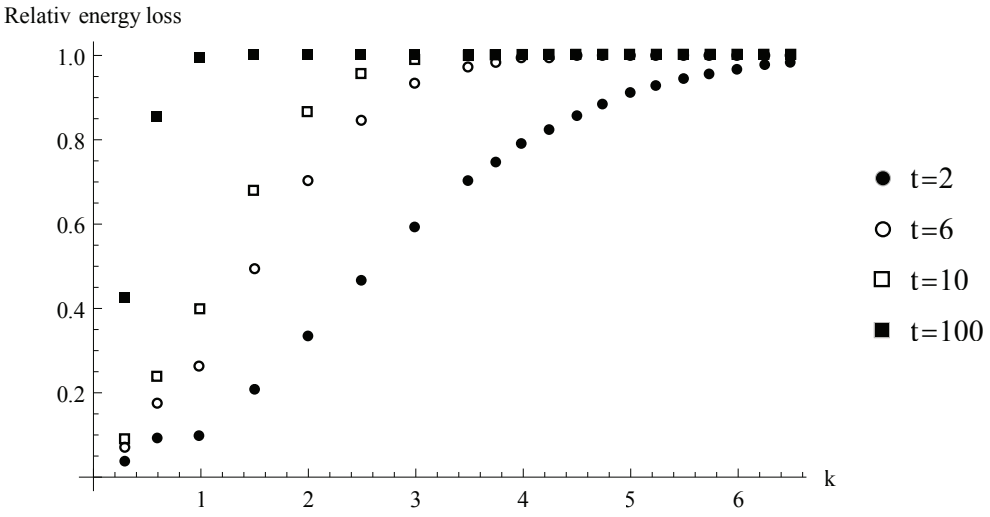

Figure 3.2.7 – Energy loss as a function of wavenumber, for different time t, in a system with viscosity.

Portrait of Hans Christian Ørsted, 1851 (© Den Store Danske, og Frederiksborgmuseet), af Wilhelm Marstrand. Was Danish physicist and chemist, and was one of the a leader of the Danish Golden Age. Beside discovering that electric currents create magnetic fields, he invented a piezometer (seen behind him) to measure waters compressibility.

Chapter 4

Sound Profiles

This chapter will treat and explain the sound profiles used in chapter 5. It will be shown how to calculate a membranes sound profile from its thermodynamic properties, and it will be done for a membrane where positive and negative solitons can propagate simultaneously.

4.1 Sound profile for DPPC membrane

In section 2.3 it was shown that solitons could propagate in a DPPC membrane at a bulk temperature of $T = 45$°C with a lateral density of $\rho = 4.035 \times 10^{-3}\ g/m^2$. The positive soliton force the membrane through the phase transition.
For a membrane in a state on the other side of the phase transition, with a lateral density of $\rho = 4.877 \times 10^{-3}\ g/m^2$, with the correspond bulk temperature at $T = 39.6$°C, will the membrane be in the gel state and just below the melting temperature. With this assumption, the sound profile can be expanded and the variables for unilamellar DPPC vesicles shown in Figure 2.3.1 can be obtained. The sound profile take the form

$$c^2 = \frac{1}{\rho^A \kappa_S^A} = c_0{}^2 + p\Delta\rho^A + q \cdot \left(\Delta\rho^A\right)^2 , \tag{4.1.1}$$

with variables $c_0 = 176.6\ m/s$, $p = 16.6\ c_0{}^2/\rho_0{}^A$, $q = 79.5\ c_0{}^2/(\rho_0{}^A)^2$ and $\rho_0{}^A = 4.877 \times 10^{-3}\ g/m^2$ and the expanded sound profile as a function of density is shown in Figure 4.1.1 .
If one chooses a bulk density larger than $\rho_0{}^A = 4.877 \times 10^{-3}\ g/m^2$, one will obtain solitons which will pass the density $\rho = 4.035 \times 10^{-3}\ g/m^2$. When the membrane density is $\rho = 4.035 \times 10^{-3}\ g/m^2$ and the corresponded temperature is $T = 45$ °C (the bulk temperature from [2]) the membrane is in the fluid state. When the membrane is in the fluid phase, the sound velocity as a function of density is not described by equation (4.1.1). The sound velocity before this point is taking a more linear and not nearly as steep slope relative to the equation (4.1.1), as illustrated in Figure 2.1.5. However, in this thesis the sound profile in the region before $\rho = 4.035 \times 10^{-3}\ g/m^2$ is described by eq. (4.1.1), as after the point. In *Lautrup et al.* [46] a soft barrier was introduced when the density exceed the phase transition. Oppo-

site, when the density exceeds the phase transition and is fully in the fluid phase, there is no soft barrier, but more the opposite of it. This assumption has no effect on the lower limit velocity, since this is dependent on the difference between the sound speed at the bulk density and minimum in the profile, from eq. (2.3.12):

$$\Delta c = c_0^2 - \left(c_0^2 + p\Delta\rho_{\min} + q\Delta\rho_{\min}\right) = c_0^2 - \left(c_0^2 + p\frac{-p}{2q} + q\left(\frac{p}{2q}\right)^2\right) = \frac{2}{3}\frac{p^2}{6q} \quad (4.1.2)$$

$$v_{\text{limit}}^2 = c_0^2 - \frac{p^2}{6q} = c_0^2 - \frac{2}{3}\Delta c \quad (4.1.3)$$

Where $\Delta\rho_{min}$ is the value of $\Delta\rho$ where c^2 has a minimum. This assumption will influence the amplitude of the solitons. The maximum amplitude for the lowest velocity depends on the difference in the density between the two points that take the value of c_0. A generalization of this is that the minimum velocity depends on the shape of the sound profile and the depth, where the amplitude depends on the wideness of the sound profile.
The result for colliding solitons presented in section 5.1.2 will in some cases have a density lower than $\rho = 4.035 \times 10^{-3}\ g/m^2$ and no significant difference was noticed. Therefore for this study, with a bulk temperature of $T = 39.6$ °C, the assumption is valid.

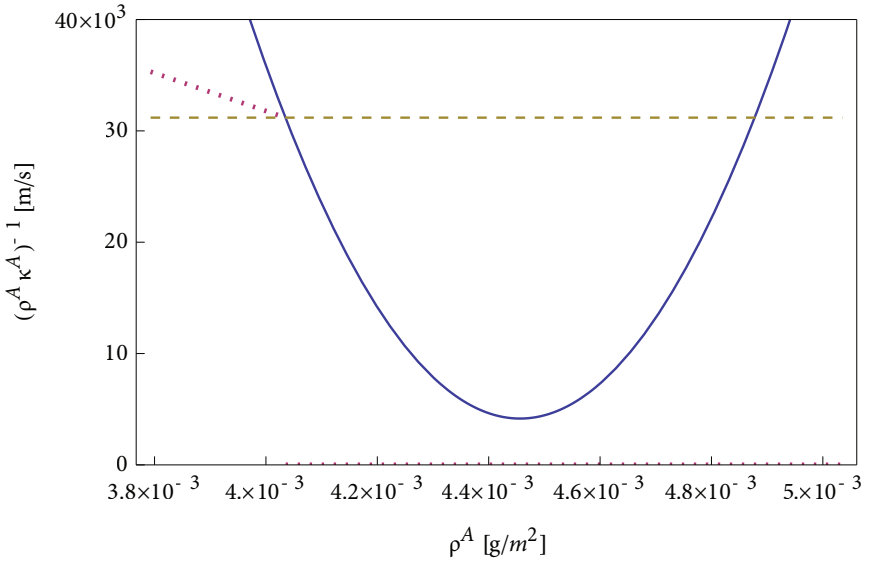

Figure 4.1.1 – The expanded lateral sound velocity for low-frequency as a function of density. The dashed line is the sound velocity of small amplitude sound c_0. Dotted line is an illustration of the sound velocity in the fluid phase.

4.2 Sound profile for a 50:50 DMPC:DSPC membrane

From the heat capacity, the total enthalpy change can be calculated by integrating the heat capacity from a temperature in gel phase to the fluid phase:

$$\Delta H = \int_{T_{gel}}^{T_{fluid}} c_p dT \tag{4.2.1}$$

The ratio of lipids in the fluid state at temperature T is then the ratio between enthalpy change at temperature T and the total enthalpy change:

$$f(T) = \frac{\Delta H_T}{\Delta H} = \frac{\int_{T_g}^{T} c_p dT}{\int_{T_g}^{T_f} c_p dT} \tag{4.2.2}$$

The lipid fraction in the solid state is then $g = 1 - f$. From [29] one knows that the specific volume, specific area and compressibilities of a membrane to a given temperature is given by:

$$\mathrm{X}(T) = (1-f)\mathrm{X}_{gel}(T) + f \cdot \mathrm{X}_{fluid}(T) = \mathrm{X}_0(T) + f \cdot \Delta \mathrm{X}(T) \tag{4.2.3}$$

X_{gel} denote the property as a function of temperature, under the assumption that the membrane only can be in the gel phase. The specific volume is the sum of the volume in the gel phase and the volume change of the membrane through the phase transition:

$$V(T) = V_0^{gel}(T) + f\Delta V(T) \tag{4.2.4}$$

A membrane that does not undergo a phase transition and is in all temperatures in the gel phase has the following specific volume expansion

$$V_0^{gel}(T) = V_{T_{gel}}^{gel}\left(1 + \frac{1}{V}\frac{dV_{gel}}{dT}\Delta T_{gel}\right), \tag{4.2.5}$$

where $(dV/dT)/V$ is the intrinsic thermal volume expansion coefficient for the gel phase, and $V_{T_{gel}}^{gel}$ is the volume of the membrane in the gel phase with temperature T_{gel}, all values can be measured experimentally, and the temperature change is defined as

$$\Delta T_{gel} \equiv T - T_{gel}\,. \tag{4.2.6}$$

The specific volume change through the phase transition is the difference between the specific volume in the fluid and gel phase

$$\Delta V(T) = V_0^{fluid}(T) - V_0^{gel}(T) = V_{T_{fluid}}^{fluid}\left(1 + \frac{1}{V}\frac{dV_{fluid}}{dT}\Delta T\right) - V_0^{gel}\,, \tag{4.2.7}$$

where *(dV/dT)/V* is the intrinsic thermal volume expansion coefficient for the fluid phase, and $V_{T_{fluid}}^{fluid}$ is the volume of the membrane in the fluid phase with temperature T_{fluid}, the temperature change is the difference between the temperature and the fluid phase temperature.
Similar, the specific area change for a membrane can be calculated as

$$A(T) = A_0^{gel}(T) + f\Delta A(T), \tag{4.2.8}$$

with the specific area change for the gel phase

$$A_0^{gel}(T) = A_{T_{gel}}^{gel}\left(1 + \frac{1}{A}\frac{dA_{gel}}{dT}\Delta T_{gel}\right), \tag{4.2.9}$$

where *(dA/dT)/A* is the intrinsic thermal area expansion coefficient for the gel phase and $A_{T_{gel}}^{gel}$ the specific area at temperature T_{gel}. The specific area change is then:

$$\Delta A(T) = A_{T_{fluid}}^{fluid}\left(1 + \frac{1}{A}\frac{dA_{fluid}}{dT}\Delta T\right) - A_0^{gel} \tag{4.2.10}$$

When the specific area and volume is known, one can calculate the lateral density and the thickness of the membrane

$$\rho(T) = 1/A(T) \qquad D(T) = V(T)/A(T) \tag{4.2.11}$$

The lateral density is choose, since the 2D case of the membrane is considered in *the soliton model*.
From equation (2.1.20) the area compressibility as the sum of the intrinsic compressibility and the lateral excess compressibility:

$$\kappa_T^A(T) = \kappa_{T,0}^A(T) + \Delta\kappa_T^A(T) \tag{4.2.12}$$

The intrinsic compressibility is due to eq. (4.2.3) a function of the intrinsic compressibility for the gel and fluid phase:

$$\kappa_{T,0}^A(T) = (1-f)\kappa_{T,0}^{A,gel}(T) + f\kappa_{T,0}^{A,fluid}(T) \tag{4.2.13}$$

The lateral excess compressibility is given by:

$$\Delta\kappa_T^A(T) = \frac{\gamma_A{}^2 T}{A(T)}\Delta c_p \tag{4.2.14}$$

Notice that lateral excess compressibility only takes values above zero in the phase transition, since the different in heat capacity between the gel and fluid phase is zero.

When the adiabatic compressibility from eq. (2.1.22) is considered, one has to consider the whole system that contains the lipid membrane, e.g. an aqueous media. The adiabatic compressibility for the lipids can be expressed as

$$\kappa_S^A(T) = \kappa_{T,0}^A(T) + \Delta\kappa_T^A(T) - \frac{T}{Ac_p}\left(\frac{dA}{dT}\right)_p^2, \tag{4.2.15}$$

where c_p is the heat capacity of the whole system. Heat capacities, there describe a heat sink, depending on the time scale of the compression so that $c_p = c_p(\omega)$. On a time scale much longer than that of relaxation processes in the membrane, the environment of the membrane serves as a heat reservoir. As a result, c_p is large and $\kappa_s \approx \kappa_T$.
If the volume expansion coefficient of the lipid chains is neglected, $dV/dT = \gamma\Delta c_p$:

$$\kappa_S^A(T) \approx \kappa_{T,0}^A(T) + \Delta\kappa_T^A(T)\left(1 - \frac{\Delta c_p}{c_p}\right) \tag{4.2.16}$$

Ultrasonic velocity measurements at a frequency of *5 MHz* show that ultrasonic velocities as a function of temperature can be calculated accurately from the heat capacity if it is assumed that there is no heat transfer between the membrane and the surrounding [2]. This means at high frequencies $c_p = \Delta c_p$ and the related term to the lipid state in adiabatic compressibility is zero.

To investigate the possibility of coexistence, behaviour and interactions of negative and positive solitons, one needs a reference media where they can coexistent at same temperature. The chosen media was a membrane with a 50:50 lipid mixture of 1,2-Dimyristoyl-*sn*-glycero-3-phosphocholine (DMPC) and 1,2-Distearoyl-*sn*-glycero-3-phosphocholine (DSPC), with a chain length of 14 and 18, and a melting point at *23.6 °C* and *54.7 °C* receptively. The heat capacity profile for 50:50 DMPC:DSPC is shown in Figure 4.2.1, where the two maxima are approximately at *30 °C* and *44 °C*, and a local minimum at *35 °C*. This can be compared to Figure 4.2.2, where the heat capacity for an ideal mixture is calculated from the enthalpy changes and the melting temperatures for DMPC and DSPC, which gives that the ideal mixture method is not suitable in use to calculate each of the individual lipid species contributions to the physiological change through the phase transition. However, with the assumption that the two lipid species will have the same properties through the phase transition, as characterized by Figure 4.2.1, one can calculate the volume, area and compressibility change. 1,2-Dipalmitoyl-*sn*-glycero-3-phosphocholine (DPPC) is a suitable lipid to assume that the lipids in a 50:50 DMPC:DSPC mixture will act like, because taking the average between DMPC and DSPC physiological properties, one gets properties very near to the ones DPPC has. DPPC has a chain length at 16, a melting temperature at $T_m = 41.3\ °C$ and enthalpy change of $\Delta H = 38.1\ kJ/mol$. DPPC's specific volume, intrinsic thermal volume expansion coefficient, volume compressibility is in the gel phase approximately below *0.5 %* and in the fluid phase approximately below *1.5%* from DMPC and DSPC values, and very close (below *0.1 %),* to the average

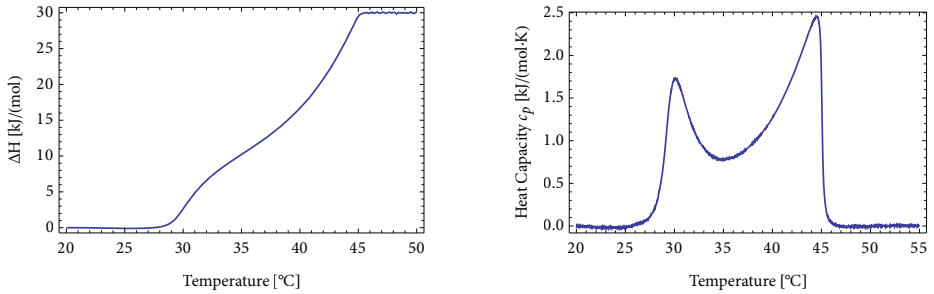

Figure 4.2.1 – Experimental heat capacity profile of a 50:50 DMPC:DSPC mixture adapted from Seeger et al. (2005) [35]. *The heat capacity profile has two maxima approximately at 30 °C and 44 °C, and a local minimum at 35 °C.*

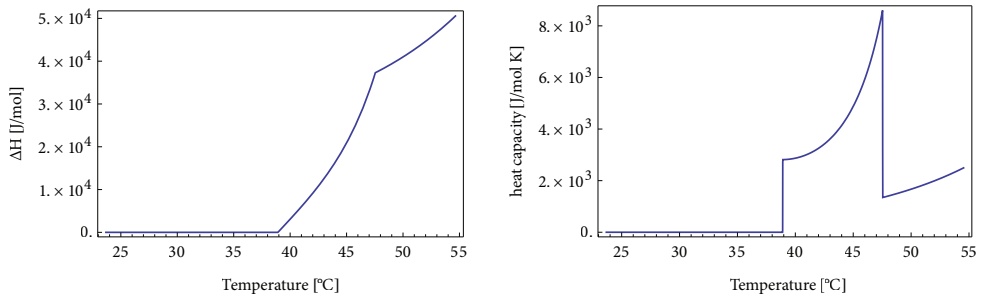

Figure 4.2.2 – Heat capacity calculated as an ideal mixture for DMPC and DSPC, with the values ΔH = 23.9 kJ/mol and T_m = 23.6 °C for DMPC, and ΔH = 50.7 kJ/mol and T_m = 54.7 °C for DSPC.

Table 4.2.1 – Literature data of membrane parameters and elastic constants of DPPC (the parentheses have the phase and temperature the properties is measured in).

		Gel	*Fluid*
	Molar mass [g/mol]	734.039	
Calorimetric	Heat capacity $c_{p,0}$ [J/molK]	1600 (21.5 °C) [57]	1650 (51.5 °C) [57]
	Melting point main transition [°C]	41.6 [29]	
Volume V	Specific volume [cm^3/g]	0.947 (L'_β, 33°C) [56]	0.999 (L_α, 41.5°C) [56]
	γ^{vol} [cm^3/g]	8.599×10^{-4} [29]	
	Intrinsic thermal volume expansion coefficient (dV/dT)/V [K^{-1}]	0.00088 [56]	0.001 [56]
	Volume compressibility κT [m^3/J]	5.2×10^{-10} [58]	7.8×10^{-10} [58]
Area A	Specific area [cm^3/g]	1.90×10^6 (L'_β, 25 °C) [29]	2.52×10^6 (L_α, 50 °C) [29]
	γ^{area} [cm^3/g]	8.93×10^3 [29]	
	Intrinsic thermal area expansion coefficient (dA/dT)/A [K^{-1}]	0.0026 (25 °C) [59]	0.0042 [a](L_α, 34 °C) [60]
	Area compressibility κ_T [m3/J]	1.0 (L'_β, 25 °C) [61]	6.9 (L_α, 50 °C) [61]

[a]value for DMPC

of DMPC and DSPC values [56]. Using the value for DPPC listed in Table 4.2.1 and the equations above, one can calculate the fractional degree of melting, membrane volume, membrane area, density and thickness shown in Figure 4.2.3(a-f). Here an assumption has been made, that the intrinsic thermal area expansion coefficient in the fluid phase is approximated to DMPC value [29]. The area compressibility can be calculate from eq. (4.2.12) and adiabatic area compressibility from

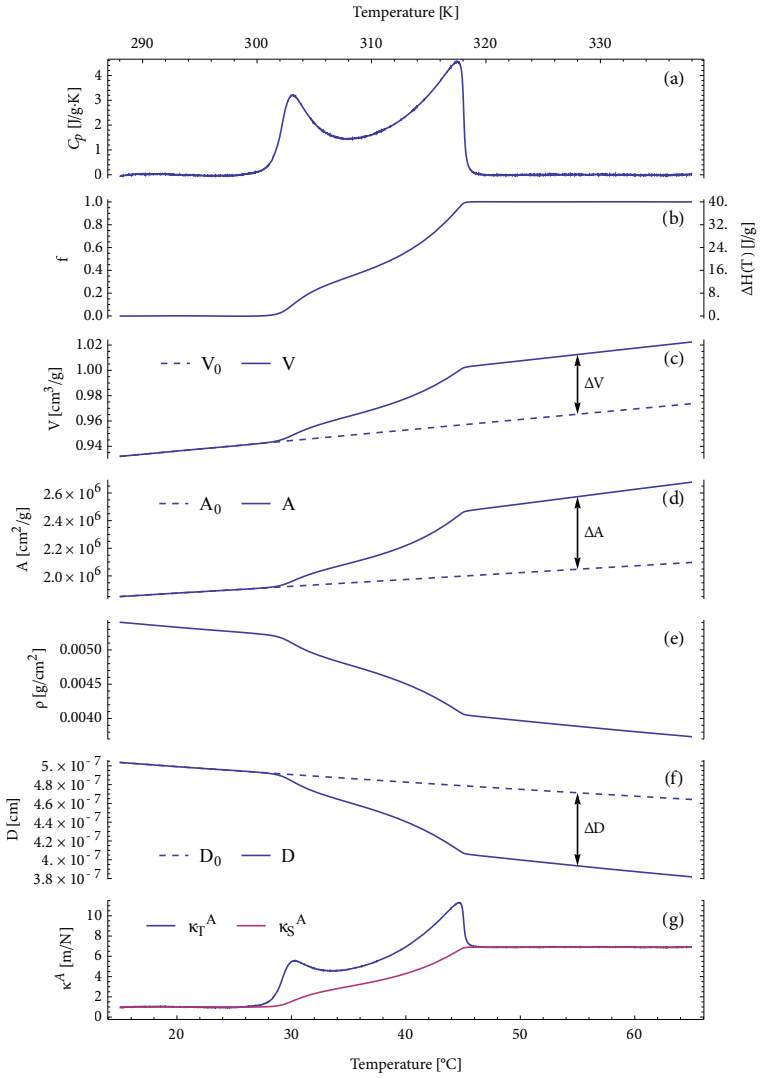

Figure 4.2.3 – Membrane dimensions of 50:50 DMPC:DSPC, calculated from the excess heat capacity. (a) Calorimetric excess heat capacity. (b) Fractional degree of melting, f, and excess enthalpy, ΔH, obtained from integrating the experimental heat capacity profile. (c) Calculated temperature dependence of the membrane specific volume, V. (d) Calculated temperature dependence of the membrane specific area, A. (e) Calculated temperature dependence of the membrane lateral density, ρ. (f) Calculated temperature dependence of the membrane thickness, D. (g) Calculated isothermal area compressibility and calculated adiabatic area compressibility, corresponding to a 5-MHz ultrasonic experiment.

(4.2.16), these are shown in Figure 4.2.3(g), for a low-frequency case ($\kappa_s \approx \kappa_T$) and a 5MHz case ($c_p = \Delta c_p$).
The sound velocity can be calculated from the lateral density and adiabatic area compressibility:

$$c^2 = \frac{1}{\rho \kappa_S^A}. \tag{4.2.17}$$

For the 50:50 DMPC:DSPC membrane the sound velocity profile as a function of density is shown in Figure 4.2.4(a). For small amplitude sound the equation takes the form $c_0 = 1/\sqrt{\rho_0 \kappa_S^A}$. As shown, the area compressibility depends strongly on the density through the phase transition, one can then expand

$$c^2 = \frac{1}{\rho \kappa_S^A} = c_0^2 + p\Delta\rho + q\Delta\rho^2 + r\Delta\rho^3 + \cdots \tag{4.2.18}$$

where $\Delta\rho = \rho + \rho_0$ with ρ_0 as the equilibrium density. For the data from 50:50 DMPC:DPPC one can choose to work with the dimensionless sound velocity

$$B(u) = \frac{c^2}{c_0^{\,2}} = 1 + B_1 u + B_2 u^2 + B_3 u^3 + B_4 u^4 + B_5 u^5 + B_6 u^6 \tag{4.2.19}$$

with the dimensionless variables (similar to section 2.3), *u, x* and *t* defined as:

$$u = \frac{\Delta\rho}{\rho_0}, \quad B_1 = \frac{\rho_0}{c_0^{\,2}} p, \quad B_2 = \frac{\rho_0^{\,2}}{c_0^{\,2}} \mathrm{q}, \quad B_3 = \frac{\rho_0^{\,3}}{c_0^{\,2}} \mathrm{r}, \quad \cdots \tag{4.2.20}$$

By fitting the function to the sound profile one can obtain[4] the values; $c_0 = 2.24988 \times 10^2$ and $\rho_0 = 4.85059 \times 10^{-3}$, and the dimensionless values $B_1 = 2.14164 \times 10^{-4}$, $B_2 = -1.30063 \times 10^2$, $B_3 = -2.41919 \times 10^2$, $B_4 = 2.42545 \times 10^4$, $B_5 = 2.45451 \times 10^5$ and $B_6 = 6.97352 \times 10^5$, assuming a bulk temperature of $T = 33$ °C. The fit is shown in Figure 4.2.4(b).
As seen in Figure 4.2.4(a) the sound velocity in the fluid phase ($\rho < 0.0405$) is al-most constant, and below the sound velocity for the equilibrium density ($\rho_0 = 0.0485$). It can be assumed that the sound velocity in the fluid phase follow the expansion. As mentioned in section 4.1, it can be shown that this approximation only effect the size of the amplitude when the velocity is near the minimum velocity, since the minimum sound velocity occurs just before the fluid phase.

4 These are not the values from the best fit, but these are the values that will be used. The dimensionless function differ less than 5 % from the function for the best fit. The two minimal has a small shift to the right, but the shape of the two functions is similar. This choice will have no effect on the results presented, more than a small variation and no influence on the phenomena presented and described. However, the membrane's sound velocity profile and the properties are all assumptions, and therefore, can these values be assume to be the ones for 50:50 DMPC:DSPC. The difference between this fit and the best fit is shown in Appendix E.

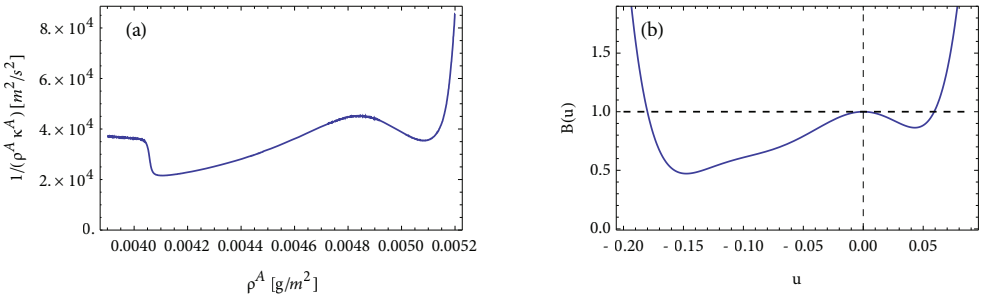

Figure 4.2.4 – (a) The lateral sound velocity, c^2, for the low-frequency case as a function of membrane density. (b) a fit to the dimensionless lateral sound velocity, B(u), as a function of u with a bulk temperature of T = 33 °C.

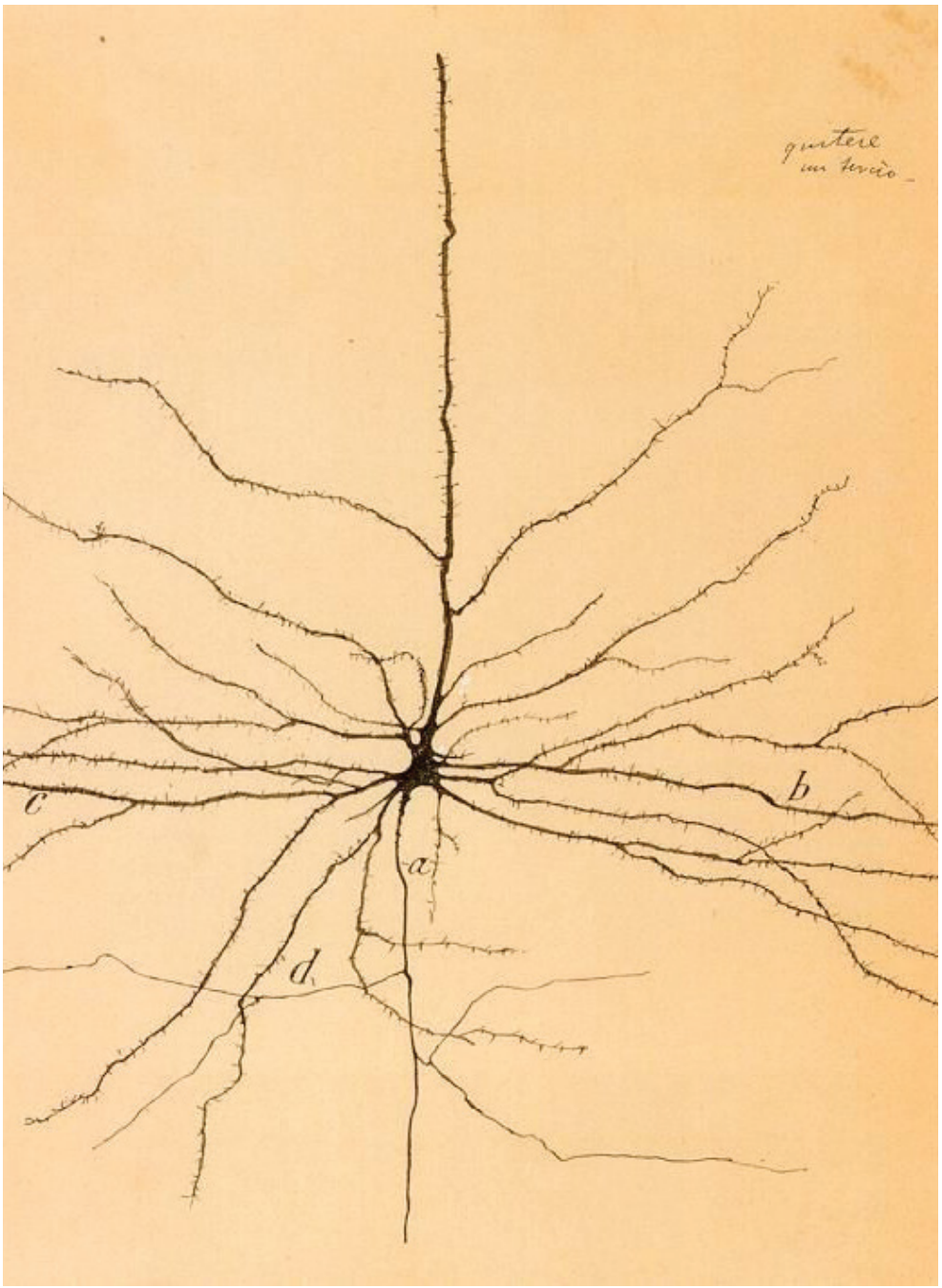

Drawing of a neuron, human retinaal cell, by Santiago Ramón y Cajal, 1899. This drawing is amoing the first drawing of a neuron. Ramón y Cajal was the Spanish physician and early neuroscientist who first discovered that the nervous system was not continuous but was comprised of interconnected individual cells.

Chapter 5

Results

One of the aims in this thesis is to investigate the possibility of negative solitons, their propagation and behaviour. Solitons in membranes have been investigated and described by *Heimburg and Jackson* [2] and *Lautrup et al.* [46], for different lipid compositions, DPPC LUV and bovine lung surfactant. They choose to assume that the membrane is slightly above the melting temperature, in the fluid state, and obtain that density waves, the solitons, are through the transition and therefore a positive change in the density. These soliton will be referred to as *positive solitons*, due to the positive density change. In literature these solitons are also called *bright solitons*. Similar, a soliton with negative density change will be referred to as *negative soliton* (*dark solitons*).
The first part of this chapter is the result for an DPPC LUV membrane, similar to the one investigated in [2], [46], [47], will be presented. But the result will be for the membrane in the state before the melting temperature, the gel state, which should allow negative solitons. Thereafter the results for a membrane of mixed lipids with two melting temperatures is presented. A membrane with two melting temperatures and thereby two phase transitions is a suitable membrane for allowing both negative and positive solitons.

5.1 Solitons in DPPC LUV Membranes

In the paper *"On soliton propagation in biomembranes and nerves"* by *Heimburg and Jackson* [2], they used DPPC vesicles as a reference. DPPC is a well-studied lipid and is a major component of biological membranes [15]. The thermodynamic data for DPPC vesicles is shown in Figure 2.3.1 and they assume a bulk temperature at $T = 45°C$ and expand the sound profile to eq. (2.3.2) and got solitons that move the membrane through the melting transition and obey eq. (2.3.3).

5.1.1 Analytic Solution

Using the same procedures as presented in section 2.3 one can obtain analytic solutions for solitons with the sound profile, presented in section 2.3. Propagation of sound in membrane is described by eq. (2.3.3) and introduce the dimensionless variables from eq. (2.3.5) we have the dimensionless sound equation for membranes:

$$\frac{\partial^2 u}{\partial t^2} = \frac{\partial}{\partial x}\left(\left(1 + B_1 u + B_2 u^2\right)\frac{\partial u}{\partial x}\right) - \frac{\partial^4 u}{\partial x^4} \tag{5.1.1}$$

Where $B_1 = 16.6$ and $B_2 = 79.5$. In [2] they required, because of the qualitative features of the empirical compression modulus, $B_1 < 0$ and $B_2 > 0$. However, in this situation, with the sound profile for the membrane in the gel state, it requires that $B_1 > 0$ and $B_2 > 0$.
From eq. (2.3.11) one has the relation that two real roots exist only when

$$1 > |\beta| > \beta_0 = \sqrt{1 - \frac{B_1^2}{6B_2}}, \tag{5.1.2}$$

where the roots is

$$a_{\pm} = -\frac{B_1}{B_2}\left(1 \pm \sqrt{\frac{\beta^2 - \beta_0^2}{1 - \beta_0^2}}\right). \tag{5.1.3}$$

When $B_1 > 0$ and $B_2 > 0$ both roots are negative and the absolute smallest root is the amplitude of the soliton described by eq. (2.3.14).
All the properties described in section 2.3, such as conservation laws and energy,

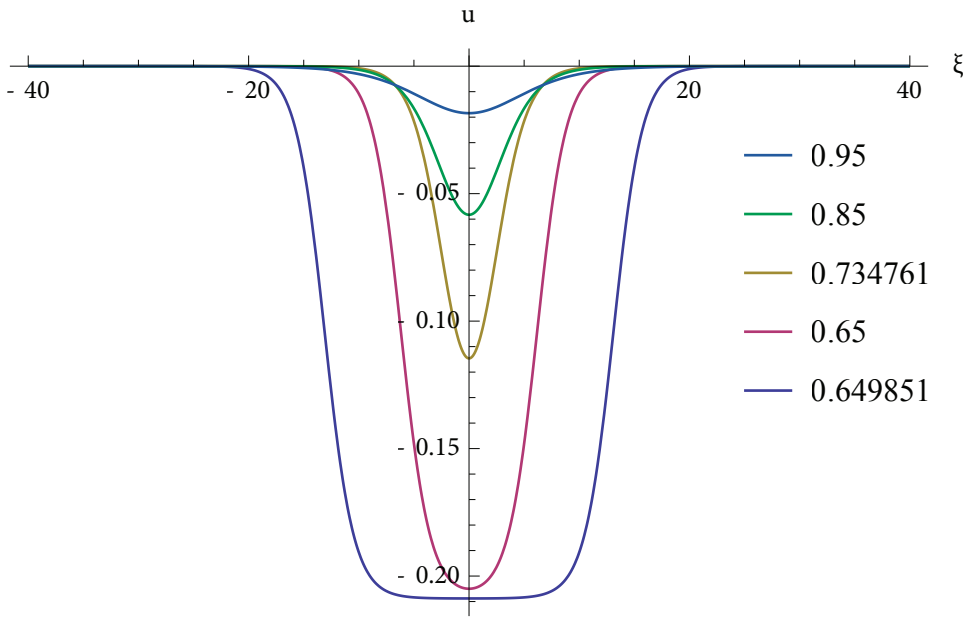

Figure 5.1.1 – Soliton profiles with different velocity, β.

for the positive solitons holds also for these negative solitons. E.g. the energy density is described by:

$$\varepsilon = u^2\left(1+\tfrac{1}{3}B_1u+\tfrac{1}{6}B_2u^2\right) \tag{5.1.4}$$

For the positive solitons u will be positive for all ξ, and B_1 negative, meaning that the second term, in the parentheses is negative, and the rest positive. For the negative solitons u will be negative for all ξ, and B_1 positive, meaning that the second term is also negative. This shows that the only difference between the stable positive solitons, and negative is the sign of the density change. Negative solitons are shown in Figure 5.1.1 for various velocities, β, compared to Figure 2.3.2 (positive solitons), which shows that the negative solitons have the same amplitude for the same velocity as the positive ones.

5.1.2 Collision of negative solitons

One of this thesis' aims is to see how these negative solitons differ from the positive, described in section 2.3.4 and by *Lautrup et al.* [46], when they collide or decay. By using the *two-step Lax-Wendroff method* the solution to a given time can be numerical calculated. *Lautrup et al.* made an analysis of small-amplitude perturbations and stability of the soliton in the *two-step Lax-Wendroff method*. The analysis can be transferred to this study, because the basic density change equation is one the same form. The negative solitons behave like the positive solitons. Figure 5.1.2 show collision of two solitons before and after collision (in Appendix C.1 a time series of two soliton colliding is shown) . The solitons with a velocity of

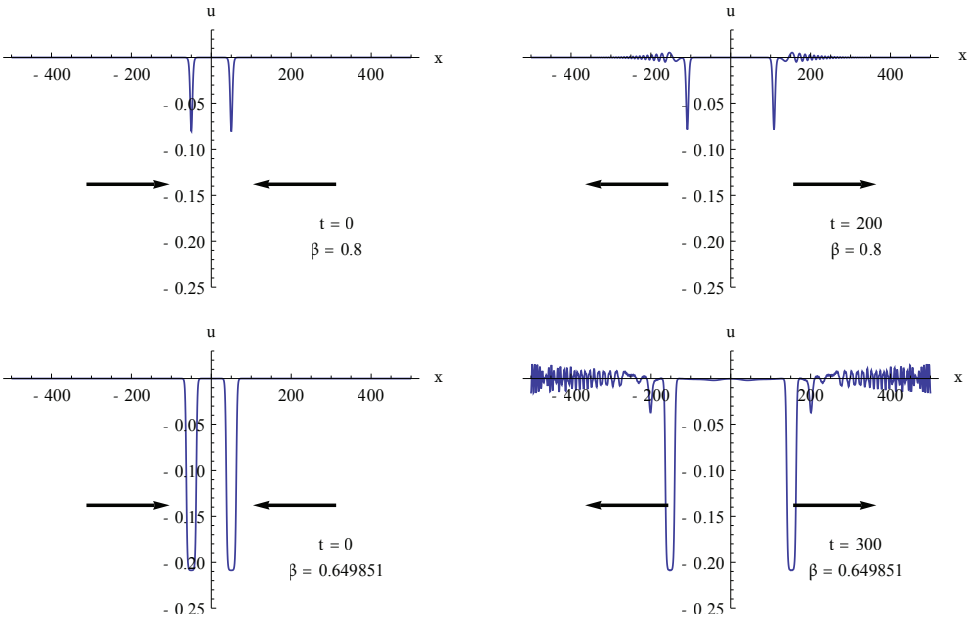

Figure 5.1.2 – Collision of negative solitons, show that they emerge from the collision almost unchanged, with small-amplitude waves ahead of them. The emission of the small-amplitudes waves make them solitary waves and not solitons, since they will emerge unchanged.

$\beta = 0.8$ have after the collision small-amplitude waves traveling ahead of them. For the $\beta = 0.649851$ solitons they have more small-amplitude waves ahead of it, and just in front of them appear a solitary wave, the solitons are falling apart into smaller solitary waves. Comparing the figure to Figure 2.3.5 (collision of positive solitons), the only difference between the collision of the negative and positive solitons with velocity $\beta = 0.8$ is the sign of the density change, the result is the same; penetration and small-amplitude waves. For the solitons with velocity $\beta = 0.649851$ the difference is bigger. The collision of the positive solitons result in several solitary waves ahead of them, where the collision of negative solitons only have one visible after the same time. This difference is because the collision of positive solitons reach the soft barrier introduced by *Lautrup et al.*. Without this barrier the result will be the same, only with different direction of the density change.

5.1.2.1 Delay of the solitons

As mentioned, the normal behaviour of two solitons colliding (in any field of physics) is that they will be delayed in their further propagation, compared to if they just pass through each other without any interaction. As shown, the collision in a biological membrane leads to a small energy loss, which result in an acceleration of the solitons. These two things combined give a complex system for the delay of solitons, because the solitons will be delayed in the collision, and right thereafter accelerate to a larger velocity. This means that depend in which point the measurement is in, the arrival of the solitons both can be before or after what is expected, if they just pass through each other. This delay as a function of velocity is shown in Figure 5.1.3. The delay is calculated from collisions of two identical solitons started with a distance of $\xi = 100$ (at $\xi = \pm 50$), where the equation of motion was found before and after the collision. The solitons have no tend to accelerate or decelerate before and after the collision, and therefore the velocity is constant. When the equation of motion of the solitons before the collision is known, one can calculate the delay after the collision by subtraction the actual time the soliton arrive at a point from the expected time from equation of motion. In Figure 5.1.3 the *"After collision"*-curve is calculated at a point between the two solitons initial state, at $\xi = 25$ (the collision happens at $\xi = 0$), and since the solitons is symmetric, the same absolute equation of motion can be obtain for both side. From the equation of motion of the solitons after the collision, the maximum delay can be approximated (*"At collision"*-curve), by the different between the collision time from the motion before and after the collision.

It can seems strange, that for velocity near the minimum limit, the delay is negative. The reason is that the acceleration of the solitons start already in the first part of the solitons in the collision, before the actual collision between the points of the theoretical maximum of the two solitons. Therefore, the movement has been accelerated and have caused to make up for the delay before the actual collision (when they are fully overlapping).

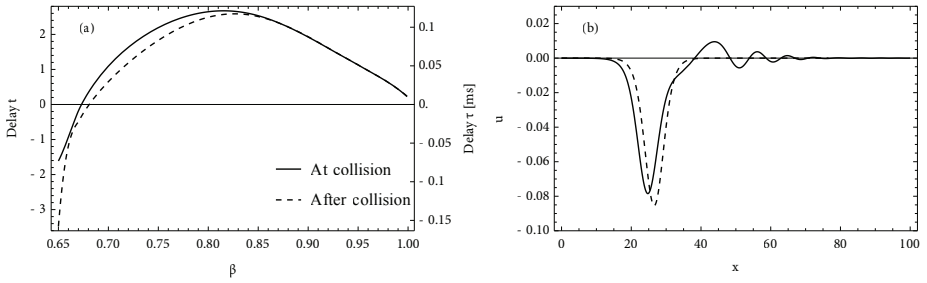

Figure 5.1.3 – (a) The delay of the soliton as a function of the velocity. The curves is the result of 25 simulations of collision of solitons at different velocities. "At collision" show the calculated delay at the collision, and "after collision" show the actual delay down of the collision. (b) Soliton with start velocity β = 0.79 after the collision (solid line), dashed is the projected solitons and represent the soliton if no collision have happen. It clearly to see that there is a delay and an amplitude change.

5.1.3 Disturbance in the soliton

In section 2.3.4, was disturbance in a positive soliton described. A distortion in the second initial condition, the velocity depended,

$$v(x,0) = p\beta u(x,0), \tag{5.1.5}$$

results in two solitons traveling in the opposite direction, and small-amplitude waves ahead of them. In Figure 5.1.4 the same is done for a negative soliton, with $\beta = 0.735$ and $p = 0.5$. The same happens as for the positive soliton with the same conditions. The negative is divided into two solitons, the big one travel in the same direction as a soliton without disturbance, and therefore is the initial soliton, where the small one travels in the opposite direction. Ahead of the solitons travels small-amplitude waves, which carry approximately 0.3 % of the initial energy. The rest of the energy is in the solitons. The two solitons quickly reach a velocity where it matches the amplitude. Subtracting the soliton, as shown in Figure 5.1.4 (c), only the small-amplitude waves is left.

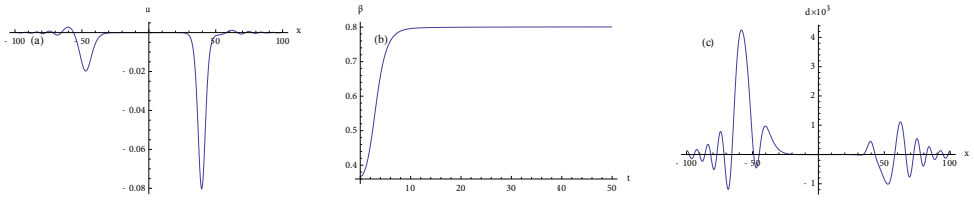

Figure 5.1.4 – (a) Soliton, shown at t = 50, with an initial amplitude corresponded to the one for the velocity β = 0.735 and with the condition p = 0.5, change shape after emission of a smaller soliton, which moves in the opposite direction. Small-amplitude waves run ahead of them. (b) Velocity of the initial soliton show that it quickly reach a stable velocity, and within the first space, ξ < 8. (c) The two solitons subtracted from (a) and only leave the small-amplitude waves.

By making a distortion in the first initial condition, the amplitude, the initial condition become

$$u(x,0) = p\,u'(\xi) \tag{5.1.6}$$

$$v(x,0) = \beta\,u(x,0) \tag{5.1.7}$$

where u' is the soliton described by equation (2.3.14) with velocity β. For $p > 1$ gives a initial soliton with a faster velocity than the stable soliton with same amplitude. The result for $p = 1.5$ and $\beta = 0.735$ is shown in Figure 5.1.5. The soliton decay to the velocity correspond to the amplitude. From the soliton, propagate small-amplitude waves in both direction. The energy carried by the small-amplitude waves is less than 1 % of the initial energy. The velocity quickly drop to a velocity near the ideal velocity, and after that slowly decay towards it. The reason that the velocity change, and not the amplitude, is that the energy released when the velocity drops is less than a change in amplitude will result in (see eq. (2.3.26)). When p takes values where the amplitude do not excess the maximum amplitude, the soliton will adjust to a velocity where it is stable, and there will be emitted small-amplitude waves. It can be shown that a small change in the velocity, both faster and slower, will result in a stable soliton that will keep the amplitude but changes to a velocity where it is stable, and in the process emits small-amplitude waves which will carry a small amount of the initial energy.
When p is increasing, the initial soliton will emit a soliton in the opposite direction as seen in Figure 5.1.6. The two solitons have a mismatch between theirs amplitude and velocity, the initial one is subsonic ($\beta < \beta_0$) but near the limit and the emitted soliton is faster than it should be, compared to the analytic soliton with same amplitude. The two solitons can be categorized as unstable solitons, but they will over many iterations decay to stable solitons, where the velocity match the amplitude. For higher p the energy ratio bound in the soliton is smaller, and the amount of small-amplitude waves is higher. Ahead of the initial soliton, there is a compressible plateau or field, which can be seen as a wide small-amplitude wave. In the opposite direction a similar plateau is found, where the emitted soliton is overlapping. The plateaus has a supersonic velocity, and it will over time become

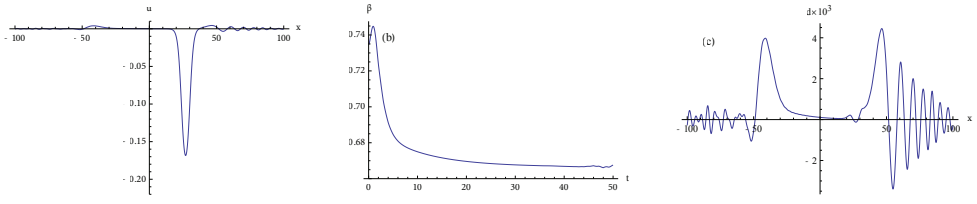

Figure 5.1.5 – (a) Soliton shown at t = 40, with an initial amplitude 1.5 the size of the corresponded velocity dictate, β = 0.735, the shape remain the same and small-amplitude waves is running away, in both direction. (b) the velocity of the soliton decay to the velocity that corresponds the amplitude. The small fluctuations in the velocity between t = 45 and 50, is collision with the small-amplitudes waves travelling the opposite direction and collide with the soliton because of the periodic boundary condition. (c) the soliton subtracted and only small-amplitude waves is left.

wider, because the velocity in the front is bigger than in the end. When the soliton is overlapping, it is speeding up and when it is just behind it, in the plateau tails, it is slowing down. When no overlapping the soliton will speed up to a constant sonic velocity and be stable. For $p = 3.5$ it will take $t = 250$ for initial soliton to get free of the plateau, where the emitted still overlap after $t = 1000$.

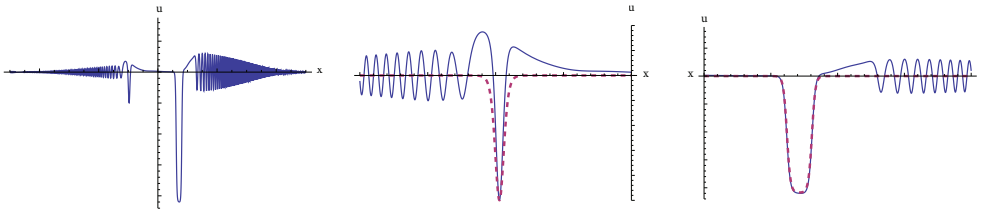

Figure 5.1.6 – Soliton shown at t = 100 with p = 3.5, show that the initial soliton emits a soliton in the opposite direction. (b) the emitted soliton have a mismatch between amplitude and velocity, the velocity is β = 0.956 (u = -0.016) and should have β = 0.870 (dashed line) to be stable with this amplitude (-0.05). The emitted soliton seems to be in a density compression field, which is speeding up the soliton, a similar field is between the initial soliton and the small-amplitude waves ahead of it. (c) the initial soliton decay to a soliton with a miss match between the amplitude and velocity. The velocity is subsonic β = 0.635 and should be 0.649852 (dashed line). The amount of the small-amplitude waves increases with bigger p, and thereby less initial energy bound in the solitons, here 65 % is bound in the solitons.

5.2 Solitons in a mixed lipid membrane

As shown in the previous section a system with negative soliton is a system where a negative density change forces the system into the phase transition. From Heimburg and Jackson [2] it was shown that a system with positive solitons, is when a positive density change force the system into the phase transition. For both systems the sound profile has to be non-linear. Therefore it is expected that a system where both a negative and positive density change forces the system into a phase transition at a certain bulk temperature. Such a system needs to have a heat capacity with two peaks. Such an environment could be a 50:50 DMPC:DSPC membrane, as mentioned before. As shown in its heat capacity it has a wide melting transition with two peaks. By choosing a bulk temperature between the peaks, it seems like it has two phase transitions, one in both direction. It is interesting to investigate this kind of heat capacity, because it looks like that of a biological membrane.

5.2.1 Stable Soliton

Using the same procedure as in the previous section and described in section 2.3, one arrives at an equation that can be numerically solved using the Euler Method. Starting with the modified dimensionless sound equation from eq. (2.3.6):

$$\frac{\partial^2 u}{\partial t^2} = \frac{\partial}{\partial x}\left(B(u)\frac{\partial u}{\partial x}\right) - \frac{\partial^4 u}{\partial x^4} \tag{5.2.1}$$

By integrating twice, then multiplying with ∂u/∂ξ and integrating once more to yield:

$$\left(\frac{\partial u}{\partial \xi}\right)^2 = \left(1-\beta^2\right)u^2 + \frac{1}{3}B_1 u^3 + \frac{1}{6}B_2 u^4 + \frac{1}{10}B_3 u^5 + \frac{1}{15}B_4 u^6 + \frac{1}{21}B_5 u^7 + \frac{1}{28}B_6 u^8 \tag{5.2.2}$$

It is seen that this equation (from left hand side) has a maxima or minima and it is symmetric around it. Solutions to this equation can both be negative and positive solitons, with a limit minimum velocity when the right hand side of the equation only has one real solution, these velocities were found to be $\beta_0 \approx 0.875681$ and $\beta_0 \approx 0.972626$, respectively for the negative and positive soliton. There exist no positive solitons with velocity below $\beta < 0.972626$. No solution that was a combination of a negative and positive density change was found. The sound profile can be split in two, and be treated as a system with only negative solitons, left hand side of the sound profile (section 5.1) and a system with only positive solitons, right hand side, (Heimburg and Jackson [2], Lautrup et al. [46]). This can be compared to the systems mentioned. Different solutions for various velocities are shown in Figure 5.2.1, and they are similar in shape to those already presented in previous sections. The amplitude is approximately inversely proportional to the velocity, and the width of half maximum goes towards infinity when the velocity goes towards the limits, minimum ($\beta = \beta_0$) and maximum velocity ($\beta = 1$). In between the limits there is one minimum, this is shown in Figure 5.2.2. This is in accordance to the

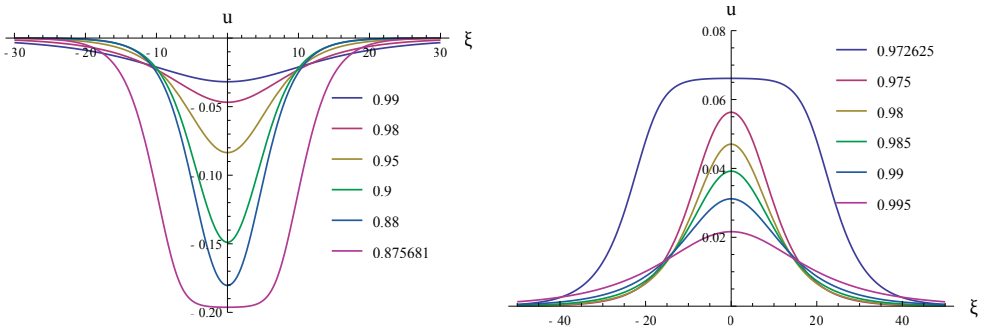

Figure 5.2.1 – Negative and positive solitons for various velocities. They have same characteristics as the soliton described in previous sections. When the velocity is near the minimal velocity the soliton become wider, and a plateau is formed in the top.

two system for DPPC with different bulk temperatures, previous described.
It can be shown, that the minimum velocity depends on the difference between the sound profiles minimum and the sound velocity for the equilibrium density. And that the amplitude for solutions with the minimal velocity depends on the distance between the equilibrium density and the density where it again reaches the sound velocity equal to the one for the equilibrium density.
No analytic solution to equation (5.2.2) could be found, and therefore the differential equation could only be solved using numerical methods. As shown in section 3.1 the error is low using *the Euler Method* when the step size is small, and it is therefore a good approximation to the exact solutions.

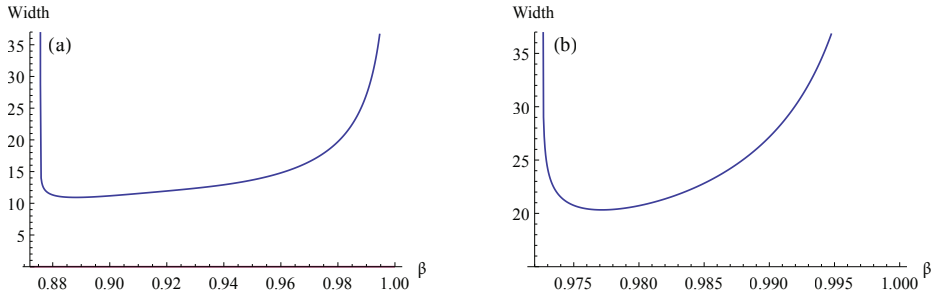

Figure 5.2.2 – Width of the solitons as a function of velocity. It is clear that the limit where the velocity goes toward the minimum velocity the width goes toward infinity, and same when the velocity goes toward 1 and amplitude towards 0. (a) Width of negative solitons as a function of velocity (b) width of positive solitons as a function of velocity.

5.2.2 Collision of Solitons

Figure 5.2.3 shows the result of collisions of positive and negative solitons for different velocities. For all collisions of solitons, the result is them passing through each other and the emission of small-amplitude waves traveling in front of them. The amount of small-amplitude waves depend on how close the solitons are to the minimum velocity, and thereby near the maximum amplitude before the collision. After the collision the solitons have a loss in their amplitude, but no more than

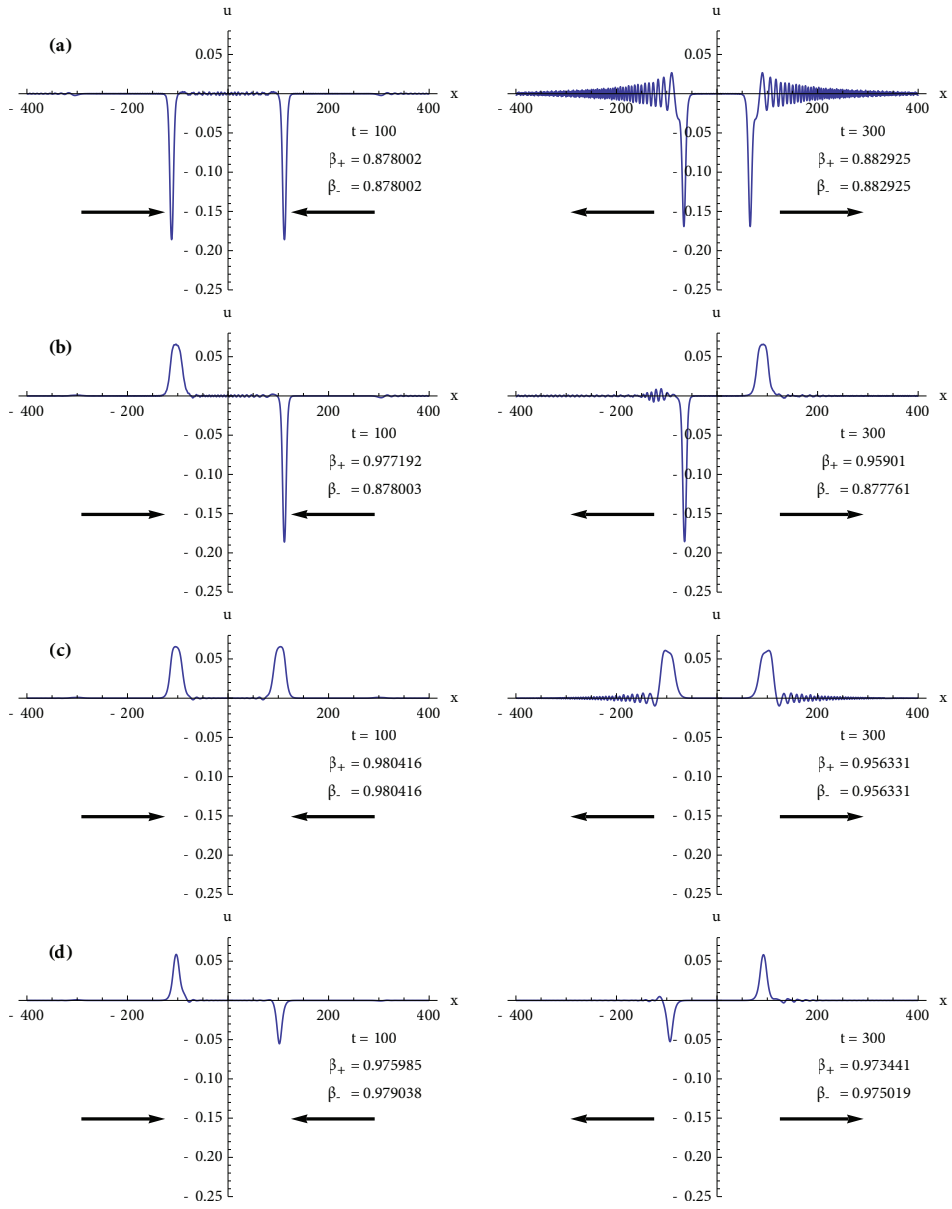

Figure 5.2.3 – Collision of negative and positive solitons with different velocities. It is clearly seen that they pass through each other. When the velocities are near the lower limits, the collision generates small-amplitude waves. (a) two solitons with a velocity near the minimum velocity for negative solitons. (b) two solitons with a velocity near the minimum velocity for a negative and positive solitons respectively. (c) two solitons with a velocity near the minimum velocity for positive solitons. (d) two solitons of approximately same absolute amplitude and shape.

6.5 % (for the minimum velocity case). This is similar to the collision for the basic density change equation.
When the solitons loose amplitude they speed up, this effect is found in most of the results. In those result where the velocity was not exactly found to speed up, the velocity was within a small margin near the velocity before the collision. The

solitons in these results have a large fluctuation in the maximum and there could not be obtained a precise measurement of the velocity, due to small-amplitude waves interfering and the error in the numerical method. One notable thing is, that most of the results, where the velocities could not be found, was the collisions between a negative and positive soliton. They was, of cause, different from each other and there shape was not exactly the same (if they has the same amplitude, then the velocity, absolute mass change and energy is different). In other collisions, was the solitons of same type, amplitude and shape. As seen in Figure 5.2.3(c) right side, the maximum of the solitons is in its front. Just after the collision this maximum is in the back of the solitons. This maximum has over time moved up to the front, and can be linked to a small-amplitude wave with almost the same velocity overlapping the soliton and slow it down, as explained in section 5.1.3 (overleaping density changes).
When the two solitons are colliding they get delayed, but because of the large fluctuation and error, the exact time delay and function for time delay as a function of velocity cannot be calculated. However, in the result where the delay could be estimated, it supported the principle described in section 5.1.2.1.
For some of the collisions, the results have been calculated to a time after they collide again because of the periodic lattice. These results show no difference from the first collision. Therefore solitons can collide several times without being unstable. There has also been calculated result for collision of soliton pairs. Such a pair could be a negative and positive soliton with a small separation. The result here also does not differ from single soliton collision, and the solitons propagate further as stable.

5.2.3 Disturbance in solitons

Finite-amplitude disturbances for negative solitons in the basic density change equation was considered in section 5.1.3. Disturbances in the expanded density change equation show similar results. However, the results differ a little because both negative and positive solitons can propagate and the relative velocity range they can have is smaller compared to those from the basic equation.
First ting to consider, is the distortion in the second initial condition (eq. (5.1.5)) and as shown in Figure 5.2.4, it look a lot like Figure 5.1.4 where it results in two solitons propagating in opposite directions. With the first initial state as a stable

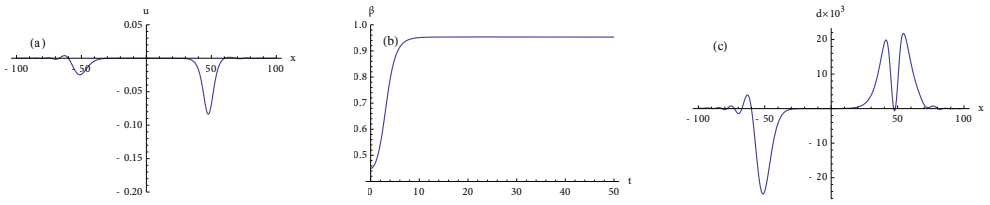

Figure 5.2.4 – Distort in velocity field, v, with p = 0.5. (a) shows a similar result than with the basic density change equation, where initial soliton split into two solitons propagation in opposite direction. However, in (a) it is only the wave in the right side is a stable soliton. (b) velocity for the initial soliton shows that it quickly reach a constant velocity. (c) the right side subtracted a soliton with same velocity, show that it is indeed a soliton.

soliton and the second initial condition with p = 0.5. Results in a stable soliton propagation in the same direction as the second initial dictate, and wit h a soliton-like wave propagating in the opposite direction. The waves in the opposite direction have a shape what could be mistaken as a soliton, but it has a velocity above $\beta > 1$, supersonic, and is too narrow compared to the numerical soliton calculated with same amplitude. The numerical method has an overshoot in the width of the solitons, and even when taking this into account, it is too narrow.
For different stable solitons, the first initial condition with a distortion in the second initial condition (p < 1), no of the results have two stable solitons propagating in opposite directions. Some waves in the opposite direction of the soliton could have sonic velocities but were too narrow to be solitons. This phenomena is not a result of an equation where negative and positive solitons can propagate, but of the small range of velocities for stable solitons. Especially the stable positive solitons have a small velocity span. The maximum density change in the basic and expanded equation is approximately the same, but the lowest velocity is not (basic: 0.649851, expanded: 0.875681). The wave propagation in the opposite direction of the soliton in Figure 5.2.4(a) has an amplitude of approximately -0.02. To have a stable soliton with this amplitude in the basic and expanded equation it must have a velocity of approximately $\beta = 0.95$ and $\beta = 0.995$ receptively. As seen in Figure 5.2.4(b) the initial soliton reaches a constant velocity shortly after the emission of small-amplitude waves. In Figure 5.2.4(c) solitons calculated with Euler method with the same velocity are subtracted from the result. As expected, the soliton from the Euler Method is wider and the soliton on a lattice becomes higher and narrower. The difference is in the same order as the error in Figure 3.2.3, and shows that it is a stable soliton taking the error into account.
If one of the initial differ a little from a stable soliton, the soliton will in short time decay to a stable soliton. The velocity will decay to a velocity corresponding to the amplitude, and small-amplitude waves are created in the process, this is seen in Figure 5.2.5.

From the basic equation it was shown that when the first initial state is an unstable soliton with a larger amplitude than any stable solitons, it will result in two solitons propagation in opposite directions and small-amplitude waves in front of them. The same is found for the expanded density change equation, but instead

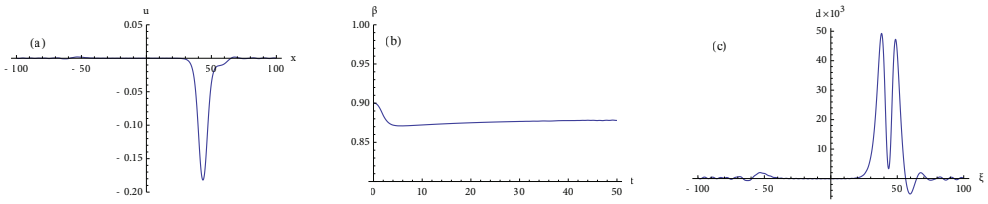

Figure 5.2.5 –Distort in first initial state, u, with p = 1.5 resulting in a bigger soliton. (a) the solitons emits small-amplitude waves in both directions where some is overleaping in front of it. Over time the wave is get free of the soliton. (b) the velocity of the soliton, shows it quickly slowdown to be stable, after that the velocity is increasing over time to a constant velocity. This increasing in velocity is because of the overleaping of a small-amplitude wave. (c) Difference from a soliton with same velocity calculated with Euler Method, where the overleaping small-amplitude wave is seen.

of two solitons, it results in four solitons. Two pairs consist of a negative and a positive soliton. As seen in Figure 5.2.6 the positive solitons are traveling in front of the negative, and a lot of small-amplitude waves are emitted from the decay. The solitons in each pair do not have the same velocity. The positive is faster than the negative, but the velocities are in the range of stable solitons. The numerical soliton calculated from the velocity, fits the negative solitons, and the positive solitons differ both in their amplitude. An explanation is that the small-amplitude waves are overleaping and speed up the solitons, as mentioned in 5.1.3. On an infinity lattice and after an amount of time where the solitons are not overleaping , results with all four solitons having a velocity which matches the amplitude. In Figure 5.2.6 the solitons are overlapping, which both affects the amplitude and the velocity of the positive soliton. In Figure 5.2.6(c) the positive is not overleaping the negative, and therefore the negative is not under the effect of other solitons or small-amplitude waves, and fit to the numerical soliton shown. The positive is under the effect of small-amplitude waves, and has a mismatch between amplitude and velocity. Over time this effect can be neglected, but since both the small-amplitude waves are traveling with $\beta \approx 1$ and the soliton is travelling with a velocity of $\beta = 0.975$, it results in the waves not overlapping until after t = 2000.
The same effect is found with a positive density change instead of a negative. However, due to the smaller velocity range and a small maximum density change, the result of a distortion in the second initial state is a soliton with small-amplitude waves travelling away from it. The distortion in the first initial condition is the same, but the negative is in front of the positive, when the initial amplitude is above the maximum amplitude of a positive soliton.

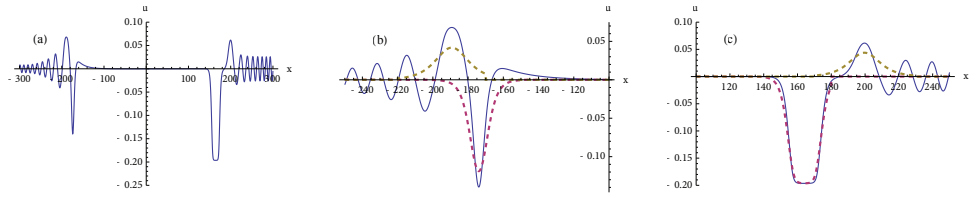

Figure 5.2.6 – When p = 3.0 in the first initial condition, u, give an initial state with a soliton with an amplitude higher than any stable, then initial soliton will split in two pairs of negative and positive solitons. The negative solitons fit approximately to calculated solitons with same velocity. However, the positive solitons seen to propagate faster than they should, since the calculated ones is smaller. Dashed lines is numerical calculated solitons with same velocity.

5.2.4 Initiation

In neurophysiology an excitation of the neuron can be made by applying a voltage pulse between two electrodes on the membrane surface, which results in two symmetrical pulses travelling in opposite direction. However, the physiology behind the excitation is not fully known, but the voltage pulse has to be above a specific threshold to initiate the pulses, meaning a certain amount of energy has to be added to the membrane.
As seen in the previous section a similar situation can be made in the soliton model. A disturbance in the initial states results in two pairs of solitons travelling in opposite direction. As seen in Figure 5.2.6 when the second initial state takes

a value different than null, the pairs propagating in opposite direction are not symmetrical. With a second initial state with the value zero, results in two symmetrical pairs of solitons travelling in opposite direction. To investigate this, the first initial state is a Gaussian function

$$u(0,x) = -Ae^{-\frac{x^2}{\sigma^2}}, \tag{5.2.3}$$

where A is the amplitude and σ is related to the width. As shown in Figure 5.2.7 the initial state(a) will over time result in two symmetrical pairs of solitons travelling in opposite directions with small-amplitude waves in front of them (b). Because of the symmetry around the origin, only one side of the system is necessary in order to calculate properties of the whole system. The results were quantified by identifying the two waves nearest to the origin as solitons or small-amplitude waves. This is done by calculating the velocity of the negative and positive wave, as illustrated in Figure 5.2.7(c) (in Appendix C.2 a time series is shown for these kind of initiation of solitons). If the velocity is sonic, $\beta < 1$, the wave is quantified as a soliton. The system can then have 2 negative solitons, if the negative wave nearest to the origin is sonic, 2 positives, if the second nearest wave or nearest positive wave is sonic, two pairs of a negative and positive soliton when both of the nearest two waves is sonic. The results show that 2 negative solitons could exist without any positive solitons, and vice versa. This was only found in a small range of situations. No results show more than 4 solitons total, and when the initial state is negative, the nearest wave to the origin is negative wave. In extreme high energy cases there was a small positive density change right after the negative soliton. This can be explained by the positive soliton being extremely wide compared to the negative soliton, and it is therefore overlapping totally the negative soliton.
All the quantities presented in this section are found at time $t = 360$, which was chosen since the positive and negative have the time to move away from each other and therefore the effect of the interaction between them is minimize. All the results were calculated on a lattice with size $N = 40{,}000$ with $\Delta x = 0.1$ and $\Delta t = 0.001$. The velocities of the nearest two wave as a function of the initial energy for different width, σ, of the Gaussian function are shown in Figure 5.2.8. As seen, the higher the initial energy is, the lower the velocity of the solitons is, until the velocity reaches the minimum velocity. For widths bigger than $\sigma > 0.85$, the velocity as a function of the width has the same form, where the negative waves become sonic first and thereafter the positive. The more energy in the initial state, the slower

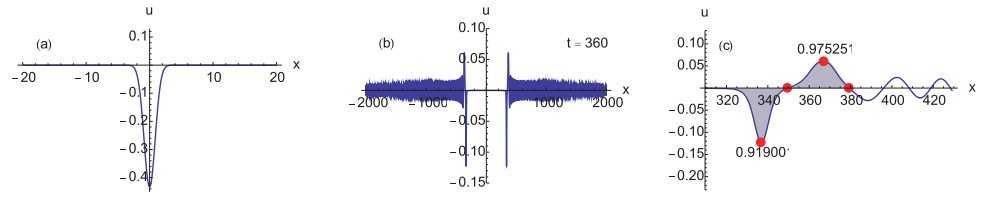

Figure 5.2.7 – (a) the initial state is a Gaussian function with σ = 1.25, A = 0.433 and E = 2.88. (b) The result for t = 360, show a lot of small-amplitude waves in front of two pairs of solitons. (c) A pair of a negative and positive soliton where the velocity is noted above and under them. Red dots indicate the minimum, maximum and roots. The filled is the area which is quantified to be the pair.

the solitons become. The transformation from small-amplitude waves to solitons happen in the same energy range approximately between initial energy 0.1 and 1. The energy needed to have solitons is decreasing as the width increase. In cases where the width is below $\sigma < 0.85$ the positive soliton is sonic before the negative, but the positive soliton is like the other cases in front of the negative soliton. But at some time the negative soliton will overtake the positive. The energy needed to get a pair of solitons as a function of the width σ follow a power law function. Cases where the width is below $\sigma < 0.85$ have many properties in common with cases where the width is above $\sigma > 0.85$, but the energy needed to get solitons is much higher. When the energy is increasing, and width constant, , the function of

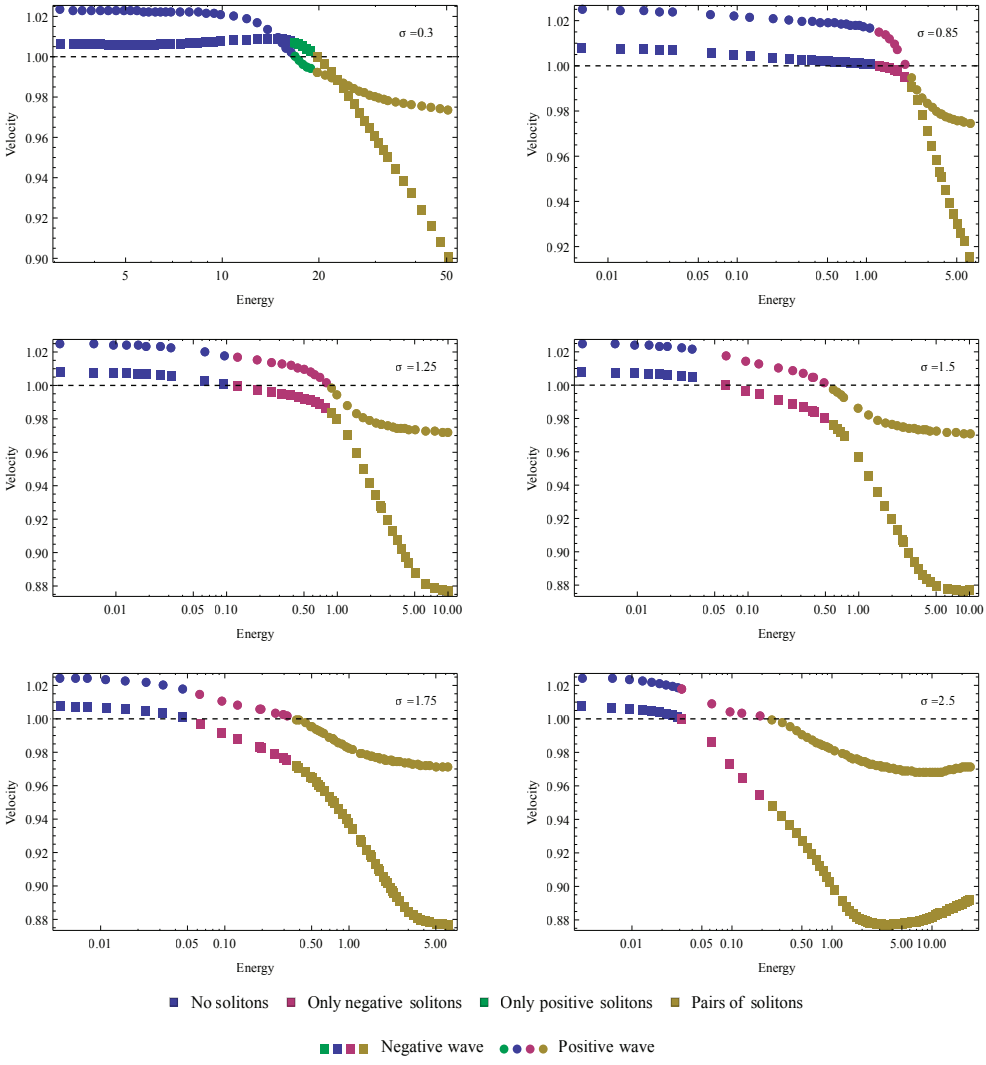

Figure 5.2.8 – Velocity for the negative and positive waves nearest the origin of the initial disturbance as a function of initial energy. Each graph is for different widths, σ. The velocity is measured at time t = 360. Each point is a calculated result for an initial state disturbance with certain width and energy. The colour indicate the quantification of the result, whenever it have no solitons, positive or negative solitons, or pairs of solitons.

energy carried by the two waves nearest to the origin follow a different path than those above $\sigma > 0.85$.
As mentioned before, overlapping of waves influences the speed of the solitons, and it is therefore expected that, because of the large amount of small-amplitude waves, some of the results will be quantified wrong. It is expected that this error is the same for all widths, and the result will not change noticeably.

The energy carried in the nearest waves to the origin can be calculated by the integral over the energy density as a function of the two states, v and u, defined as:

$$\varepsilon(t,x) = \frac{1}{2}v(t,x)^2 + \frac{1}{2}\left(\frac{\partial u(t,x)}{\partial x}\right)^2 + \frac{1}{2}A(u(t,x)) \tag{5.2.4}$$

Where $A(u)$ is eq. (4.2.19) integrated twice, and is the compressive energy density. In Figure 5.2.9 the ratio of the initial energy carried in the two waves as a function of the initial energy shown. Again, it is seen that widths below and above $\sigma > 0.85$ show different tendencies. Where the widths below $\sigma < 0.85$ show that the ratio of the initial energy carried in the two waves increases with the initial energy. The amount of the initial energy that ends up in the two waves is very low. The widths above $\sigma > 0.85$, where negative solitons appear first and thereafter pairs, show all the same similarity in the ratio of the initial energy as the energy increasing. As seen the functions start rising from low energies until a point where they fall. In this fall the first soliton appear. For larger widths the first solitons appear just before the fall in ratio. When the energy is increasing the function has a bump. At the start of this bump, when it start to raise, is where the pairs of solitons appear in the results. When the slope for the fall is fitted to a power law function, it is seen that this bump has the same height above for all widths above $\sigma > 0.85$ of approximately 0.04 points. It therefore shows, that when the pairs of solitons appear, the system becomes more efficient by using the solitons to carry the initial energy instead of the small-amplitude waves.
The initial state is a disturbance in the mass, which is like the energy carried away with the waves. The mass change can be calculated by integrating $u(t,x)$ over the waves. The ratio of initial mass change carried away by the two nearest waves to the origin starting with approximately 0.8 and fall to a minimum (the fall become smaller when the widths is increasing) where it raises again in the pairs domain. However, most of the mass change is in the two waves. The mass change in the negative solitons are bigger than the initial mass change. For example in Figure 5.2.7 the initial disturbance is a mass change of -0.96 and the mass change in the negative solitons at time $t = 360$ is -2.37 and in the positive solitons it is 1.83. The larger mass change found in the solitons than found in the initial state, is an effect of energy and mass conservation. This means that to conserve the energy and mass it has to link the positive and negative solitons together to make a pair where the negative soliton borrows mass to the positive solitons, so the total mass change is below the initial state. The soliton pairs are carrying most of the mass from the initial state and a lot of the energy, the rest of the energy and mass change is then carried in the small-amplitude waves.
As seen in Figure 5.2.9, the larger the width, or distribution of the initial energy

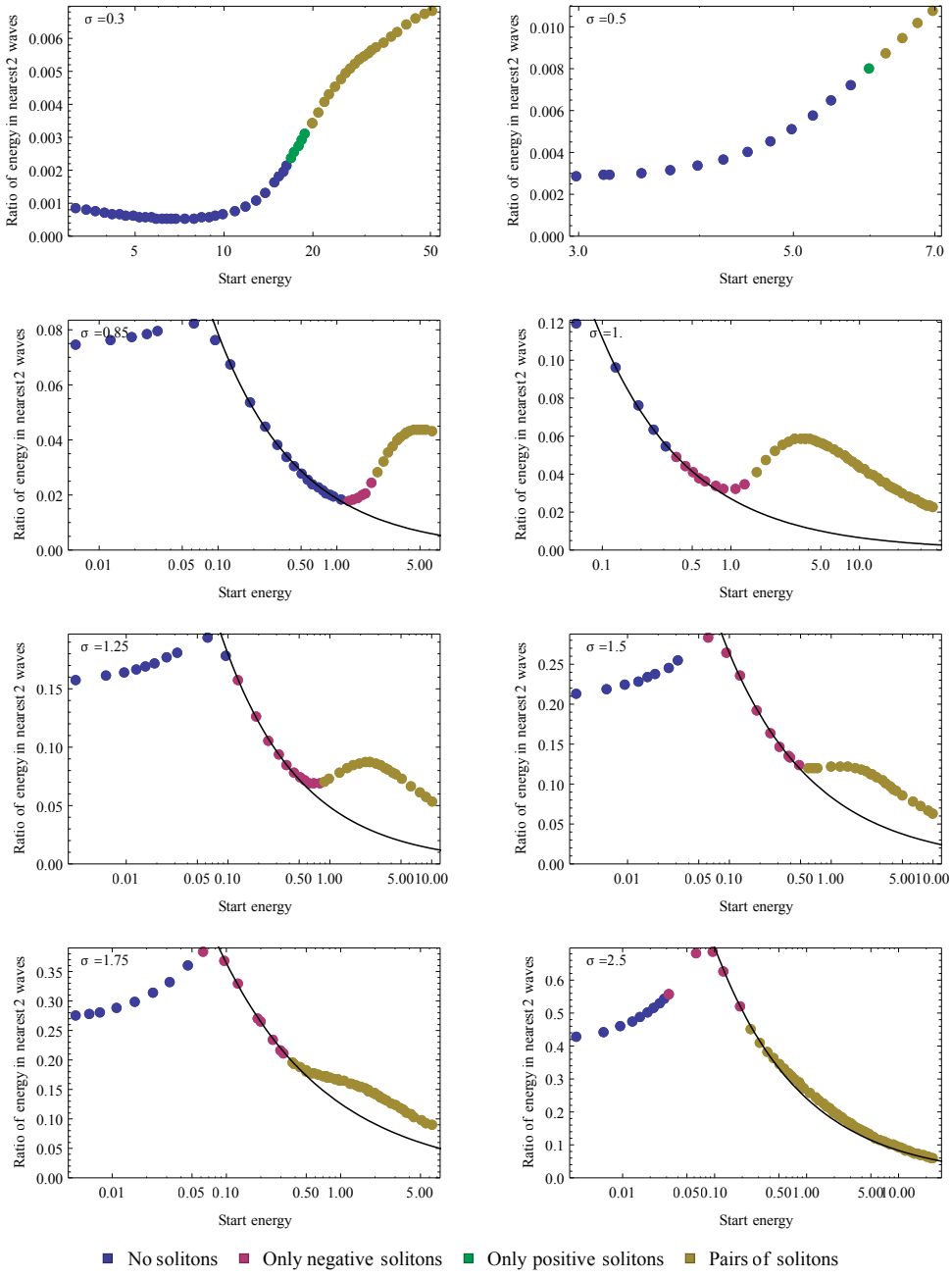

Figure 5.2.9 – The ratio of the initial energy in the two nearest waves to the origin of the initial state disturbance as a function of the initial energy for different widths, σ. Each point is a result and the ratio is calculated at time t = 360. The black line is a fitted power law function to the slope decreasing from the top point.

is, the less energy is needed to have a result with pairs of solitons. In Figure 5.2.10 the initial energy from the results as a function of the width of the initial disturbance is seen. With the quantification of the result, it is seen that the result falls into domains – a domain where no solitons exist, a domain where only negative solitons exist, a domain where only positive solitons, and a domain where pairs of solitons exist. The domains was found by fitting the first points at a certain width where the result first shows that domain. E.g. the pair domain was found by fitting the points, representing a result, at a certain width and energy, where the point just below with same width and less energy do not contain pairs. The pair domain follows, with a very small standard error a power law function

$$E = 1.40\sigma^{-2.20} \tag{5.2.5}$$

And the other domains have a small standard error when fitted to a power law function. All three function approximately cross each other at a point at $\sigma = 0.77$ and $E = 2.5$. See Appendix B for the fits and error.
No widths above $\sigma > 2.5$ was investigated fully, and one can imagine that this symmetry will break when the width become too big (E.g. should an initial state $u(0,x) = const.$ use little energy to have pairs, but this is the same as moving the bulk temperature, and no waves will propagate). The predicted initial energy with a width of $\sigma = 5$ ($E = 0.04$) is five times smaller than needed ($E = 0.2$), leading to the symmetry only holding for a finite range of widths and thereby a certain distribution of the initial energy. Other patterns from the result is shown in Appendix D.

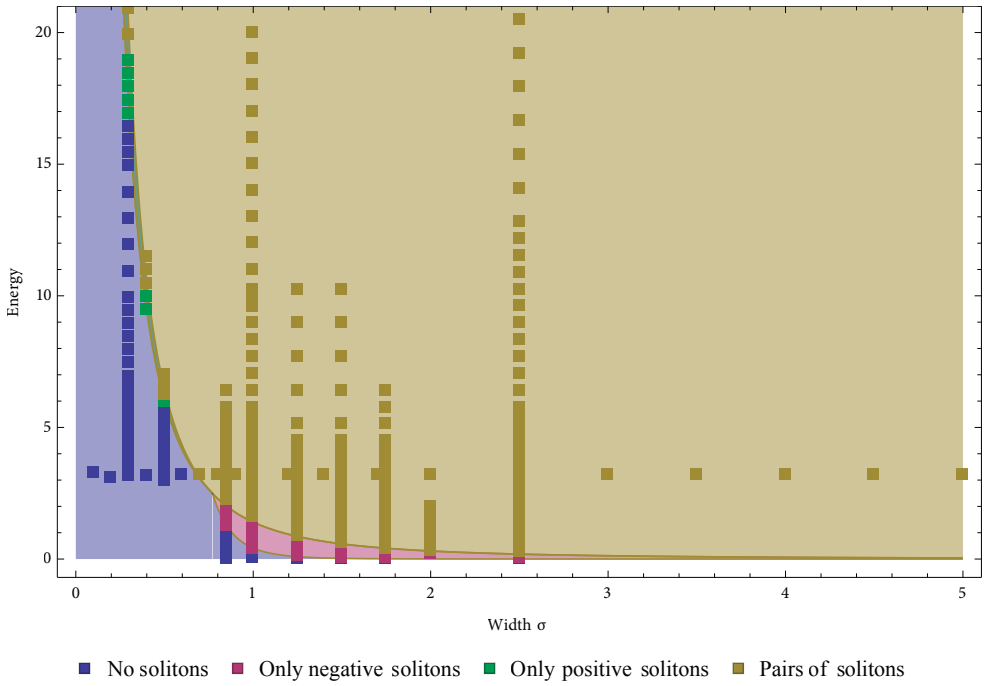

Figure 5.2.10 – When the initial energy as a function of the width, σ, is plotted with the quantification of the result, one get a phase diagram of when different solitons exist. Each point is a result with width, σ, and initial energy. Total 421 results.

5.2.4.1 *Initiation in a system with viscosity*

In the process of initiation of solitons a lot of small-amplitude waves are emitted. Introducing viscosity into the system the amount of small-amplitude waves is reduced, as seen in Figure 5.2.11. The solitons can propagate over a great distance with a very little decay per time, shown by *Lautrup et al.* [46]. An example is shown in Figure 5.2.11, the solitons in the system with viscosity is smaller than them in the system without, and only carrying half the amount of energy than the solitons from the viscosity-less system at time $t = 360$. The system has only less than one-tenth of the initial energy at time $t = 360$, where 96.4% is in the solitons. The viscosity term does not prevent the emission of the small-amplitude waves, but only prevents them from propagate very far.

5.2.5 Thickness change and heat release

From the density change the thickness can be calculated and found to be in the order of 6 Å to -10 Å, Figure 5.2.12 shows the displacement of a cylinder mem-

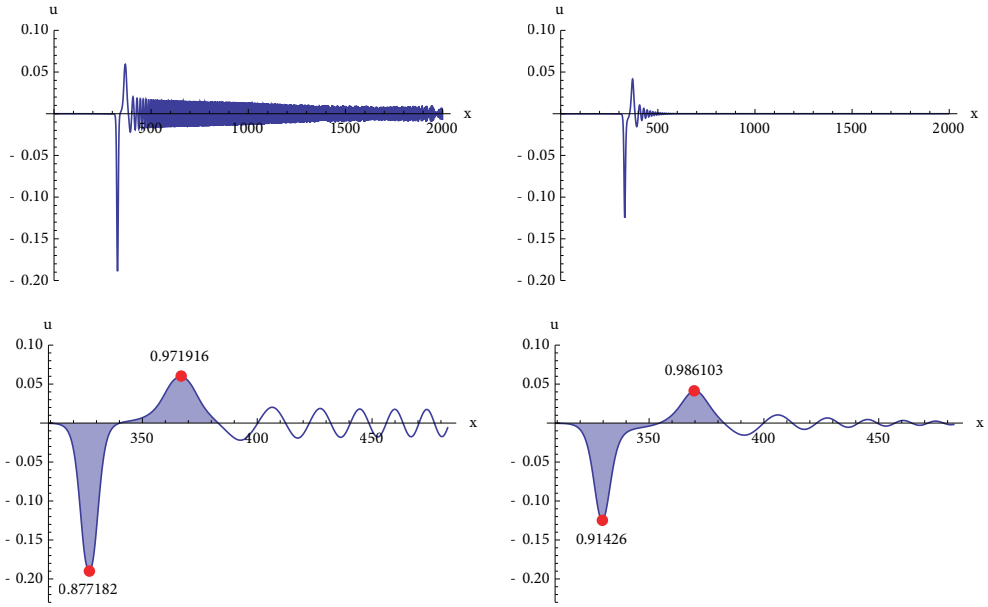

Figure 5.2.11 – With and without viscosity for solitons from an initial state with width σ = 2.5, amplitude A = -0.402382 and initial energy E = 2.81. Left, show a pair of solitons at time t = 360 in a system without viscosity. Right, show a pair of solitons at the same time in a system with viscosity. It is clear that the small-amplitude waves propagating is reduce, and the solitons is smaller due to the viscosity. There is twice the energy in the solitons without viscosity than in them with.

brane when a pair of solitons pass, and follow the density change. The density and displacement is biphasic.

The heat release through a passage of a pair of solitons can be calculated from the density change, when the heat capacity as a function of lateral density, and the temperature for any densities is known (see Figure 4.2.3). The heat change can be calculated by integrating the heat release over time. In Figure 5.2.13 it is shown

that the heat is reversible and it is biphasic, whereas the heat release is triphasic. The absolute maximum of heat release does not exceed the maximum energy density in the soliton.
The heat change is a factor 1000 bigger than any recorded heat change in the literature. However, it cannot be compared, since it is here shown as heat per gram lipid membrane, where literature values show it as heat per gram nerve, which includes, beside the lipids, proteins, water and cell material, which make up for most of the neuron mass.

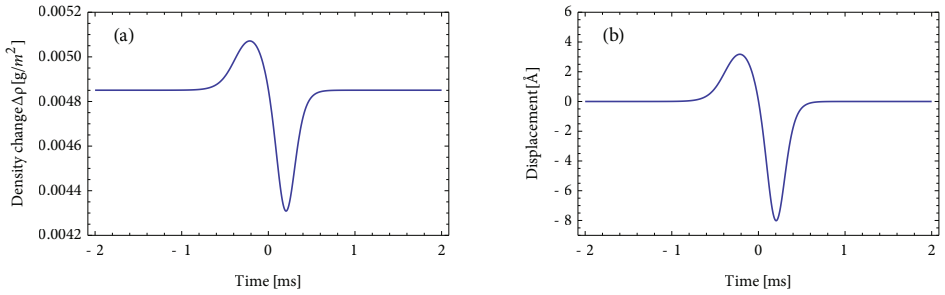

Figure 5.2.12 – (a) Density change for two solitons with velocities β = 0.90 and β = 0.95 for the negative and positive soliton respectively. (b) Calculated thickness change of a membrane of a membrane cylinder (displacement).

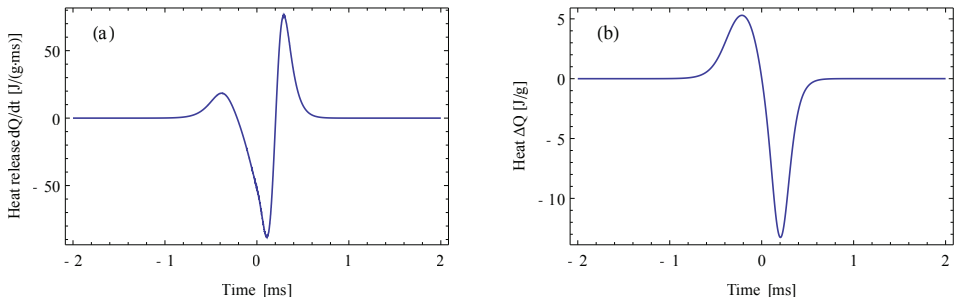

Figure 5.2.13 – (a) Calculated heat release and (b) calculated heat change during the passage of a pair of solitons.

Chapter 6

Discussion

The results presented in the previous chapter have many similarities with what is known of the nerve pulses mechanical behaviour. However, it also raises the question of how the biomembrane obtains these thermodynamic and mechanic properties, which will be discussed in this chapter.

It was shown by *Iwasa and Tasaki* [44] that during the passage of an action potential the thickness of the membrane follows the action potentials phases (see Figure 2.2.2). The membrane becomes thicker under the positive part of the action potential, and thinner under the negative, before it gets back to equilibrium. As shown in Figure 4.2.3 the lateral density and thickness are both a function of the temperature. The thickness can be expressed as a function of the lateral density, where it can be found to be proportional to the density, Figure 5.2.12. In section 5.2 it was shown that pairs of negative and positive solitons are a common phenomenon, where the density change was first positive and then negative. Depending on the sound profile and the initial state, it could be opposite. The membrane will therefore, first be thicker with the positive density change and thereafter thinner with the negative density change. Both the experimental findings and the results shown are biphasic.
The heat change during an action potential was found to be experimentally reversible and biphasic [40], [42], [43], [62]. It was shown to first release heat, and thereafter absorbs the same amount of heat. This process follows the action potential, where it releases under the positive part of the action potential and absorbs under the last part, the negative path, and is biphasic. The integrated heat release, the heat change, is monophasic. In Figure 5.2.13 the calculated heat release for a pair of solitons was found to be triphasic, and the heat change biphasic, and that is not in consensus with the experimental findings. This means that a pure lipid membrane cannot have a biphasic heat release and a biphasic displacement in *the soliton model*.

The heat profile used for the expanded basic density change equation has many similarities with the ones found in living cells. The difference is that the used heat capacity seems to have two melting transition, when the bulk temperature is between the two peaks, see Figure 4.2.1. The same is found for biomembranes, see Figure 2.1.5. But where the two melting transitions in the expanded basic density

change equation were an effect of mixed lipids, the peaks found in biomembranes are an effect of lipids and proteins. The first peak is when the lipids melt and the second where the protein unfolds. A second scan of a biomembrane does not give the same heat capacity as the first scan, because after the protein unfolds in the first scan, it does not fold back again, meaning it is an irreversible process. However, no evidence is recorded that a nerve signal unfolds its propagation media's proteins, due to the temperaute changes during the nerve signal, which would result in a damaged neuron for every signal. The length the nerve signal spans over is approximately *2 ms*, and the heat change corresponds to a temperature change of *10 °C*. No recording has been found on, that a short heat influence has been should be enough to unfold the proteins. This means that the speed of sound in the biomembrane as a function of lateral density in this range cannot alone be found from the heat capacity of a biomembrane.
The soliton model does not include proteins as an active part of the solitons propagation, where *the Hodgkin-Huxley model* describes proteins role as essential. The sound profile used here was calculated from area compressibility, where for a biological membrane it was assumed that the protein was solid particles, and do not alter the area compressibility on stress. The neurons have a large population of mechanosensitive proteins which can alter the compressibility under stress [63]–[65]. Mechanosensitive proteins are channels in the membrane, which can change from an open state to an closed and visa versa due to a mechanical change in the environment. Some of the best known mechanosensitive proteins is TREK-1 and TRAAK, both of which are found in mammalian neurons [66], [67]. TREK-1 and TRAAK are both member of the potassium channel subfamily K, and are responsible for the potassium transport through the membrane. It is known that these proteins open when one stretches the membrane, and can be seen as a damper of the lateral stress under stretching. One can therefore speculate of these proteins role under soliton propagation. To have a pair of negative and positive soliton to propagate, the area compressibility has to have a peak on both sides of the bulk density. If one is from the area compressibility of lipids and the other one from the mechanosensitive proteins, it could explain the biphasic displacement and monophasic heat change. The following will then happen under propagation of a pair of solitons – first the positive soliton will change the lipids lateral density of the membrane and the membrane becomes thicker and heat will be released and then absorbed. It is assume that the mechanosensitive proteins are closed. When the negative solitons pass, the mechanosensitive proteins will open and the density of the lipid areas will be constant, but the total density will change, resulting in no heat release and the membrane will overall become thinner, which results in a biphasic displacement and a monophasic heat change. No evidence of such a mechanism and cooperation between lipids and solitons in a short time scale has been observe. It is also questionable, since the heat change and displacement was found to be over the whole action potential. And the mechanosensitive proteins effect on the thickness of the membrane is also unclear, since the thickness change then should only be on the difference between the protein open and close state, and with no contribution from the lipids. But the mattress-model could be used to explain this effect, because the lipids may be distributed inhomogeneously and thickness of membrane near the protein will therefore be affected.

In section 5.1.2 and 5.2.2 it was shown that collision of solitons did not result in instability or annihilation. Which is a controversy with what is common knowledge of nerve signals, but in agreement with common knowledge of solitons and the results from our lab [4]. It has been shown that collisions only result in small-amplitude waves, and that several solitons could collide without any instability occurring. When solitons collide they become delayed, but as shown in Figure 5.1.3, the solitons in a membrane could be either earlier or later than expected compared to the situation where no interaction happens. After the collision the solitons have lost a small amount of energy, and is therefore accelerated. The acceleration and energy loss depends on how near the velocity is to the minimum velocity before the collision. This delay was found to be in the order of one tenth of a single soliton width, and is therefore possible to experimental measure it.

In neurophysiological experiments the nerve signal is initiated by a disturbance in the axon, made by a voltage pulse. The voltage pulse has to be above a threshold before a nerve pulse will propagate. When the voltage pulse is above the threshold, an action potential starts to propagate. A similar thing is seen in section 5.2.4, where a certain amount of energy distributed over a finite and small area compared to the solitons width results in two pairs of solitons travelling in opposite direction. If the system has viscosity, the small-amplitude waves will not travel very far from its origin, but the soliton could travel a great distance without any sign of instability. However, a soliton, with the values presented, have a width of approximately 10 cm and travel with a speed of up to 200 m/s. These solitons correspond to the one in myelinated neurons [2], which nerve pulses travels with a speed of 100 m/s. The solitons travel faster because of the membrane and choice of bulk temperature. The small-amplitude waves in a system with viscosity can propagate more than one soliton width, and would therefore be seen in recordings of membrane potential, if the density change is proportional to the membrane potential. This connection between density and membrane potential is not fully understood, and no clear evidence is found on small waves propagating in front of an action potential.
It was also shown that the two solitons in the pairs have different velocities, which would over time result in a separation of the solitons. The solitons was found to be overleaping slightly, at time $t = 360$ or after *10 ms* and after travelling over two meters. Most neurophysiological experiments are not made in meters scale, but in a centimetres or millimetres. The velocity was found to be a factor two higher than any recorded velocities, this because of the choice of reference. In neurons larger than 2 meters it could be expected that the nerve pulse would arrived as a broader signal than at the start. This is seen in recorded nerve signal of few centrimetres, but both *the Hodgkin-Huxley model* and *the soliton model* describe it as an effect of the change in the axon's diameter. It was also shown that the velocity of the solitons depend on the initial energy. And in the situations, where the result contains only one type of solitons, was found unlikely, becuase this domain was narrow.
In a system where the initial energy was varied, but distributed over a constant width, the different systems have the same pattern of energy effeciency as function of initial energy. The system becomes more energy effective when the pairs of solitons appears. This effectiveness was of the relative same size for all systems, and could be predicted, since the domains of solitons follow a power law. If the width

of the area becomes too narrow a different kind of similarity appears. The domain where the pairs appeared, followed the same power law function and could be likewise predicted. But the system was much less energy effective, and positive solitons, instead of negative, appeared just before the pair did.
One of the largest width of distribution of energy investigated was *2.5*, which corresponds to *1.5 cm*, and results in solitons with a width of *10 - 20 cm*. In neurophysiological experiments on non-myelinated neurons, which have typically a velocity of *5 m/s*, the distance the voltage pulse is applied over is typically about 3 mm where the pulse is approximately *4 - 17 mm* in width [4].

Chapter 7

Conclusion

It was the aim for this thesis to find a suitable environment for propagation of negative and positive solitons, and investigate such a medium and the medium's properties of the solitons propagating. Such an environment was found, it has been discussed, and it was found that such an environment could be neurons, but because of the complexity and the amount of things there should be involve in the signal. It is more likely that the nerve signal is one soliton, instead of pairs, since it is shown that a soliton can propagate in a pure lipid membrane, and therefore also in other biological membranes. *The soliton model* only explains a part of the mechanic properties seen in the nerve signal, and the heat and displacement, and could not at the same time be explain by the theory. The properties for solitons in such an environment was presented, and it was found that unstable solitons decay to stable solitons, and collision between solitons does not lead to annihilation. Further, initiations of solitons was discussed, and it was shown that the energy needed to make a distortion in the membrane, and to initiate solitons, versus the distribution of the energy (or width of the distortion) followed a power law function. The system becomes slightly more efficient when pairs of the solitons appear. This is in agreement with what there is expected of the nerve signal, where the initiation voltage pulse have to be above a threshold, before the signal propagate. All pulses energy under the threshold is lost in the membrane.

In general not much work has been made on solitons in such an environment, which at the same time allows propagation of negative and positive solitons. And no one has looked at it in combination with the biological membrane and the nerve signal. Results from this thesis can be used in other fields of physic, where the same characteristic is present.

Chapter 8

Perspectives

One of the key features in the soliton model is that it can explain how anaesthesia works. When a membrane is exposed to anaesthesia, the melting temperature becomes lower, and the membrane will be fully in the fluid phase. It is therefore difficult for solitons to propagate, since the phase transition is moved away. When the solitons have difficulty propagating, no nerve signal is transmitted between the neurons, and then one does not feel pain [68]. Moving the bulk temperature in the present work will give the same effect as anaesthesia. By moving the phase transition it will still allow one of the solitons to propagate. It is therefore interesting to explore what is happening in these situations, if there are still seen pairs of solitons or waves that look like solitons, and what initiation result in and do they show the same pattern as shown. In Appendix F it is demostrated that it can result in waves that could look like solitons.

In the discussion, mechanosensitive proteins were mentioned, which could explain the heat release and displacement, but not much and not enough is known of these proteins and their role under stress in the membrane and their contribution to the compressibility. These kind of proteins are rich presented in the neuron, and an investigation and formulation of their role on the compressibility is needed.

It was shown that when two solitons collide, the soliton could either be earlier than expected or delayed. The time was dependent on the velocity of the solitons. This is a prediction, which can be investigated experimentally. Further it was shown that the more energy there is used to initiate the pulses, the slower the solitons will propagate. This is also a thing that can be investigated experimentally.

In neurophysiology the recorded action potential is recorded near the excitation point, and no research has been found where the signal has been recorded far away. Most recording of the action potential is done by measuring with a two point electrode that does not record the shape of the signal, but measures the voltage difference between two points. One of the main things in the thesis is that the two solitons in the pairs after an initiation have different velocities. This gives the prediction that far away from the signals starting point, the signal will arrive separated. This distance is in a myelinated-nerve greater than 2 meters. Myelinated nerves are mostly long nerves, where the signal has to travel fast over a long

distance, e.g. toe to hip, where non-myelinated nerves are short and present in the brain, where the signal travels over a short distance and not necessarily fast. This give rise to the question, what is then the nerve signal, the first part or last part. Or is the length of the longest nerves in the nervous system in time evolved to a length where this separation is prevented.

Acknowledgments

First of all I want to thank my supervisor Thomas Heimburg, for the opportunity to make this project.

A special thank goes to Lars D. Mosgaard, for the inspiring debates on the soliton model. Giving answers to my countless questions and for his help through this thesis, and last minut proofreading.

I want to thank Ann-Katrine Vransø West for proofreading the thesis and her the support. Trine Meldgaard for proofreading and critical comments on my thesis, however that consensus was almost impossible to reach.

I would like to thank all members of the Membrane Biophysics Group at Niels Bohr Insitute: especially Alfredo Gonzélez-Pérez for answer my question on nerves, Henrike Sasse-Middelhoff for the good company at the office and for all thing she didn't noticed.
Thanks to the BioComplexity group for being one way or another an anchor for me through most of my study.

Thanks to Kitt Lindgaard for the help and support doing this thesis.

Last, but definitely not least, I would like to thank my family that in all aspects of my education have been infinite source of support.

References

[1] J. S. Russell, "Report on Waves," *Rep. 14th Meet. Br. Assoc. Adv. Sci.*, pp. 311–390, 1844.

[2] T. Heimburg and A. Jackson, "On soliton propagation in biomembranes and nerves," *PNAS*, vol. 102, no. 28, pp. 9790–9795, 2005.

[3] A. Hodgkin and A. Huxley, "A Quantitative Description of Membrane Current and its Application to Conduction and Excitation in Nerve," *J. Physiol.*, vol. 117, pp. 500–544, 1952.

[4] A. Gonzalez-Perez, R. Budvytyte, L. D. Mosgaard, M. T. Stauning, S. Nissen, and T. Heimburg, "Penetration of action potentials during collision in the medial giant of the earthworm," *Publ. early April ArXiv.org*, 2014.

[5] W. Pfeffer, *Pflanzenphysiologie: ein Handbuch der Lehre vom Stoffwechsel und Kraftwechsel in der Pflanze*, 2nd ed. Leipzig: Engelmann, 1897.

[6] E. Overton, *Ueber die allgemeinen osmotischen Eigenschaften der Zelle, ihre vermutlichen Ursachen u. ihre Bedeutg fd Physiologie*. Fäsi & Beer, 1899.

[7] E. Gorter and F. Grendel, "On bimolecular layers of lipoids on the chromocytes of the blood," *J. Exp. Med.*, pp. 439–443, 1925.

[8] J. Danielli and H. Davson, "A contribution to the theory of permeability of thin films," *J. Cell. Comp. …*, pp. 495–508, 1935.

[9] E. Harvey, "The properties of elastic membranes with special reference to the cell surface," *J. Cell. Comp. Physiol.*, pp. 251–260, 1936.

[10] E. N. Harvey and J. F. Danielli, "Properties of the Cell Surface," *Biol. Rev.*, vol. 13, no. 4, pp. 319–341, 1938.

[11] J. F. Danielli, "Morphological and molecular aspects of active transport," in *Symp. Soc. Exp. Biol*, 1954, vol. 8, pp. 502–516.

[12] J. D. Robertson, "New observations on the ultrastructure of the membranes of frog peripheral nerve fibers.," *J. Biophys. Biochem. Cytol.*, vol. 3, no. 6, pp. 1043–8, Nov. 1957.

[13] S. J. Singer and G. L. Nicolson, "The fluid mosaic model of the structure of cell membranes.," *Science*, vol. 175, no. 4023, pp. 720–31, Feb. 1972.

[14] O. G. Mouritsen and M. Bloom, "Mattress model of lipid-protein interactions in membranes.," *Biophys. J.*, vol. 46, no. 2, pp. 141–53, Aug. 1984.

[15] T. Heimburg, *Thermal biophysics of membranes*, 1st ed. Berlin: Wiley-VCH, 2007.

[16] J. R. Hazel and E. E. Williams, "The role of alterations in membrane lipid composition in enabling physiological adaptation of organisms to their physical environment.," *Prog. Lipid Res.*, vol. 29, no. 3, pp. 167–227, Jan. 1990.

[17] a G. Marr and J. L. Ingraham, "Effect of Temperature on the Composition of Fatty Acids in Escherichia Coli.," *J. Bacteriol.*, vol. 84, no. 6, pp. 1260–7, Dec. 1962.

[18] M. Sinensky, "Homeoviscous adaptation--a homeostatic process that regulates the viscosity of membrane lipids in Escherichia coli.," *Proc. Natl. Acad. Sci. U. S. A.*, vol. 71, no. 2, pp. 522–5, Feb. 1974.

[19] J. R. Hazel, "Influence of thermal acclimation on membrane lipid composition of rainbow trout liver.," *Am. J. Physiol.*, vol. 236, no. 1, pp. R91–101, Jan. 1979.

[20] E. DeLong and A. Yayanos, "Adaptation of the membrane lipids of a deep-sea bacterium to changes in hydrostatic pressure," *Science (80-.).*, vol. 228, no. 4703, pp. 1101–1103, May 1985.

[21] T. Heimburg, "A model for the lipid pretransition: coupling of ripple formation with the chain-melting transition.," *Biophys. J.*, vol. 78, no. 3, pp. 1154–1165, 2000.

[22] D. Marsh, "General features of phospholipid phase transitions.," *Chem. Phys. Lipids*, vol. 57, no. 2–3, pp. 109–20, Mar. 1991.

[23] J. F. Nagle, "THEORY OF THE MAIN LIPID BILAYER PHASE," 1980.

[24] G. Cevc, "Isothermal lipid phase transitions.," *Chem. Phys. Lipids*, vol. 57, no. 2–3, pp. 293–307, Mar. 1991.

[25] N. I. Liu and R. L. Kay, "Redetermination of the pressure dependence of the lipid bilayer phase transition.," *Biochemistry*, vol. 16, no. 15, pp. 3484–6, Jul. 1977.

[26] F. Anthony, R. Biltonen, and E. Freire, "Modification of a vibrating-tube density meter for precise temperature scanning," *Anal. Biochem.*, vol. 167, pp. 161–167, 1981.

[27] H. Ebel, P. Grabitz, and T. Heimburg, "Enthalpy and Volume Changes in Lipid Membranes. I. The Proportionality of Heat and Volume Changes in the Lipid Melting Transition and Its Implication for the Elastic Constants ‡," *J. Phys. Chem. B*, vol. 105, no. 30, pp. 7353–7360, Aug. 2001.

[28] U. R. Pedersen, G. H. Peters, T. B. Schrøder, and J. C. Dyre, “Correlated volume-energy fluctuations of phospholipid membranes: a simulation study.,” *J. Phys. Chem. B*, vol. 114, no. 6, pp. 2124–30, Feb. 2010.

[29] T. Heimburg, “Mechanical aspects of membrane thermodynamics. Estimation of the mechanical properties of lipid membranes close to the chain melting transition from,” *Biochim. Biophys. Acta (BBA)-Biomembranes*, vol. 1415, pp. 147–162, 1998.

[30] D. Steppich, J. Griesbauer, T. Frommelt, W. Appelt, a. Wixforth, and M. F. Schneider, “Thermomechanic-electrical coupling in phospholipid monolayers near the critical point,” *Phys. Rev. E*, vol. 81, no. 6, p. 061123, Jun. 2010.

[31] A. G. Lee, “Lipid Phase Transitions and Phase Diagrams,” *Biochim. Biophys. Acta*, vol. 472, pp. 285–344, 1977.

[32] I. P. Sugár, T. E. Thompson, and R. L. Biltonen, “Monte Carlo simulation of two-component bilayers: DMPC/DSPC mixtures.,” *Biophys. J.*, vol. 76, no. 4, pp. 2099–110, Apr. 1999.

[33] A. E. Hac, H. M. Seeger, M. Fidorra, and T. Heimburg, “Diffusion in two-component lipid membranes--a fluorescence correlation spectroscopy and monte carlo simulation study.,” *Biophys. J.*, vol. 88, no. 1, pp. 317–33, Jan. 2005.

[34] V. P. Ivanova, I. M. Makarov, T. E. Schäffer, and T. Heimburg, “Analyzing heat capacity profiles of peptide-containing membranes: cluster formation of gramicidin A.,” *Biophys. J.*, vol. 84, no. 4, pp. 2427–39, Apr. 2003.

[35] H. M. Seeger, M. Fidorra, and T. Heimburg, “Domain Size and Fluctuations at Domain Interfaces in Lipid Mixtures,” *Macromol. Symp.*, vol. 219, no. 1, pp. 85–96, Jan. 2005.

[36] K. S. Cole and H. J. Curtis, “Electric Impedance of the Squid Giant Axon During Activity.,” *J. Gen. Physiol.*, vol. 22, no. 5, pp. 649–70, May 1939.

[37] L. M. N. Wu, A. Williams, A. Delaney, D. L. Sherman, and P. J. Brophy, “Report Increasing Internodal Distance in Myelinated Nerves Accelerates Nerve Conduction to a Flat Maximum,” *Curr. Biol.*, vol. 22, no. 20, pp. 1957–1961, 2012.

[38] Y. Kobatake, I. Tasaki, and A. Watanabe, “Phase transition in membrane with reference to nerve excitation.,” *Adv. Biophys.*, 1971.

[39] I. Tasaki, “Evidence for phase transition in nerve fibers, cells and synapses,” *Ferroelectrics*, 1999.

[40] B. C. Abbott, A. V. Hill, and J. V. Howarth, “The Positive and Negative Heat Production Associated with a Nerve Impulse,” *Proc. R. Soc. B Biol. Sci.*, vol. 148, no. 931, pp. 149–187, Feb. 1958.

[41] I. Tasaki and P. Byrne, “Rapid structural chances in nerve fibers evoked by electric current pulses,” *Biochem. Biophys. Res. Commun.*, vol. 188, no. 2, pp. 559–564, 1992.

[42] J. M. Ritchie and R. D. Keynes, “The production and absorption of heat associated with electrical activity in nerve and electric organ.,” *Q. Rev. Biophys.*, vol. 18, no. 4, pp. 451–76, Nov. 1985.

[43] I. Tasaki, K. Kusano, and P. M. Byrne, “Rapid mechanical and thermal changes in the garfish olfactory nerve associated with a propagated impulse.,” *Biophys. J.*, vol. 55, no. 6, pp. 1033–40, Jun. 1989.

[44] K. Iwasa and I. Tasaki, “Mechanical changes in squid giant axons associated with production of action potentials,” *Biochem. Biophys. Res. Commun.*, no. 3, pp. 1328–1331, 1980.

[45] S. Mitaku and T. Date, “Anomalies of nanosecond ultrasonic relaxation in the lipid bilayer transition.,” *Biochim. Biophys. Acta*, vol. 688, no. 2, pp. 411–21, Jun. 1982.

[46] B. Lautrup, R. Appali, A. D. Jackson, and T. Heimburg, “The stability of solitons in biomembranes and nerves,” *Eur. Phys. …*, vol. 34, no. 57, pp. 1–9, Jun. 2011.

[47] E. V. Vargas, A. Ludu, R. Hustert, P. Gumrich, A. D. Jackson, and T. Heimburg, “Periodic solutions and refractory periods in the soliton theory for nerves and the locust femoral nerve,” *Biophys. Chem.*, vol. 153, no. 2–3, pp. 159–67, Jan. 2011.

[48] I. Tasaki, “Collision of two nerve impulses in the nerve fibre,” *Biochim. Biophys. Acta*, vol. 3, pp. 494–497, 1949.

[49] R. FitzHugh, “Impulses and Physiological States in Theoretical Models of Nerve Membrane,” *Biophys. J.*, vol. 1, no. 6, pp. 445–466, Jul. 1961.

[50] J. Nagumo, S. Arimoto, and S. Yoshizawa, “An active pulse transmission line simulating nerve axon,” *Proc. IRE*, vol. 117, no. m V, pp. 2061–2070, 1962.

[51] M. Argentina, P. Coullet, and V. Krinsky, “Head-on collisions of waves in an excitable FitzHugh-Nagumo system: a transition from wave annihilation to classical wave behavior.,” *J. Theor. Biol.*, vol. 205, no. 1, pp. 47–52, Jul. 2000.

[52] G. Whitham, *Linear and nonlinear waves*. New York: John Wiley & Sons, 1974, p. 636.

[53] S. Gatz and J. Herrmann, "Soliton propagation and soliton collision in double-doped fibers with a non-Kerr-like nonlinear refractive-index change.," *Opt. Lett.*, vol. 17, no. 7, pp. 484–6, Apr. 1992.

[54] S. K. Sharma, a. Boruah, and H. Bailung, "Head-on collision of dust-acoustic solitons in a strongly coupled dust*ys. Rev. E*, vol. 89, no. 1, p. 013110, Jan. 2014.

[55] W. Press, B. Flannery, S. Teukolsky, and W. Vetterling, *Numerical recipes*, Third Edit. 2007, p. 1262.

[56] J. F. Nagle and D. a Wilkinson, "Lecithin bilayers. Density measurement and molecular interactions.," *Biophys. J.*, vol. 23, no. 2, pp. 159–75, Aug. 1978.

[57] A. Blume, "Apparent molar heat capacities of phospholipids in aqueous dispersion. Effects of chain length and head group structure," *Biochemistry*, vol. 22, no. 23, pp. 5436–5442, Nov. 1983.

[58] R. E. Tosh and P. J. Collings, "High pressure volumetric measurements in dipalmitoylphosphatidylcholine bilayers.," *Biochim. Biophys. Acta*, vol. 859, no. 1, pp. 10–4, Jul. 1986.

[59] W. J. Sun, S. Tristram-Nagle, R. M. Suter, and J. F. Nagle, "Structure of gel phase saturated lecithin bilayers: temperature and chain length dependence.," *Biophys. J.*, vol. 71, no. 2, pp. 885–91, Aug. 1996.

[60] D. Needham and E. Evans, "Structure and mechanical properties of giant lipid (DMPC) vesicle bilayers from 20 degrees C below to 10 degrees C above the liquid crystal-crystalline phase transition at 24 degrees C.," *Biochemistry*, vol. 27, no. 21, pp. 8261–9, Oct. 1988.

[61] R. Rand and V. Parsegian, "Hydration forces between phospholipid bilayers," *Biochim. Biophys. Acta (BBA)-Reviews …*, vol. 988, no. 19159, 1989.

[62] J. Howarth, R. Keynes, and J. Ritchie, "The origin of the initial heat associated with a single impulse in mammalian non-myelinated nerve fibres," *J. Physiol.*, pp. 745–793, 1968.

[63] F. Guharay and F. Sachs, "Stretch-activated single ion channel currents in tissue-cultured embryonic chick skeletal muscle.," *J. Physiol.*, pp. 685–701, 1984.

[64] P.-A. Boucher, C. E. Morris, and B. Joós, "Mechanosensitive closed-closed transitions in large membrane proteins: osmoprotection and tension

damping.," *Biophys. J.*, vol. 97, no. 10, pp. 2761–70, Nov. 2009.

[65] I. R. Booth, M. D. Edwards, S. Black, U. Schumann, and S. Miller, "Mechanosensitive channels in bacteria: signs of closure?," *Nat. Rev. Microbiol.*, vol. 5, no. 6, pp. 431–40, Jun. 2007.

[66] M. Fink, F. Duprat, F. Lesage, R. Reyes, G. Romey, C. Heurteaux, and M. Lazdunski, "Cloning, functional expression and brain localization of a novel unconventional outward rectifier K+ channel.," *EMBO J.*, vol. 15, no. 24, pp. 6854–62, Dec. 1996.

[67] M. Fink, F. Lesage, F. Duprat, C. Heurteaux, R. Reyes, M. Fosset, and M. Lazdunski, "A neuronal two P domain K+ channel stimulated by arachidonic acid and polyunsaturated fatty acids.," *EMBO J.*, vol. 17, no. 12, pp. 3297–308, Jun. 1998.

[68] T. Heimburg and A. D. Jackson, "The thermodynamics of general anesthesia.," *Biophys. J.*, vol. 92, no. 9, pp. 3159–65, May 2007.

[69] C. Leirer, "Dynamik und Struktur in der Phasenkoexistenz von Lipidmembranen," PhD Thesis, Universität Augsburg, Nov. 2008.

Appendix

A. Small-amplitude waves

The small-amplitude waves were found to depend on the wavenumber, but not linearly. The amplitude of the waves and velocity depend on the wavenumber. The dependency of the wavenumber was approximately the same for the small-amplitude waves created from distortions in the solitons, initiation and collisions. However, the size of a wave with same wavenumber is not the same across the different ways of creation. It was chosen to use the small-amplitude waves created from the collision of two negative solitons with velocity $\beta = 0.649851$. The waves have been propagating for $t = 200$ and the smallest of the waves have vanish due to the error in the numerical method. The small-amplitude waves is shown in Figure A.1. The smallest waves have no interest, but the waves between them and the solitons has. Because it is them, there could interfere with the solitons. For the small-amplitude waves from the collision, was the following dependency of the amplitude and wavenumber found:

$$u(0,x) = 0.0107 - \frac{1}{95.6 + \exp(12.9 - 6.97k)} \sin(xk) \tag{A.1}$$

Where the velocity field was found to be:

$$v(0,x) = (0.801k + 0.625) \cdot u(0,x) \tag{A.2}$$

The fit can be seen in Figure A.2. The structure of the wave's dependency were found in numerous situations (collision, initiation and distortion). However, when the waves got larger in amplitude, the amplitude as a function of wavenumber become more a decaying exponential function, than a combination of exponential functions. The velocity field was found to be linear for all way of creation of small-amplitude waves.

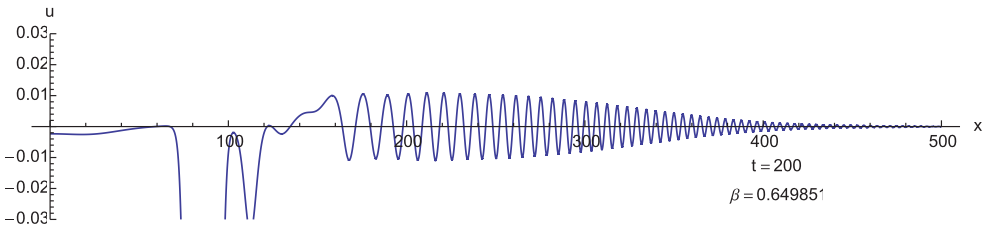

Figure A.1 – The small-amplitude wave created from a collision of two negative soliton with velocity $\beta = 0.649851$.

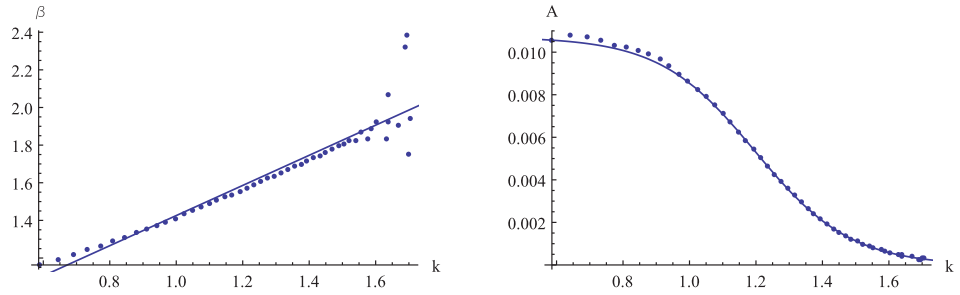

Figure A.2 – The function for velocity (left) and amplitude(right) as a function of wavenumber, k.

B. The initiations domains

The three domains, mentioned in section 5.2.4, was found by fitting the points where the effect of increased energy, on the previous state energy over a finite width of the distortion result in the system entered the domain. The fits is shown in Figure B.2, and it is seen that the fit for the pair domain has a very small error, where the one for the domain of only negative solitons has a larger one. The fit for the domain of only positive solitons, has also a small error, however the fit contains of only 3 points. The three fits has almost the same crossing point, as seen in

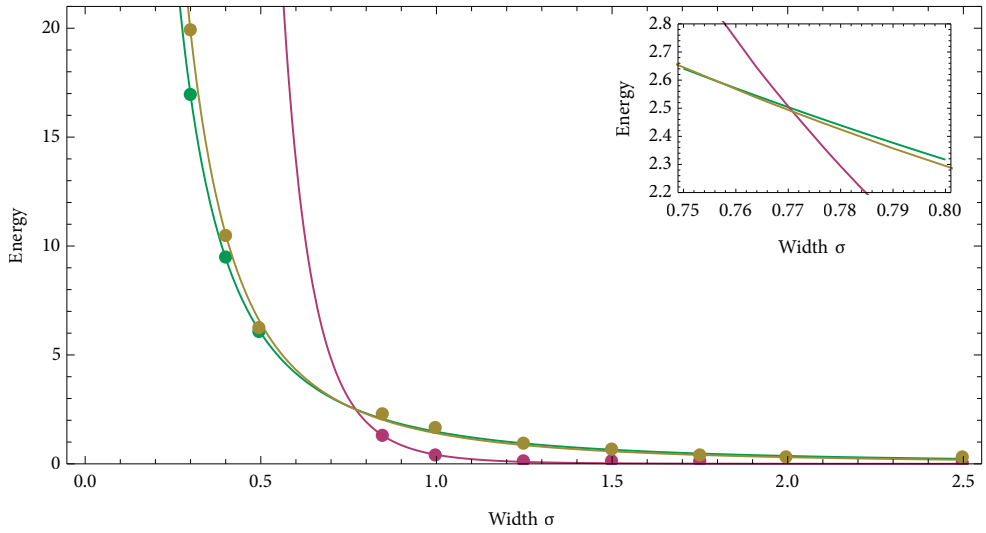

Figure B.1 – All three fits together, show that they all meets in the same point.

Figure B.1.

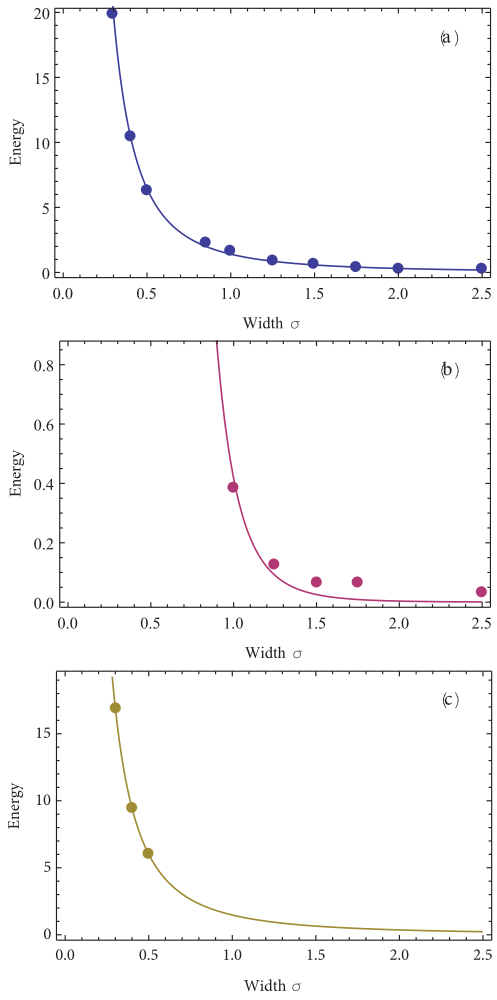

$$\frac{1.40306}{x^{2.2008}}$$

	Estimate	Standard Error	t-Statistic	P-Value
a	1.40306	0.045181	31.0542	1.25701×10^{-9}
b	- 2.2008	0.0289665	- 75.9776	1.00361×10^{-12}

$$\frac{0.41645}{x^{6.8669}}$$

	Estimate	Standard Error	t-Statistic	P-Value
a	0.41645	0.0390937	10.6526	0.000439778
b	- 6.8669	0.60552	- 11.3405	0.000344698

$$\frac{1.47385}{x^{2.02751}}$$

	Estimate	Standard Error	t-Statistic	P-Value
a	1.47385	0.0157269	93.7151	0.00679288
b	- 2.02751	0.00961185	- 210.939	0.00301801

Figure B.2 – The fits for different domains with the estimate and standard error listed.. (a) domain with pairs of solitons. (b) only negative solitons. (c) only positive solitons.

C. Time series

C.1 Collision of two solitons

Time series of the collision of two negative solitons with velocity $\beta = 0.649851$ in the basic equation.

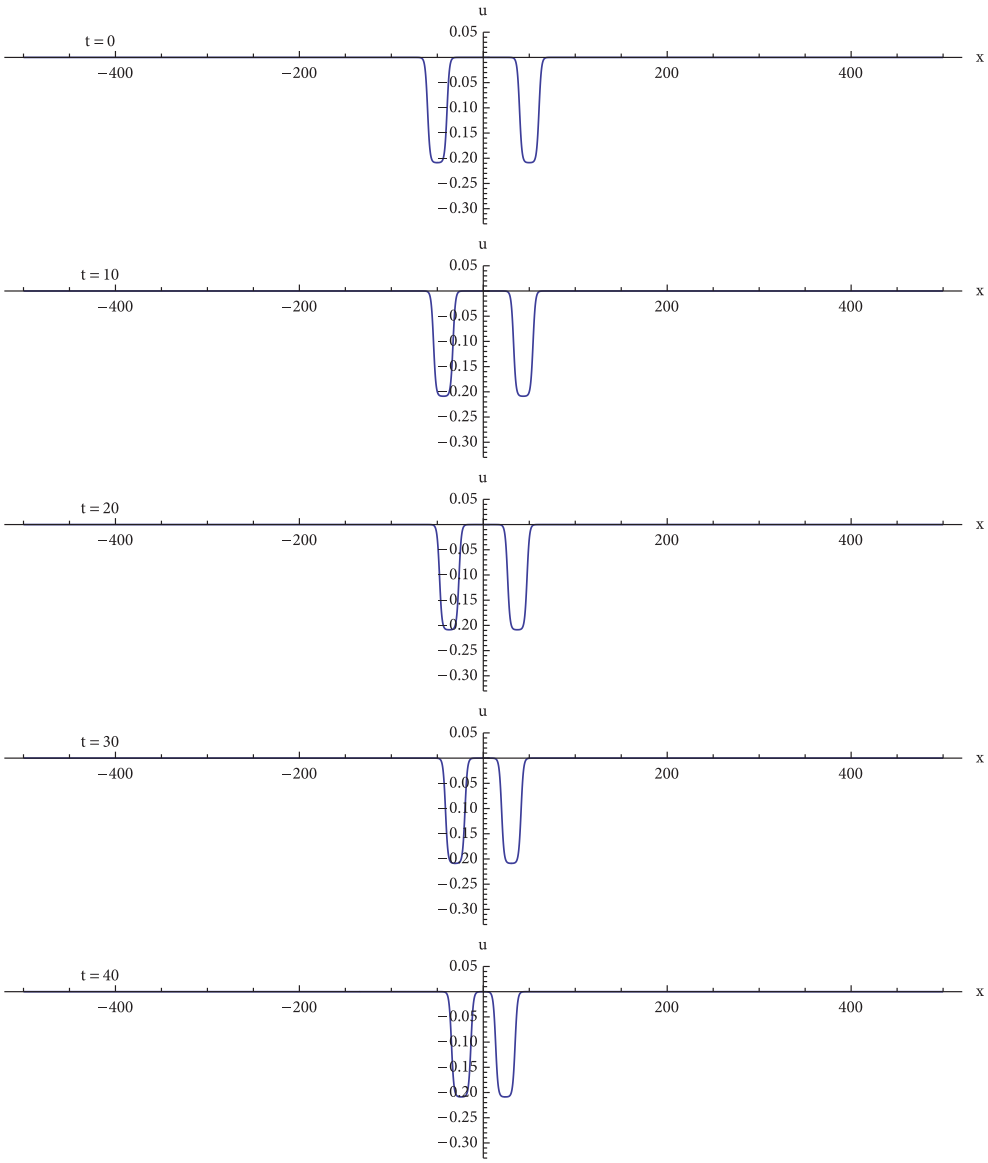

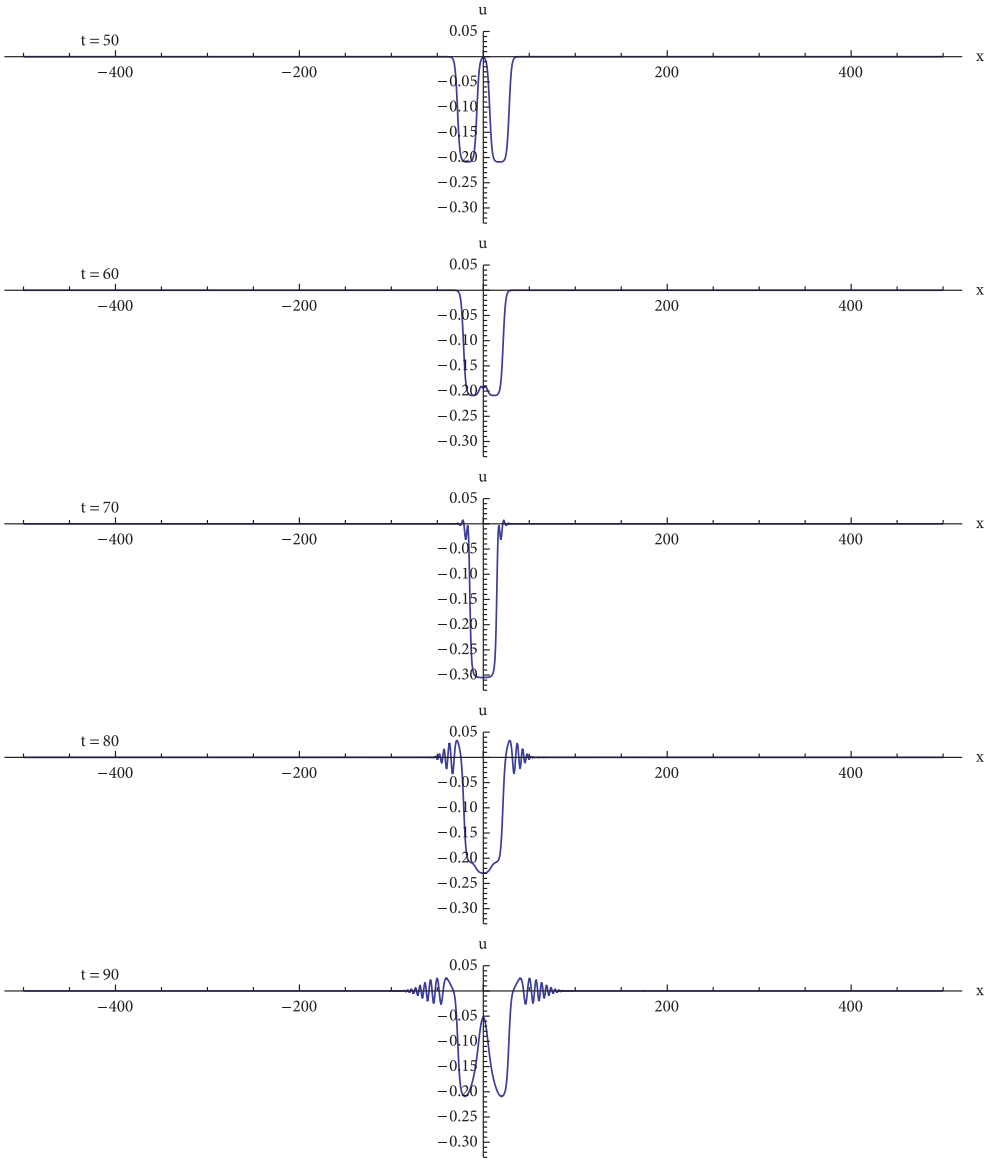
t = 50
t = 60
t = 70
t = 80
t = 90
u
x
0.05
−0.05
−0.10
−0.15
−0.20
−0.25
−0.30
−400
−200
200
400

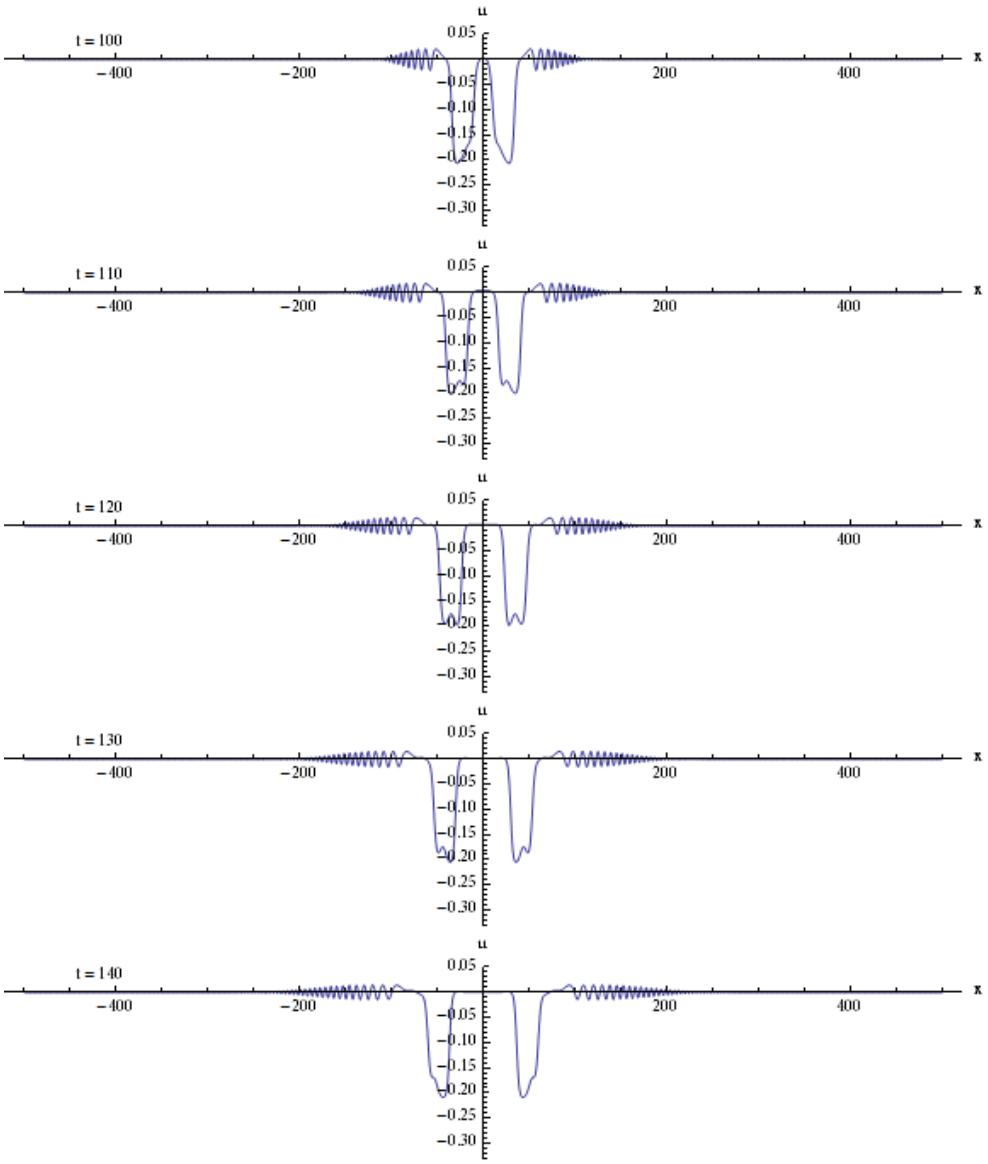
t = 100
t = 110
t = 120
t = 130
t = 140
u
x
0.05
−0.05
−0.10
−0.15
−0.20
−0.25
−0.30
−400
−200
200
400

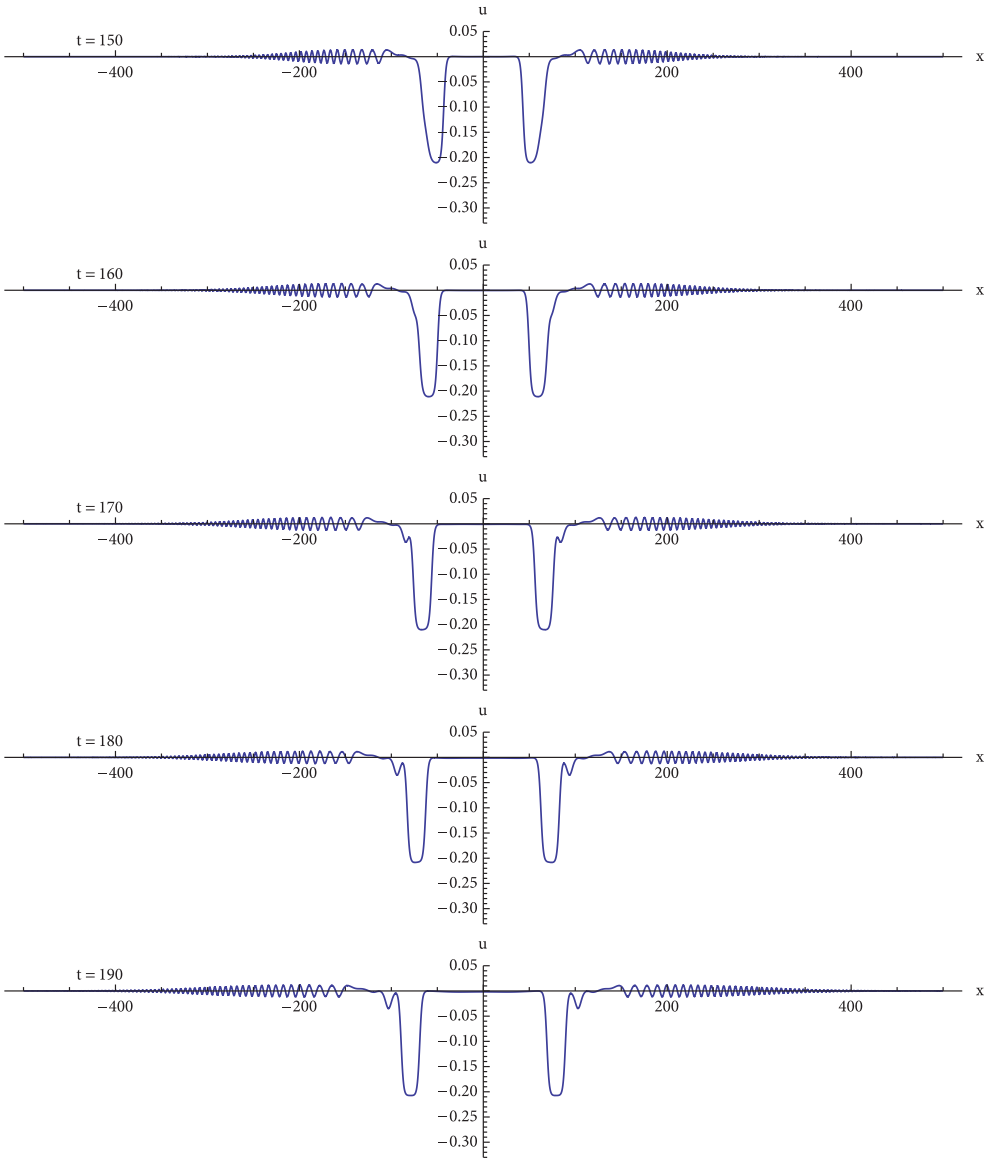
t = 150
t = 160
t = 170
t = 180
t = 190
u
x
0.05
−0.05
−0.10
−0.15
−0.20
−0.25
−0.30
−400
−200
200
400

C.2 Initiation of solitons

Time series of initiation of two pairs of solitons in the expanded basic equation. The initial state is a Gaussian function described in section 5.2.4 with the values $\sigma = 5$ and $A = 0.386441$.

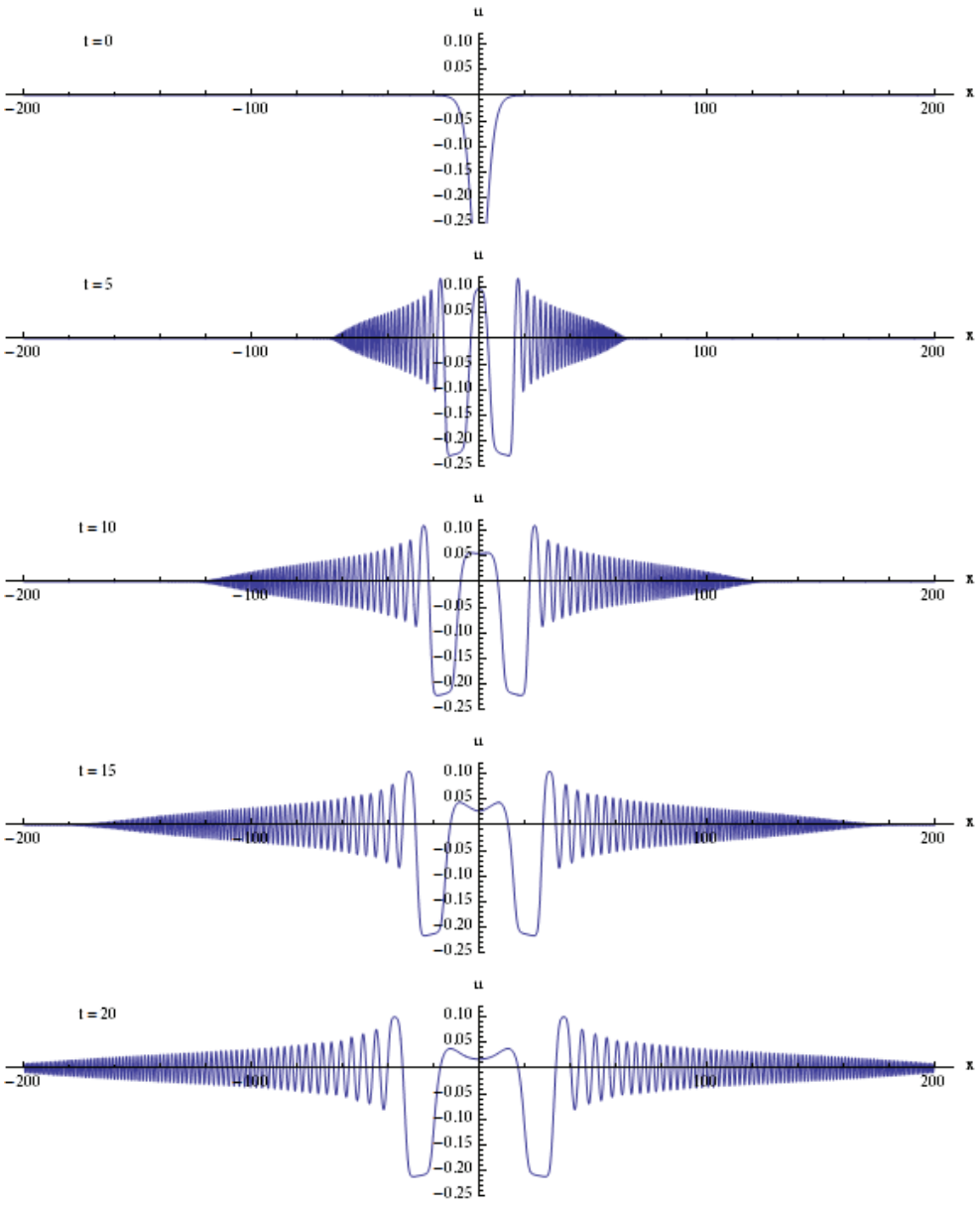

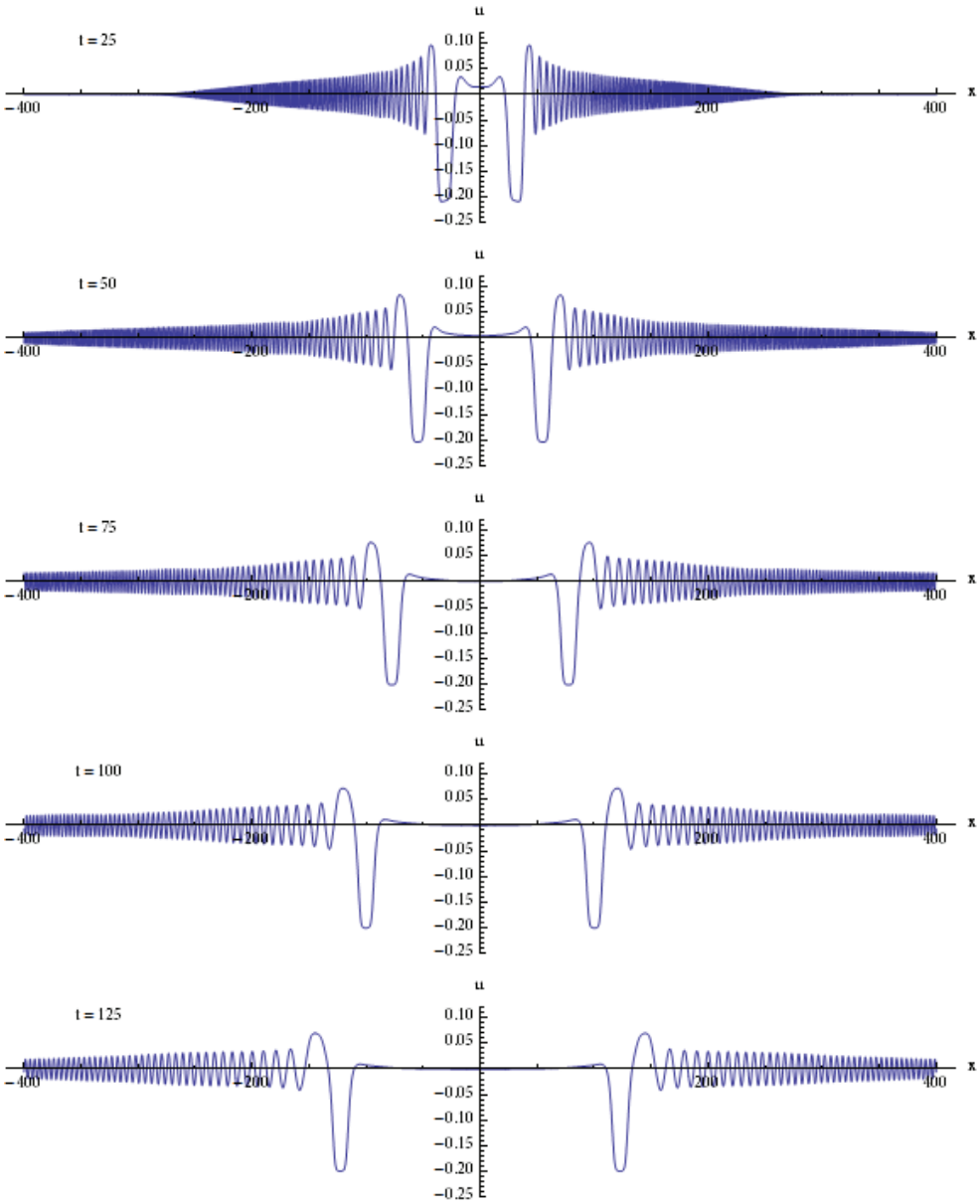
t = 25
t = 50
t = 75
t = 100
t = 125
u
x
0.10
0.05
−0.05
−0.10
−0.15
−0.20
−0.25
−400
−200
200
400

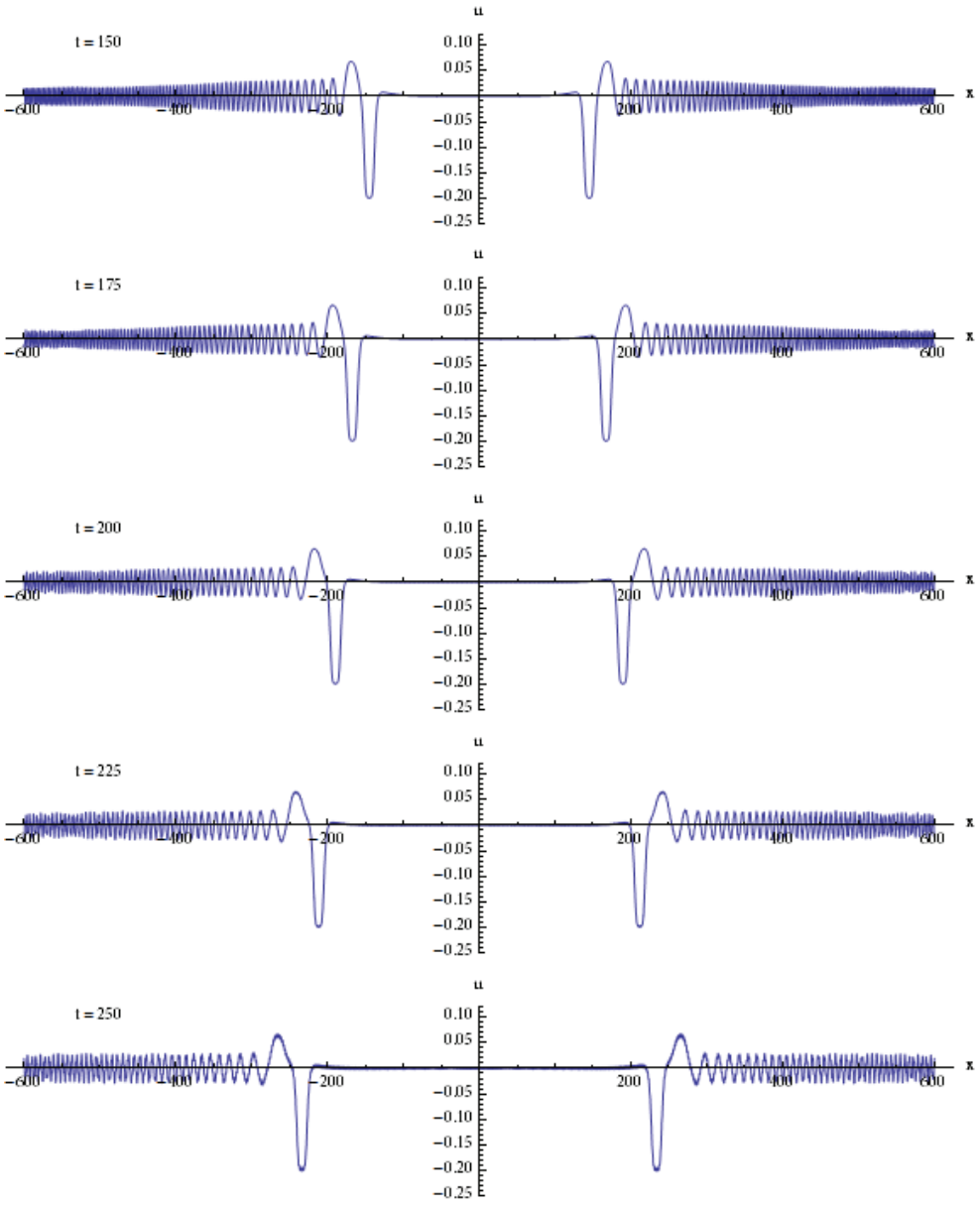
t = 150
t = 175
t = 200
t = 225
t = 250
u
x
0.10
0.05
−0.05
−0.10
−0.15
−0.20
−0.25
−600
−400
−200
200
400
600

D. Initiation (other similarities)

As shown in section 5.2.4, the systems follow the same pattern for energy over a finite width is increased. Beside what is shown (energy in the soliton as a function of initial energy and velocity of the waves as a function of initial energy) other things follow the same pattern across different widths.

In Figure D.1 the ratio of initial mass change, in the two nearest waves as a function of the initial energy is shown. As seen for the widths over σ = 0.85 have the

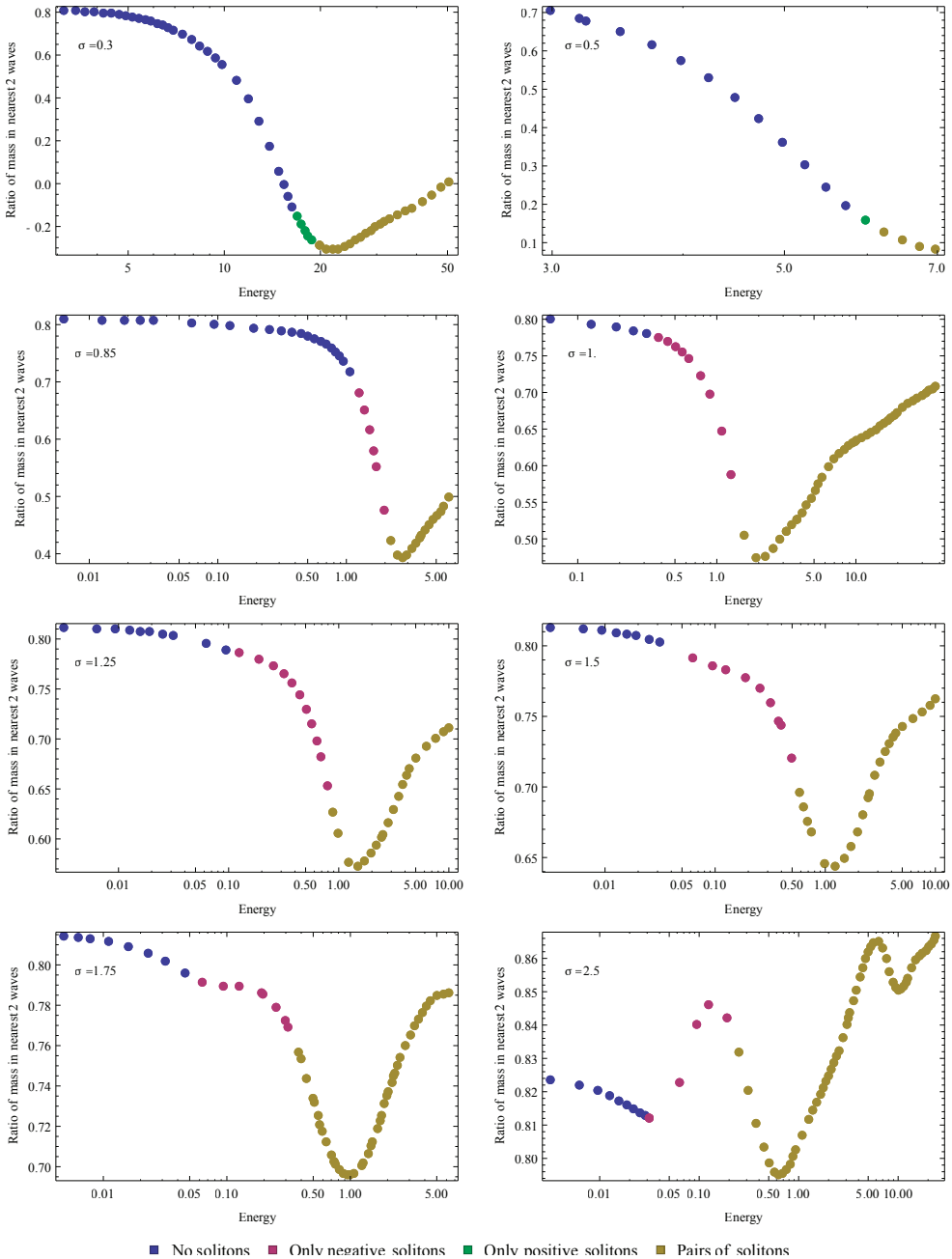

Figure D.1 – The ratio of initial mass in the nearest two waves as a function of initial energy for different widths.

same pattern, however increasing the width results in a smaller fluctuation and a more stable ratio of mass in the two nearest waves. E.g. the width σ = 0.85 fluctuate between 0.8 and 0.4, where σ = 2.5 fluctuate between 0.86 and 0.78. All patterns show a local minimum in the function, this local minimum follow a power law function of the width (see Figure D.2).

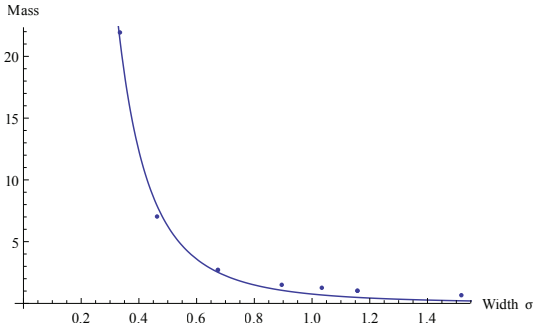

$$\frac{0.756001}{x^{3.04793}}$$

	Estimate	Standard Error	t-Statistic	P-Value
a	0.756001	0.121771	6.20838	0.000441637
b	- 3.04793	0.152689	- 19.9617	1.98087×10^{-7}

Figure D.2 – The minimum mass ration for each width follow a power law function.

E. Best fit to 50:50 DMPC:DSPC sound profile

As mentioned in section 4.2 was the best fit to the sound profile for 50:50 DMPC:DSPC not used, because of an early mistake, which was noticed until too late. However, the different between the best fit and the used fit is not big, as shown in Table E.1 and Figure E.1. Therefore was it assumed that this difference, and taken all the others assumptions into account, can be neglected.

Table E.1 - The difference between the best fit and the used on

	Used fit	*Best fit*
c [m/s]	224.988	212.621
ρ_0 *[g/m²]*	0.0696462	0.069568
β_-	0.875679	0.878868
β_+	0.972625	0.957121

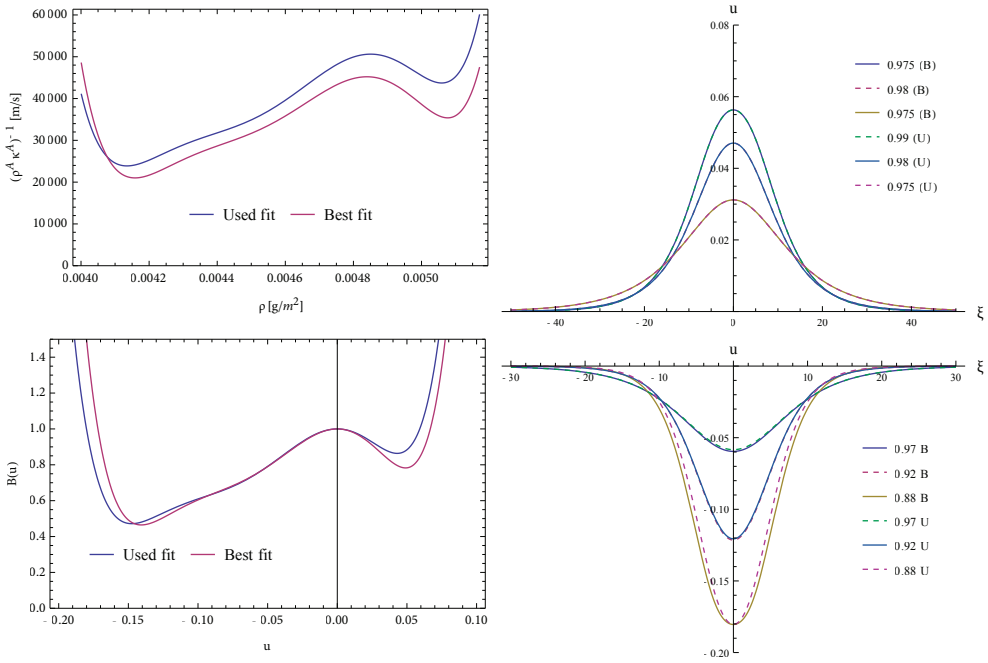

Figure E.1 - The difference between the best fit and the used fit. Upper left, the sound profile. Bottom left, the dimensionless sound profile. Right, positive and negative solitons for various velocities for both fits. Solid and (B) as the best fit, and dashed and (U) the used fit.

F. Soliton propagation in a shifted sound profile

It is unlikely that a membrane constantly stay at the same temperature, to be at the local minimum in the compressibility. Therefore it is interesting to know what happens to soliton propagation, when the bulk temperature change and stay within the two compressibility maximum. Such a shift in the temperature is shown in Figure F.1, where the bulk temperature is 37.6 °C, raised from a bulk temperature of 33 °C, the sound profile used in this thesis. When the bulk temperature is shifted, can only one type of stable solitons exist. When the temperature is raised, only stable negative solitons can propagate. However, using an initial state, as the Gaussian function described in the *Initiation* (section 5.2.4), one obtain a result their have similarities with the result with same initial values and with the non-shifted sound profile. In Figure F.2, it is shown the difference between a system with a shift and not. The system has viscosity, and in the result for the non-shifted sound profile it is clear to see four solitons. Where the one with the shifted sound profile clearly have two solitons, and two waves that could look like solitons. One should notice when shifting the sound profile, the same initial distortion have only the same mass change, and not the same energy. A study of this effect, when shifting the sound profile was not further made, due to other priorities.

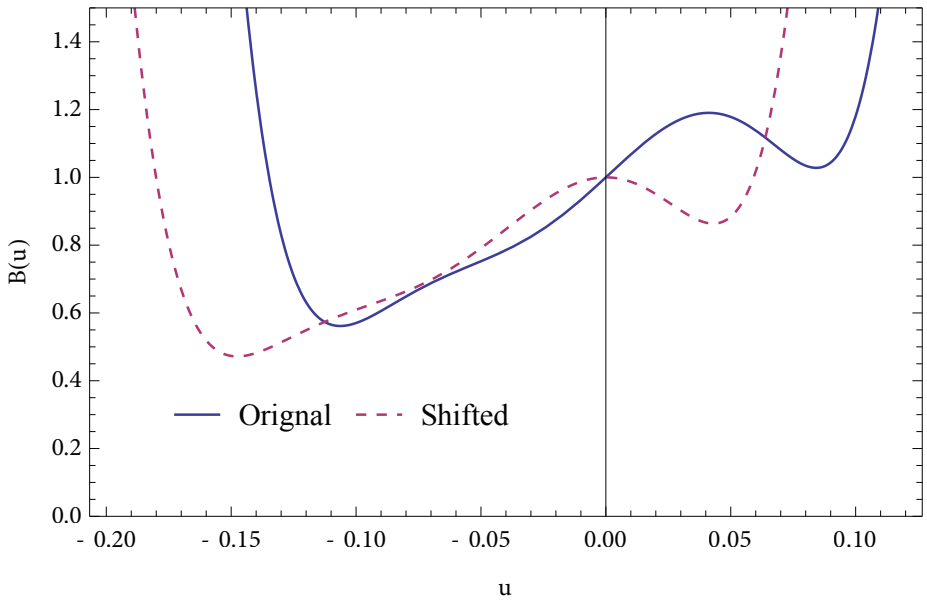

Figure F.1 – The shifted sound profile and the used sound profile in the thesis.

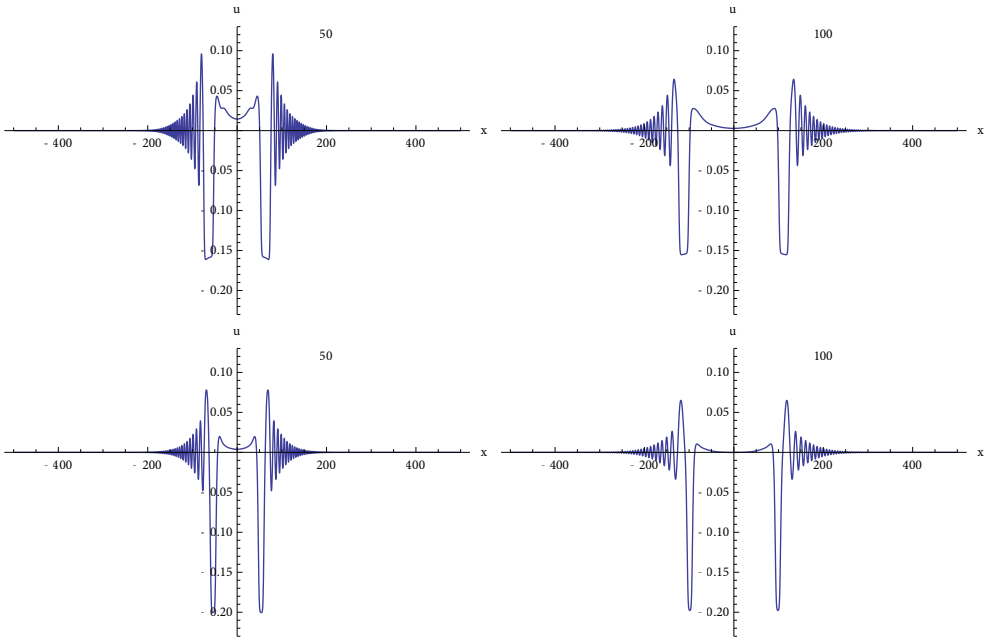

Figure F.2 – Top: the result with a shifted sound profile for time t = 50 and t = 100, where the initial state was described by a Gaussian function with σ = 5 and A = 0.386441, the system have viscosity of κ = 0.05. Bottom: the result for the non-shifted sound profile at the same time for the same initial state, and with same viscosity.

Niels Bohr Institutet
københavns universitet

Blegdamsvej 17
2100 københavn